Developing a minimal-input one-dimensional methodology for modelling axial compressors using a diffuser analogy

Prepared by:

Daniel Barlin

BRLDAN001

Department of Mechanical Engineering

University of Cape Town

Supervisor:

Assoc. Prof. Wim Fuls

February 2023

Submitted to the Department of Mechanical Engineering at the University of Cape Town in partial fulfilment of the academic requirements for a Masters of Science degree in Mechanical Engineering

Key Words: Axial compressor, Mean-line method, Flownex, Diffuser analogy

Abstract

Despite notable advances in Computational Fluid Dynamics as a tool for gas turbine design, the analysis and performance prediction of turbomachinery still benefits greatly from the use of one-dimensional mean-line modelling, as it can provide results of acceptable accuracy while requiring fewer geometric inputs, as well as comparatively lower computational expenses. However, even mean-line codes are often limited by the amount of geometric and operational data available, often withheld by Original Equipment Manufacturers for proprietary reasons. As a result, a large number of tuning factors are often employed in mean-line simulations to achieve more accurate results.

This report describes the development of a one-dimensional modelling methodology which requires minimal geometric inputs and tuning factors for predicting the performance of a transonic axial compressor stage, for use in a gas turbine. The minimal input model is achieved through development of a diffuser analogy, whereby the stage's rotor and stator rows are modelled as simple diffusers with passage flow areas approximately equal to those in the compressor stage. A design point calibration operation is first performed to estimate all diffuser flow path areas using a set of industry knowledge-based assumptions, and blade angles are determined using widely adopted correlations from open literature. The estimated geometries are then used as inputs for an off-design model built in Flownex SE. Using correlations of total pressure loss from the open literature, the Flownex model is then able to predict the stage's performance over a range of off-design operating conditions.

The model was validated against a well-documented axial compressor stage from NASA through four successive models. First, Flownex's built-in Designer function was used to determine the rotor losses that would result in good agreement with experimental data of stage total pressure ratio. The second model adopted a simple total pressure loss correlation from the literature. The third model employed a single calibration factor for adjusting flow path areas, in order to obtain better agreement with the experimental data. Further definition of the area calibration factor was achieved by applying the third model to three other NASA compressor stages. Finally, correlations determined from this exercise were evaluated.

The methodology presented an efficient means of predicting compressor stage performance with acceptable accuracy, while requiring minimal geometric inputs and only a single calibration factor, thus allowing gas turbine operators and analysts to gain greater insight into the compressor's off-design behaviour with the limited geometric and operational data available to them.

Declaration

I, Daniel Barlin, hereby declare the work contained in this dissertation to be my own. All information which has been gained from various journal articles, textbooks or other sources has been referenced accordingly. I have not allowed and will not allow anyone to copy my work with the intention of passing it off as their own work or part thereof.

Signed by candidate

Daniel Barlin

3 August 2023

Date

Acknowledgements

First and foremost, I would like to express my gratitude to my supervisor, Prof. Wim Fuls, whose constant guidance and encouragement have made my Masters journey incredibly enjoyable and fulfilling. It has been an absolute pleasure being under his supervision.

I would like to extend my gratitude to the management team of the Applied Thermofluid Process Modelling Research Unit. I have gained invaluable knowledge under your leadership, and it has been a great honour to be a part of your academic community.

I would also like to extend my gratitude to the students of the ATProM office with whom I have shared my academic journey. I am forever grateful for your moral support. You have all made these last two years truly memorable.

Lastly, I would like to thank my parents, Patti and Colin, whose undying love, support and investment in my future have carried me through my academic career. To you both, I owe you a lifetime of gratitude.

Table of Contents

List of Figures

List of Tables

List of Nomenclature

General symbols

b	Deviation angle exponent	[-]
c	Absolute velocity magnitude	m/s
c_p	Specific heat at constant pressure	kJ/kg.K
h	Specific enthalpy	kJ/kg
i	Incidence angle	°
l	Blade chord length	mm, m
m	Reference deviation angle slope function	[-]
n	Reference incidence slope function	[-]
p	Pressure	kPa
r	Radius	mm, m
s	Blade spacing	mm, m
t	Blade thickness	mm
u	Blade velocity magnitude	m/s
v	General velocity magnitude	m/s
w	Relative velocity magnitude	m/s
M	Mach number	[-]
N	Number of blades	[-]
R	Gas constant/Reaction ratio	kJ/kg.K, [-]
T	Temperature	K
Y	Total-pressure loss coefficient	[-]

Greek symbols

Δ	Change in value	
Π	Total-pressure ratio	[-]
T	Total-temperature ratio	[-]
α	Absolute flow angle	°
β	Relative flow angle	°
γ	Ratio of specific heats	[-]
δ	Deviation angle	°
θ	Camber angle	°

κ	Blade angle	°
ρ	Density	kg/m^3
σ	Blade solidity	[-]
ψ	Stage loading	[-]
ω	Angular velocity	rad/s
ϕ	Flow coefficient	[-]

Acronyms and Abbreviations

AVDR	Axial velocity density ratio
CFD	Computational fluid dynamics
DCA	Double circular arc
DF	Diffusion factor
MCA	Multiple circular arc
OEM	Original equipment manufacturer

Subscripts

h	Hub
D	Design-point condition
M	Mach number
R	Rotor
S	Stator
$crit$	Critical condition
m	Mean-line
rel	Relative condition
s	Isentropic condition
t	Tip
x	Axial direction/condition before shock
y	Condition after shock
θ	Tangential direction
0	Total or stagnation property
$1, 2, 3, 4$	Station in compressor stage

1. Introduction

1.1 Background

Computational simulation has become a key component in the design and analysis of axial compressors in modern gas turbines. Advances in three-dimensional simulation such as CFD allow compressor designers access to vast amounts of information describing complex three-dimensional flow phenomena within the turbomachinery that help inform design improvements and optimisation. However, such simulation tools typically demand significantly larger computational requirements when compared to lower-order modelling methods, and often require extensive simulation run-times, even with access to high-performance computing resources. Over and above this, CFD modelling requires a near-complete knowledge of the turbomachine geometry in order to obtain accurate prediction of performance. Such an extensive knowledge of the machine's geometry is often unavailable to machine operators or analysts, as it is withheld by Original Equipment Manufacturers (OEMs) for proprietary reasons. This can make it difficult to perform simulations if operators wish to gain greater insights into the machine's behaviour beyond the information that was made available to them by the OEMs at the time of commissioning.

Although the benefits of CFD in turbomachinery design often justify its large computational expenses, it remains a nonviable option as an analysis tool for applications such as high-level powerplant simulations, in which the turbomachine is a single component in a much larger system. This remains true for each component within a gas turbine, including the axial compressor. Moreover, if one needs to perform a wide range of simulation test cases, the time to complete this task is significantly lengthened if higher-order models are employed. It is clear, therefore, that in the case of system-level analyses, where only the compressor's overall performance is of interest to the larger system, analysts can benefit greatly from the use of lower-order modelling methodologies.

The one-dimensional mean-line method is a favourable simulation tool in such cases, as it is able to produce predictions of turbomachinery performance with acceptable accuracy, while requiring significantly fewer geometric inputs when compared to higher-order methods. Furthermore, the one-dimensional method allows for significantly lower simulation run-times, as its computational requirements are notably lower than those of higher-order models. This enables the rapid assessment of compressor performance across a broad range of operating conditions.

Nevertheless, even mean-line codes can be limited by the extent of geometric and operational data available, often resulting in a greater number of assumptions and calibration factors required to obtain accurate results. Therefore, in cases where such information is limited, a minimal-input modelling methodology that is able to produce reasonably accurate results is required.

1.2 Research aims and objectives

Based on the problem set defined above, this study aims to develop and validate a one-dimensional modelling methodology which is capable of predicting the performance of a transonic axial compressor stage with acceptable accuracy, while requiring minimal geometric inputs and knowledge of the compressor's operation. Furthermore, this study aims to minimize the number of tuning factors required to obtain accurate results, when compared to previous works.

The work performed in this study largely builds on from the Nozzle Flow Analogy previously developed by Fuls [1], which, as will be discussed in later sections, demonstrated an efficient means of predicting the performance of gas- and steam-turbine stages with minimal known geometric inputs. This was achieved by modifying the classic mean-line method to model the stator and rotor rows of the stage as simple one-dimensional nozzles in series. It was hypothesized that an "inverse" formulation of the Nozzle Flow Analogy, titled the Diffuser Analogy, will provide a suitable modification to the classic compressor mean-line method in order to achieve the study's aims.

Therefore, the study's aims will be met through the following objectives:

- A modification of the classic compressor mean-line method will be formulated using a diffuser analogy;
- Appropriate loss correlations will be identified from the open literature for use in the model;
- The model will be implemented in the Flownex Simulation Environment using the software's existing component library to create a new compound component, and
- The developed Flownex model will be validated against a well-documented set of compressor performance data from the open literature.

1.3 Limitations

As is common in research, the greatest impediment to this study was the extent of available compressor performance data for model validation because such data is often withheld by OEMs to protect intellectual property. As such, the data used for validation in this study was limited to some extent, and as a result, the range of validation performed was restricted.

The various assumptions that make up the mean-line method are discussed in later sections, but it is worth noting here that the developed model was formulated using the compressible ideal gas assumption and is therefore not suitable for fluids that deviate significantly from the ideal gas law. Furthermore, the model was developed to model axial compressors only, thereby omitting the radial flow component of other types of compressors.

It is also important to note that this study focusses specifically on developing the one-dimensional method itself. As such, discussion of various performance modelling methods such as deviation and loss sources are greatly limited. Formulation and comparison of these methods and correlations are therefore outside the scope of the present work. Nevertheless, a broad overview of the relevant performance models and their relevance to the present work will be discussed.

1.4 Dissertation outline

This dissertation comprises of a further four chapters which cover the following content:

Chapter 2: Literature review

In this chapter, the basic function of an axial compressor is described. Compressor geometry and cascade nomenclature are discussed, and conventional performance metrics are outlined. Following this, the various modelling methodologies employed in the open literature are discussed, including correlations of loss, deviation, shock treatment, and prediction methods of surge and choke. Assessment of these previous works will help inform decisions in developing the new model.

Chapter 3: Modelling methodology

Here, development of the new methodology is described, including choices of loss, deviation, and shock models. The design-point calibration and off-design methods are discussed in detail, and implementation of the model in Flownex is outlined.

Chapter 4: Results and discussion

This chapter discusses the process of validating the developed model against a set of well-documented performance data from the open literature. The performances of several sub-models are compared. The progression of model validation is concluded with the description of the final model developed in this study.

Chapter 5: Conclusions and Recommendations

Drawing on major findings in previous chapters, this chapter summarises the study's key conclusions, including choices of loss and deviation models, the model's capabilities and restrictions, and the degree to which the study's primary aims have been met. Finally, recommendations for future studies are made.

2. Literature Review

The axial compressor is often an integral component of a gas turbine, achieving the first process in the Brayton cycle, as is employed in applications such as power generation and aero-propulsion. Its primary function is to increase the pressure of the working fluid, in many cases air, to the optimal conditions for combustion in the combustion chamber. Therefore, a complete understanding of the factors affecting compressor performance is essential for the design of a robust model. This literature review investigates the various aspects of compressor operation that influence compressor modelling and performance prediction. First, context is given to the reader by discussing the various fundamentals of axial compressors, including their geometry and various parameters that describe their performance. Following this, the various modelling methodologies of loss, deviation and shock found in the open literature are discussed and assessed. Finally, discussion around these methods will outline a path of development for the new method.

2.1 Compressor fundamentals

An axial compressor achieves a desired increase in pressure by performing mechanical work on the working fluid. This is done by increasing the kinetic energy of the fluid through a moving rotor blade row. A portion the fluid's kinetic energy is then converted into a pressure rise through a stator blade row. A single rotor and stator pair in series is referred to as a compressor stage. Modern axial compressors typically achieve the desired total pressure ratio through multiple successive stages. For control of flow direction at the compressor inlet, a guide vane is often placed before the rotor of the first stage. This basic layout is observed in Figure 1 below:

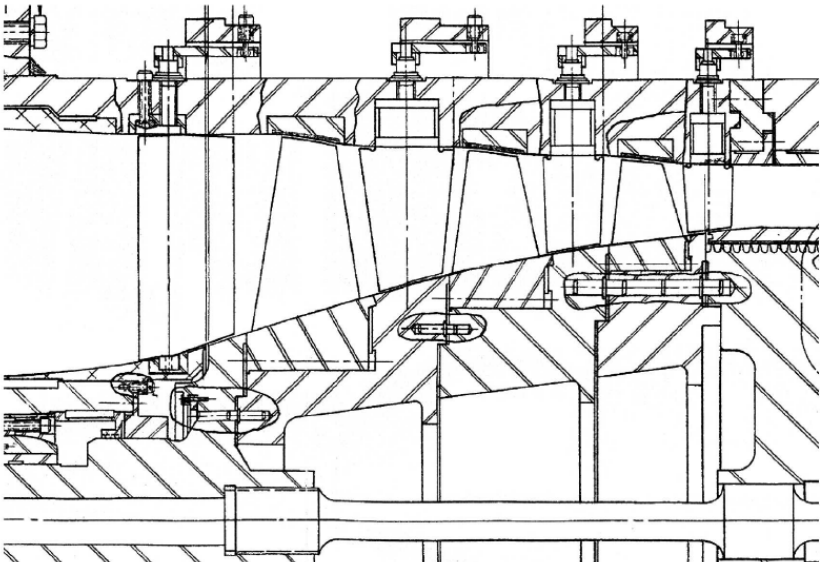

Figure 1: NASA 74-A three stage axial compressor – Taken from [16]

Although fluid flows through modern compressors are typically highly complex and three-dimensional in nature, one can describe the average flow path through a compressor stage by examining only the flow along the stage's geometric mean-line, using the velocity triangles illustrated in Figure 2 below:

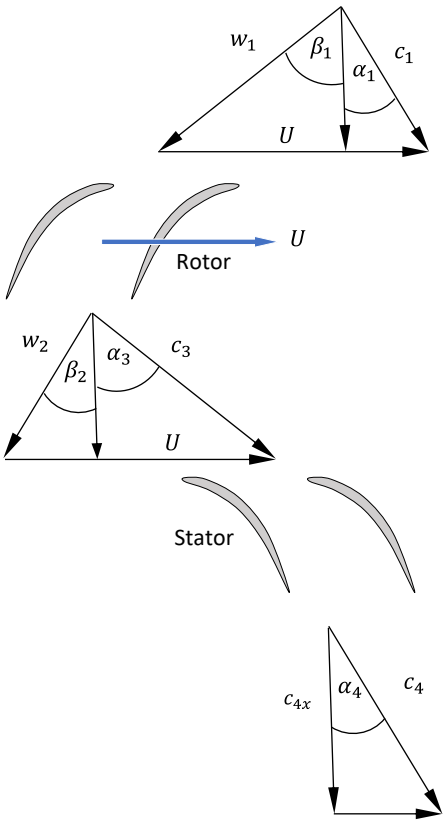

Figure 2: Axial compressor velocity triangles

The velocity triangles above illustrate the transfer of work, as well as processes of diffusion in the rotor and stator rows. The work addition by the rotor is observed from the increase in magnitude of tangential absolute velocity from $c_{1\theta}$ to $c_{3\theta}$, while diffusion and subsequent pressure recovery in the stator is observed from the decrease in velocity from c_3 to c_4. However, one can also observe diffusion of the relative flow through the rotor, shown by the decrease in magnitude of relative velocities from w_1 to w_2. For computational consistency, angles are defined as positive if their corresponding velocity vector's tangential component is in the same direction as the rotor speed vector, U. Otherwise, the angle is defined as negative. Therefore, under typical operation, relative flow angles β_1 and β_2 in Figure 2 are negative.

Many modern compressor stages are often initially designed under the normal, repeating-stage assumption, whereby the axial velocity through the stage is constant, and absolute angles α_1 and α_4 are equal [2].

2.1.1 Compressor geometry and nomenclature

Blade and flow path geometries in modern compressors are typically complex. Modern compressor blades are often three-dimensional in design, comprising of variable spanwise cross-sectional profiles and high degrees of twist. However, the assumptions of average flow discussed above allows one to analyse a blade row in a two-dimensional frame, only considering the blade profile at the blade's mean-section. This is illustrated in Figure 3:

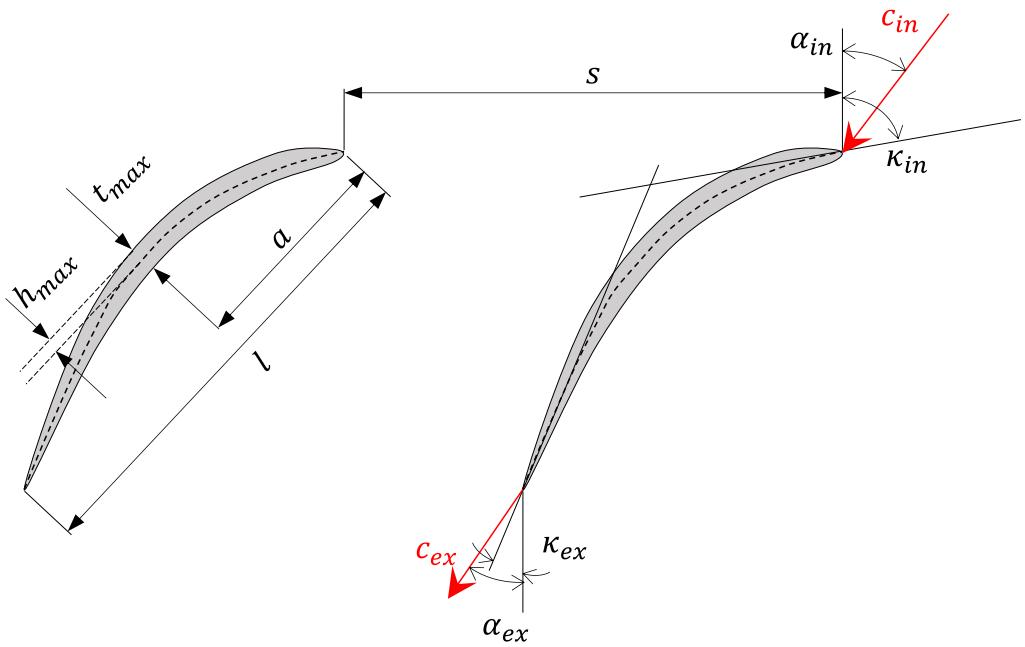

Figure 3: Compressor cascade nomenclature – Adapted from [2]

In the above figure, α_{in} and α_{ex} denote the flow angles at the blade inlet and exit, respectively. Similarly, κ_{in} and κ_{ex} denote the average physical inlet and exit blade angles. All angles are measured from the axial direction.

The difference between inlet flow angle and blade angle is referred to as the incidence angle, and in the absolute frame is denoted as:

$$i = \alpha_{in} - \kappa_{in} \tag{2.1.1}$$

Similarly, the difference between exit flow and blade angles is referred to as the deviation angle, and is denoted as:

$$\delta = \alpha_{ex} - \kappa_{ex} \tag{2.1.2}$$

The difference between the inlet and exit blade angles is referred to as the camber angle, and is denoted as:

$$\theta = \kappa_1 - \kappa_2 \tag{2.1.3}$$

Similarly, the difference between inlet and exit flow angles is known as the deflection angle, and is denoted in the absolute frame as:

$$\varepsilon = \alpha_{in} - \alpha_{ex} \tag{2.1.4}$$

Other notable geometric features in Figure 3 include the blade chord, l, maximum blade thickness, t_{max} , blade spacing, s, and the maximum camber height, h_{max}. Additionally, a denotes the distance to the point of maximum camber from the leading edge.

The blade solidity is defined as the ratio of a blade's chord length to blade-spacing, and can be estimated at the mean-line knowing the mean-radius and number of blades:

$$\sigma_m = \frac{l_m}{s_m} = \frac{l}{2\pi r_m} \cdot N \tag{2.1.5}$$

2.1.2 Compressor performance parameters

One of the most common methods of visualising compressor performance is the compressor map. A typical compressor map of total pressure ratio is illustrated in Figure 4 below:

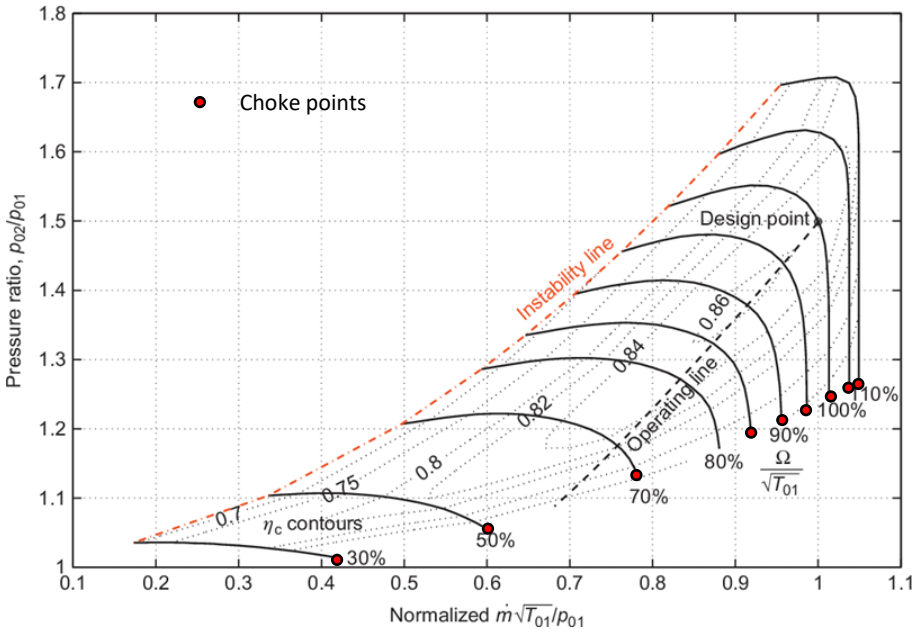

Figure 4: Typical compressor performance map – Taken from [2]

The above compressor map plots total pressure ratio against normalised mass flow rate and includes lines of normalised rotor speed. A single speed line is bound by the compressor's surge limit (instability line) and its choke limit. The design point represents the mass flow and total pressure ratio at which the compressor is designed to operate. However, a compressor must also be designed

such that it is able to operate under adverse, off-design conditions without exceeding surge or choke limits.

In the preliminary stages of compressor design, several non-dimensional design parameters are employed to characterise the compressor's flow geometry for design-point operation. Three predominant design parameters are the reaction ratio, stage loading and flow coefficient, each discussed in more detail below:

Reaction ratio

Reaction ratio is defined as the ratio of the rotor static enthalpy rise to the stage static enthalpy rise:

$$R = \frac{h_2 - h_1}{h_4 - h_1} \tag{2.1.6}$$

In modern compressors, reaction ratios are typically chosen to be between 0.5 and 0.8 [2].

Stage loading

The stage loading of a normal, repeating stage is expressed as:

$$\psi = \frac{h_{03} - h_{01}}{U^2} = \frac{\Delta c_\theta}{U} \tag{2.1.7}$$

Equation (2.1.7) indicates that higher stage loading results in an increased work done per stage, and thus a higher achieved pressure ratio. However, excessive stage loading results in greater flow turning, and subsequently higher degrees of diffusion, thus decreasing stage performance. For this reason, axial compressors typically comprise of a large number of stages with a lower loading per stage. As a result, stage loading is typically selected to be around 0.4 [2].

Flow coefficient

The flow coefficient is defined as the ratio of axial flow velocity to blade velocity:

$$\phi = \frac{c_x}{U} \tag{2.1.8}$$

Typically, a large flow coefficient is desired as this results in a higher mass flow per stage annulus area, and thus greater potential stage loading [2]. This translates to fewer stages required to achieve a desired pressure ratio, which is beneficial from a cost point of view. The flow coefficient is however limited by flow choking, and is thus typically chosen to be between 0.4 and 0.8 [2].

Through derivation of the of the stage loading and flow coefficient in a normal repeating stage, the rotor-exit relative flow angle can be determined from Equation (2.1.9) [2]. The negative sign adopted here is to ensure conformance with the study's sign convention.

$$\beta_2 = -\arctan\left(\frac{1-\psi_D}{\phi_D} - \tan(\alpha_1)\right) \tag{2.1.9}$$

2.2 Modelling methodologies

The various successive stages of compressor design each require modelling capabilities of increasing complexity. As outlined by Kidikian [3], the compressor design life-cycle typically begins with one-dimensional mean-line modelling to set initial sizing and boundary conditions. Following this, two-dimensional throughflow analysis is performed to further define flow path geometry and spanwise variations of blade profile. Three-dimensional modelling, such as Computational Fluid Dynamics (CFD), is then employed to define full three-dimensional aerofoil geometry. This process is often iterative and requires several repetitions to achieve optimal design. Although higher-order models (2D and 3D) enable greater design capabilities, their suitability specifically in analysis applications must be evaluated.

Three-dimensional modelling

Over the past several decades, CFD has become an increasingly popular tool for turbomachinery design. Based on the discrete solving of the Navier-Stokes equations for momentum, energy and mass conservation, CFD modelling can provide extensive information of the complex, turbulent three-dimensional flows typically observed in modern turbomachines. CFD simulations also do not require extensive empirical correlations of loss or flow deviation, as these are determined within the solving methodology and chosen turbulence and friction model. However, CFD models are typically computationally expensive, requiring large computational resources and extensive simulations run-times. The convergence and overall accuracy of CFD simulations rely heavily on

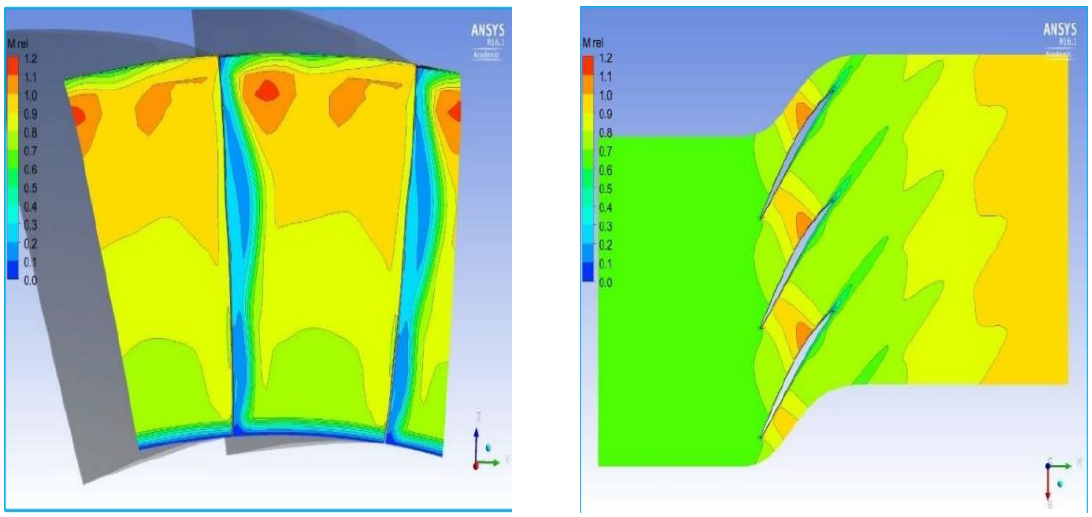

Figure 5: CFD modelling of axial compressor – Taken from [3]

mesh quality and construction, and analysis typically requires a complete knowledge of the compressor geometry, usually only available to Original Equipment Manufacturers (OEMs).

Two-dimensional modelling

Also referred to as throughflow modelling, two-dimensional compressor modelling involves a finite-element-based approach of discretely solving for momentum conservation and stream function equations along a blade's span. As such, the method is capable of predicting variations in flow characteristics in both axial and spanwise directions. An example of a throughflow solving grid is illustrated in Figure 6 below:

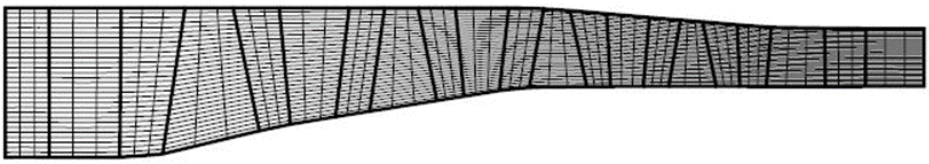

Figure 6: Finite element grid for a 4-stage axial compressor – Taken from [11]

In contrast to 3D modelling, however, throughflow modelling requires empirical correlations of loss, flow deviation, and spanwise mixing. Nevertheless, the method's two-dimensional nature makes it less computationally expensive, resulting in comparatively lower run-times. Although to a lesser extent than CFD, throughflow modelling also requires a detailed understanding of flow path geometry.

One-dimensional modelling

Otherwise known as the mean-line method, one-dimensional compressor modelling is performed under the assumption that one can adequately estimate the average flow conditions through a compressor stage by only considering flow along the stage's meridional mean-line. The method involves determining the velocity triangles (kinematics) and fluid properties (thermodynamics) at the leading and trailing edges of the rotor and stator rows. In achieving this, one is able to predict the compressor stage's overall performance characteristics at varying operating conditions.

The mean-line thermodynamics and kinematics are related through the definition of total enthalpy, which is expressed for both absolute and relative frames in Equations (2.2.1) and (2.2.2), respectively.

$$h_0 = h + \frac{1}{2}c^2 \tag{2.2.1}$$

$$h_{0,rel} = h + \frac{1}{2}w^2 \tag{2.2.2}$$

The above equations are derived from the definition of rothalpy, which describes the conservation of stagnation enthalpy through a blade passage. For a rotor blade row in the relative frame, the conservation of rothalpy is expressed as:

$$h_{01rel} - \frac{1}{2}\omega_1^2 r_1^2 = h_{02rel} - \frac{1}{2}\omega_2^2 r_2^2 \tag{2.2.3}$$

If changes in streamline radius are negligible, and rotor speed is assumed constant, Equation (2.2.3) indicates that the relative total enthalpy over a rotor blade row remains constant. This is a common assumption in many simplified axial mean-line models. Similarly, the absolute total enthalpy through the stator row can be assumed constant since the stator passage does not perform any work on the fluid.

As is the case for two-dimensional modelling, mean-line codes also require correlations for losses and flow deviation. With suitable correlations, mean-line modelling is capable of predicting overall compressor performance over a wide range of operation with acceptable accuracy. The knowledge of compressor geometry required to perform mean-line analysis is significantly less compared to higher-order methods, typically including only information of flow areas and general blade characteristics. The mean-line method remains one of the oldest and most reliable methods for preliminary compressor design and is therefore regarded as one of the most popular methods of compressor simulation.

2.3 Performance modelling

Much of the research in the open literature concerning compressor performance has evolved from the low-speed two-dimensional cascade studies of Lieblein [4]–[6] and Carter [7], as well as other prominent studies such as that of Koch and Smith [8]. The correlations of loss, incidence, deviation and surge developed in these studies laid the foundations for further development in compressor modelling. The progression of research in the open literature from these works is discussed in the following sections.

2.3.1 Reference incidence angle

Low-speed cascade tests performed by Lieblein [5] revealed that the off-design behaviour of axial compressors was significantly influenced by off-design incidence angle. The studies showed that a minimum total pressure loss would be observed at some reference incidence angle, and for incidence angles smaller or greater than the reference incidence, total pressure loss would increase almost parabolically. The general nature of loss vs. incidence is illustrated in Figure 7 below:

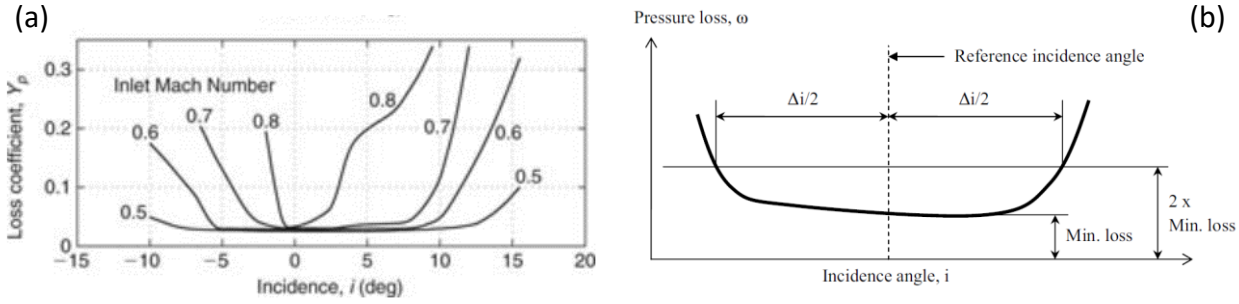

Figure 7: (a) Observed compressor loss behaviour, and (b) idealised loss bucket – Taken from [2] and [9], respectively

Lieblein's findings also suggested that compressibility has negligible effect on the reference incidence angle, since it would remain fairly constant for a range of inlet Mach numbers, as illustrated in Figure 7(a). This led to the definition of the idealised "loss bucket", illustrated in Figure 7(b).

Lieblein's correlation of reference minimum loss incidence angle was developed based on cascade data of 10-percent-thick NACA 65-series blades [5]. The correlation, also referred to as the NASA 2D method, is presented in Equation (2.3.1) below:

$$i_{2D}^{*} = (K)_{sh}(K_i)_t(i_0)_{10} + n\theta \tag{2.3.1}$$

In the above equation, $(K)_{sh}$ and $(K_i)_t$ are correction factors for blade shape and maximum thickness distributions, respectively, $(i_0)_{10}$ is the zero-camber incidence angle for a 10-percent-thick NACA 65-series aerofoil, n is the reference incidence slope factor, and θ is the camber angle defined in Equation (2.1.3). The zero-camber reference incidence and slope factor are functions of both inlet flow angle and blade solidity, and all angles are defined in degrees.

Lieblein estimated values for shape correction factor $(K)_{sh}$ based on general blade profile classification. This was done for double-circular-arc (DCA), C-Series, and NACA 65-Series aerofoils. The estimated values for $(K)_{sh}$ are shown in Table 1 below:

Table 1: Values of shape correction factor for various blade types [5]

Blade type	$(\mathbf{K})_{\mathbf{sh}}$
DCA	0.7
C-Series	1.1
NACA 65-Series	1.0

Values for $(i_0)_{10}$, n and $(K_i)_t$ can be interpolated from Figures 137, 138 and 142 in Lieblein's paper, respectively [5]. However, Falck [9] derived multivariable equations that describe the original data with good agreement:

The zero-camber incidence angle $(i_0)_{10}$, based on 10-percent-thick NACA 65-series, is expressed as:

$$(i_0)_{10} = \alpha_1^2(1.64\cdot10^{-5} - 2.38\cdot10^{-4}\sigma) + \alpha_1(-0.002364 + 0.0913\sigma) - 0.0674\sigma + 0.0325 \quad (2.3.2)$$

The zero-camber incidence angle is defined with the same sign convention as mentioned in 2.1.1. The slope factor n is then defined as:

$$n = -\alpha_1^2(3.79\cdot10^{-5} + 1.11\cdot10^{-5}\sigma) + \alpha_1(-0.0035 + 0.0029\sigma) - 0.02274\sigma - 0.063 \quad (2.3.3)$$

In the above two equations, α_1 and σ denote the inlet flow angle and solidity, respectively. In the case of a rotor row, α_1 is replaced in the above equations with the relative inlet flow angle β_1.

The thickness-distribution correction factor $(K_i)_t$ is a function of maximum-thickness-to-chord ratio, and was estimated by Falck [9] as:

$$(K_i)_t = 312.5\left(\frac{t}{l}\right)^3_{\max} - 122.3\left(\frac{t}{l}\right)^2_{\max} + 19.17\left(\frac{t}{l}\right)_{\max} - 0.0214 \quad (2.3.4)$$

In a study evaluating several compressor performance modelling methods, Çetin et al. [10] determined that a modified form of the NASA 2D method provided the greatest agreement in a range of experimental data. Çetin's modified correlation accounted for effects due to inlet Mach number, and was determined for DCA and multiple-circular-arc (MCA) blading as:

$$i^*_{DCA} - i^*_{2D} = 0.7238M_1 + 7.5481 \quad (2.3.5)$$

$$i^*_{MCA} - i^*_{2D} = 1.3026M_1 + 5.7380 \quad (2.3.6)$$

Other studies adopted a modified form of the standard NASA 2D method by adding a calibration factor C_i to achieve better agreement with experimental data. Petrovic et al. [11] found that a C_i of 2° for NACA profiles and 2.5° for DCA profiles achieved the best agreement in throughflow simulations. The study however did not identify a value of C_i for MCA bladings.

It is important to note that definitions of optimum incidence vary throughout the literature. Carter [12] defined optimum incidence as being associated with a fixed stagnation point on a blade's leading edge, while Lieblein [5] defined it as the incidence at point of minimum-pressure losses. Over and above this, Lieblein notes that the reference minimum-loss incidence is not necessarily the design-point incidence, as this would likely be determined by compressor designers after more in-depth analysis. However, in absence of further information, it can be assumed that there is little distinction between the actual design-point incidence and Lieblein's definition of reference incidence.

2.3.2 Deviation angle

The deviation angle describes the degree of flow deviation from the mean blade exit angle, which is typically caused by diffusion effects resulting from high adverse pressure gradients often occurring in axial compressor blade rows [2]. This is a common phenomenon in compressor flow passages which are subjected to high adverse pressure gradients [2] . Deviation angle forms a key component in compressor performance modelling, as it influences the degree of flow turning and thus the amount of diffusion in a blade row, as illustrated in Figure 8 below, which shows the realistic exit velocity w'_2 of a rotor blade against the ideal case w_2 in which no deviation occurs.

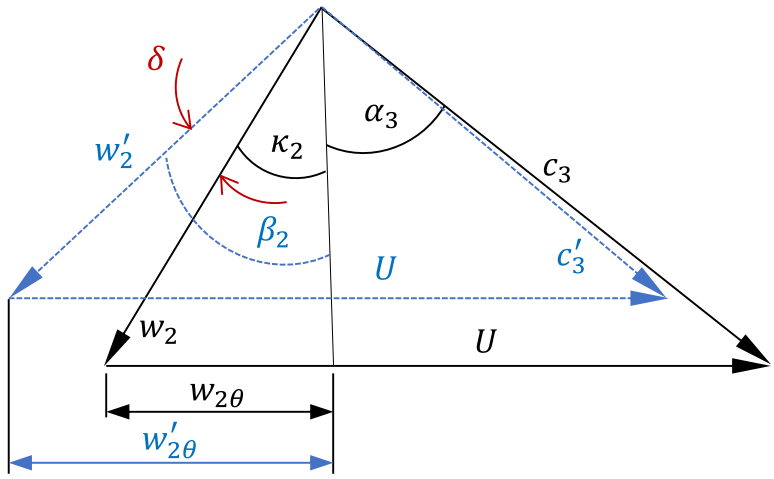

Figure 8: Influence of deviation angle on velocity triangle

As can be observed from Figure 8, an increase in the tangential component of w_2 will result in a decrease in that of c_3, assuming blade velocity U remains constant. If one considers the work performed by the rotor as being equal to $\Delta(Uc_\theta)$, then it is clear that a higher deviation angle will result in reduced rotor compressor work and can therefore be considered as a source of loss in work potential.

As is the case with incidence angle, off-design compressor performance prediction relies on information of the machine's performance characteristics at design-point operation. Therefore, several methods of determining the design-point deviation angle have been explored in the literature and are discussed below.

Reference deviation angle

In an effort to derive methods of compressor performance analysis without the need for lengthy calculations, Carter [7] presented a simple method of determining the deviation angle in cascades at reference incidence. This has come to be known as Carter's Rule and is widely cited throughout the literature:

$$\delta^*_{CAR} = m\frac{\theta}{\sigma^b} \tag{2.3.7}$$

In Equation (2.3.7), m is a function of blade profile and stagger angle, and b is some experimental exponent. It is typically approximated with b equal to 0.5 for compressor cascades and 1 for turbine cascades and inlet guide vanes [2]. Through use of blade solidity in the denominator, Carter's rule intuitively describes the effect of blade spacing on flow deviation, whereby a greater number of blades (and thus reduced blade spacing) allows for greater control of flow direction, therefore reducing deviation angle.

The value of m can be determined from experimental data plotted by Carter, however Dixon and Hall [2] cited a typical correlation for m in compressor cascades:

$$m = 0.23\left(2\frac{a}{l}\right)^2 + \frac{\alpha_2^*}{500} \tag{2.3.8}$$

In Equation (2.3.8), α_2^* is the cascade exit flow angle at reference incidence, and a is the distance of maximum camber from the blade's leading edge, illustrated in Figure 3.

Çetin et al. [10] presented a modified form of Carter's Rule for achieving better agreement with data of transonic compressor cases, and also including 3D effects:

$$\delta^* = -0.1988\left(\delta^*_{CAR}\right)^2 + 3.0186\left(\delta^*_{CAR}\right) - 1.099379 \tag{2.3.9}$$

In a similar fashion to the NASA 2D method for reference incidence, Lieblein [5] derived a method for determining deviation angle at minimum-loss reference incidence. Similar to Equation (2.3.1), Lieblein's method takes into account variations in blade profile and thickness distribution in relation to the NACA 65-Series blades:

$$\delta^*_{2D} = \left(K\right)_{sh}\left(K_\delta\right)_t\left(\delta^*_0\right)_{10} + m\theta \tag{2.3.10}$$

As in Equation (2.3.1), $(K)_{sh}$ and $(K_\delta)_t$ are correction factors for blade shape and thickness distribution, respectively, $(\delta_0)_{10}$ is the reference zero-camber deviation angle of NACA 65-Series blades, and m is a deviation slope factor. As is the case for reference incidence, values of $(K)_{sh}$ for reference deviation can also be taken from Table 1. Values of $(\delta_0)_{10}$, m, and $(K_\delta)_t$ can be interpolated from Figures 161, 162 and 172 in Lieblein's paper [5], respectively. However, Falck [9] also derived correlations for these variables to represent the original graphical data. It must first be noted that Falck adopted the alternative correlation for m:

$$m = \frac{m'}{\sigma^b} \tag{2.3.11}$$

Falck's correlations for $(\delta_0)_{10}$, m' and b are described in Equations (2.3.12) to (2.3.15) below, noting that values of m' vary for different blade profiles:

$$\left(\delta_0\right)_{10} = \alpha_1^2\left(-0.0004 + 0.00076\sigma\right) + \alpha_1\left(0.0209 - 0.0186\sigma\right) + 0.1057\sigma - 0.0443 \tag{2.3.12}$$

For NACA 65-Series blades:

$$m' = 3.33\cdot10^{-5}\alpha_1^2 - 3.33\cdot10^{-4}\alpha_1 + 0.17 \tag{2.3.13}$$

For DCA and C-Series blades:

$$m' = 3.16\cdot10^{-7}\alpha_1^3 - 1.32\cdot10^{-5}\alpha_1^2 + 7.4\cdot10^{-4}\alpha_1 + 0.249 \tag{2.3.14}$$

$$b = -1.3\cdot10^{-6}\alpha_1^3 + 4.221\cdot10^{-5}\alpha_1^2 + 2.538\cdot10^{-3}\alpha_1 + 0.9655 \tag{2.3.15}$$

As before, α_1 is replaced in the above equations with the relative inlet flow angle β_1 for the rotor row.

Falck's estimation for the thickness-distribution correction factor $(K_\delta)_t$ was determined as:

$$\left(K_\delta\right)_t = 36.61\left(\frac{t}{l}\right)_{\max}^2 + 6.172\left(\frac{t}{l}\right)_{\max} + 0.0142 \tag{2.3.16}$$

Petrovic et al. [11] also adopted a modified form of Equation (2.3.10) by adding a calibration factor C_δ. Petrovic found that C_δ values of 0° and 1.1° returned the best agreement with experimental data for NACA and DCA blades, respectively. However, no correction factors were identified for MCA blades.

Off-design deviation angle

The most commonly cited method for determining off-design deviation angle is that employed by Boyer [13], which describes the total off-design deviation as the sum of various deviation contributions:

$$\delta = \delta_{ref} + \delta_{3D} + \delta_M + \delta_{va} + \delta_i \tag{2.3.17}$$

The deviation contributions in Equation (2.3.17) are as follows:

- δ_{ref} – reference, minimum loss deviation angle
- δ_{3D} – deviation due to three-dimensional flow effects
- δ_M – deviation due to Mach number effects
- δ_{va} – deviation related to axial velocity ratio
- δ_i – deviation due to off-design incidence effects

The reference deviation angle δ_{ref} is calculated using Lieblein's reference minimum-loss correlation discussed earlier [5]. δ_{3D} accounts for the complex three-dimensional flows through a blade row, including secondary and tip-leakage flows. This is calculated from graphical data in NASA SP-36 [14]. δ_{va} accounts for streamtube contraction through a blade row, and is typically calculated as:

$$\delta_{va} = k\left(1 - \frac{c_{x2}}{c_{x1}}\right) \tag{2.3.18}$$

In the above equation, c_{1x} and c_{2x} are the meridional velocities at the blade inlet and exit, respectively, and k is a calibration factor which can initially be chosen as 10.0 [13].

For off-design deviation due to incidence effects (δ_i), Çetin et al. [10] found that the method of Creveling and Carmody [15] produced the most accurate results among a number of investigated methods. Based on data collected from NACA-65 tests, the method plots change in deviation angle from design-point as a function of change in incidence angle, as illustrated in Figure 9 below:

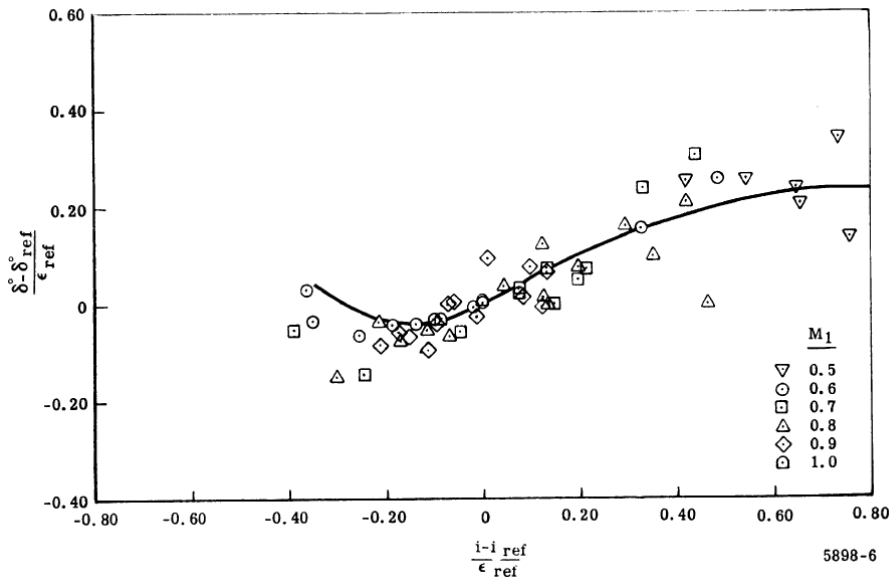

Figure 9: Off-design deviation angle due to incidence effects – Taken from [15]

Although the method is widely adopted throughout the literature, it is evident from Figure 9 that Creveling's test data was greatly limited for values of $(i - i_{ref})/\varepsilon_{ref}$, with values only ranging between approximately -0.05 and 0.25. Furthermore, the tests only included data in the subsonic range, with Mach numbers not exceeding 1.0. In any case, Figure 9 shows that insignificant change in normalised deviation angle is observed for the range of incidence angles investigated, with a maximum possible increase of 0.2.

Boyer found that Mach number had an insignificant effect on off-design deviation, and thus chose to omit δ_M from their model.

It may be argued that determining each contribution to off-design deviation leads to a lengthy process involving a notable number of steps and calibration factors. Many authors have in fact chosen to perform off-design analysis using a constant deviation angle equal to the design-point deviation determined using Carter's Rule [3], [7], based on the assumption that deviation does not vary significantly from the design condition. For example, Veres [16] indirectly selected a constant deviation angle for off-design analysis by fixing slip factor between 0.93 and 0.96. A sample output presented by Boyer [13] suggested that the off-design deviation angle did not vary significantly from the reference point at the mean-line radius. One may therefore conclude that considerations for off-design deviation angle may be ignored for mean-line analysis. Its importance however may still hold for two-dimensional analysis where spanwise variations are considered.

2.3.3 Design-point total pressure loss

Predicting compressor loss behaviour at off-design operation requires knowledge of the machine's loss sources at the design point. Therefore, a means of predicting the design-point losses is required to perform further analysis.

The total pressure loss coefficient is a primary means of representing losses through a compressor blade row. In compressor cascades, the total pressure loss coefficient is defined as:

$$Y = \frac{p_{01} - p_{02}}{p_{01} - p_1} \tag{2.3.19}$$

The ratio presented in Equation (2.3.19) can be represented as a "run-over-rise" relationship, as illustrated in Figure 10:

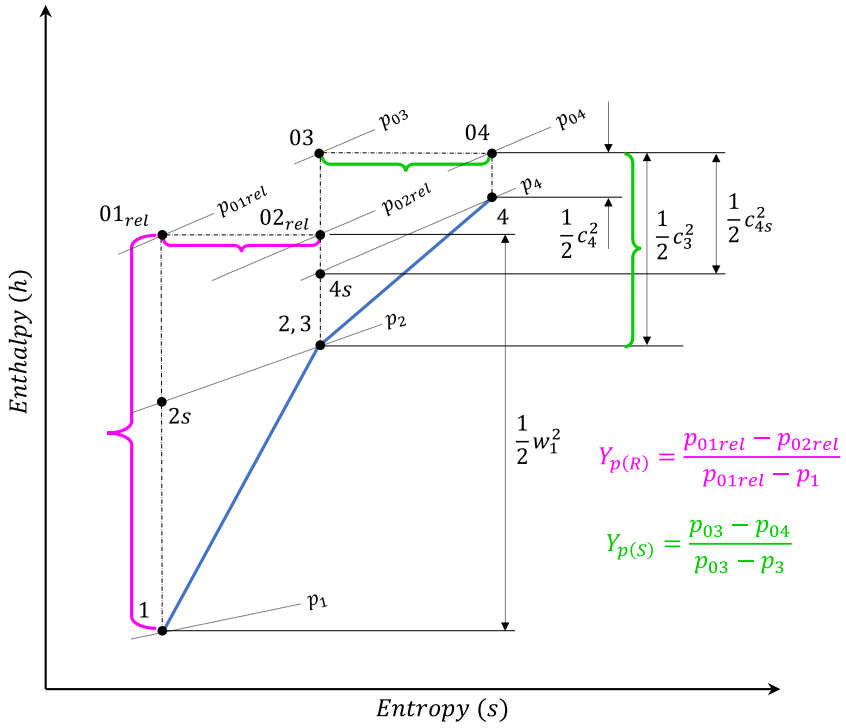

Figure 10: Visual representation of total pressure loss coefficient

Determining the rotor and stator total pressure loss coefficients is often a complex exercise, due to the fact that many factors of blade passage flow each have a markable effect on the row's total entropy generation. It is generally agreed throughout the literature that the total pressure loss coefficient can be represented as the sum of individual loss contributions. Kidikian [3] described the predominant loss sources modelled in the open literature as being: Profile loss Y_p, secondary or vortex loss Y_S, Clearance loss Y_{CL}, and shock loss Y_M. The various loss sources arise from the complex flow structures typically observed in a compressor blade passage, as illustrated in Figure 11:

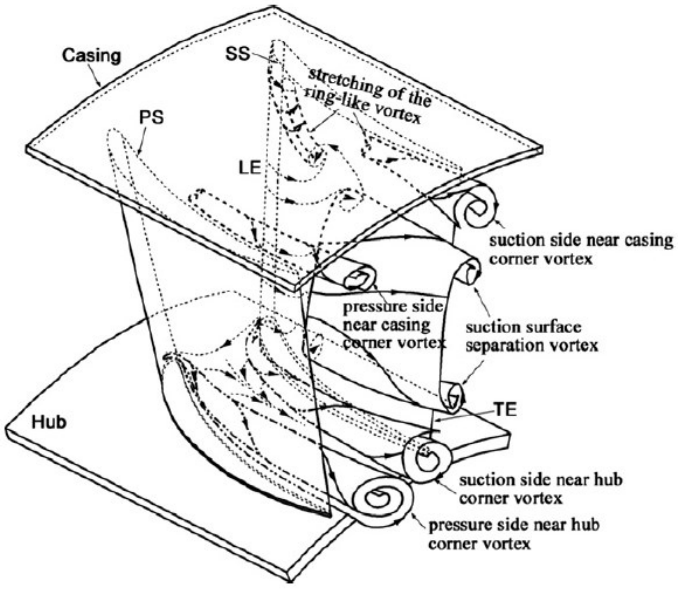

Figure 11: Three-dimensional flows through compressor flow passage – Taken from [39]

Having investigated loss modelling trends from a wide range of publications, Kidikian [3] found that the most adopted methods for estimating design-point losses are those of Koch and Smith [8] and Wright and Miller [17]. Çetin et al. [10] also compared several methods, and found Koch and Smith's method to be the most complete. In addition to the already-listed loss sources, Koch and Smith's method also included a means of estimating the loss generated from part-span shrouds.

Much of the research concerning profile loss has evolved from low-speed cascade tests performed by Lieblein [5]. Lieblein's original work, strongly based in boundary-layer theory, formulated a relationship between cascade loss and the degree of diffusion through the cascade. Lieblein estimated the equivalent amount of diffusion through a cascade from the ratio of maximum blade suction-surface velocity to cascade inlet velocity, as well as the momentum thickness of the wake at the blade trailing edge. Lieblein's method was however limited to incompressible flows only. König et al. [18] modified Lieblein's model to account for effects of streamline curvature, change in axial velocity, and compressibility, thus extending the method's applicability to transonic cascades. Studying various loss models, Manfredi [19] found that König's method was the most complete, and needed no revision. Crutzen [20] also found König's method to be the most adequate over a number of investigated profile loss models.

Shock losses arise as a result of shock structure formation in compressor flow passages when blade inlet flows are supersonic ($M_1 > 1$), or of high-enough subsonic Mach number to cause the maximum Mach number on the blade suction surface to be supersonic [19]. The shock losses are attributed to the viscous dissipation across these shock structures, as well the shock's interaction with the blades' surface boundary layers [19].

Of the various shock loss models available in the open literature, some of the more popular include the simple flow model of Miller et al. [21], the leading edge and passage shock model of Koch and Smith [8], and the modified two-shock model developed by König et al. [22]. For the purpose of this study, the formulations of the above loss and shock models will not be discussed in this report as an alternative method was used to treat supersonic flows.

Several papers are dedicated to outlining the various loss sources in detail, such as that of Crutzen [20]. Nevertheless, discussion of the various loss sources is still relevant in the following paragraphs, and the relevant shock models will be discussed in later sections.

2.3.4 Off-design total pressure loss

For predicting loss behaviour at off-design operation, several studies have adopted the idealised "loss bucket" approach, which determines the total pressure loss coefficient as a function of off-design incidence angle at a given Mach number. Smith [23], for example, employed the quadratic loss approximation function:

$$Y_{tot} = \left(Y_{\min} + Y_M\right)\left[1 + \left(\frac{i - i_{ref}}{W}\right)^2\right] \tag{2.3.20}$$

In the above equation, Y_{min} represents the profile losses, Y_M represents shock losses, i_{ref} is the reference minimum-loss incidence angle discussed in Section 2.3.1, and W defines the width of the loss bucket, which is illustrated in Figure 12 below[1]:

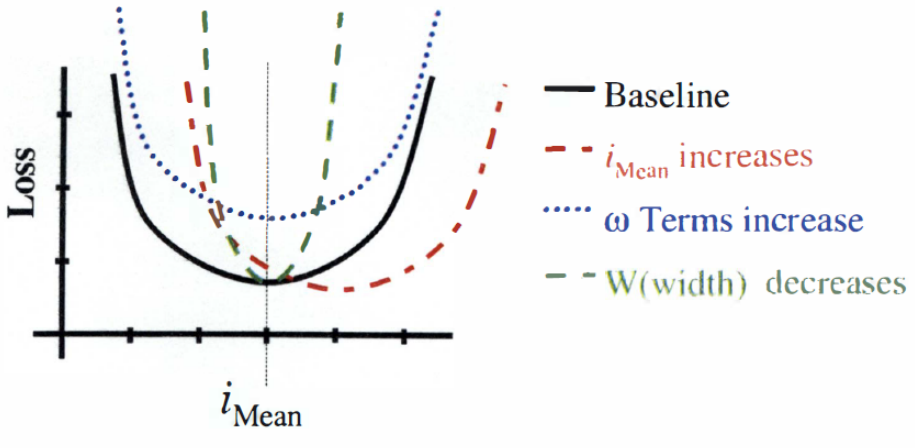

Figure 12: Idealised loss bucket – Taken from [23]

[1] Note that the ω term used by Smith [23] denotes $Y_{\min} + Y_M$ of Equation (2.3.20).

Figure 12 demonstrates the effect of varying the width parameter W, as well as the loss bucket's positioning relative to the point of minimum loss, similar to Figure 7(b).

In addition to profile and shock losses, Boyer [13] also included tip and hub (endwall) losses in the first set of parentheses in Equation (2.3.20).

A typical alternative method to the idealised loss bucket is to calculate the sum of the various loss contributions at off-design from appropriate correlations. The loss bucket method has several benefits over this alternative, as it introduces assumptions which consequently reduce the amount of computation and known inputs required. Nevertheless, even the loss bucket method requires calculation of some individual loss contributions. Furthermore, the method introduces a considerable number of calibration factors, including the width parameter W, and a number of others required for determining the individual loss sources. With each additional calibration factor, the difficulty in determining the appropriate value for each calibration factor increases. This may affect the overall robustness of the model and increase the complexity of validation.

Based on the above argument, several studies have disputed the method of calculating individual loss sources. Assessing the various correlations of loss, Çetin et al. [10] argued that the task of determining each source of loss independently is an extremely complex process, since the mechanisms of loss in modern compressors are cumulative and interrelated, rather than being independent as the method may suggest. On this basis, Çetin developed a new total pressure loss correlation by fitting curves to experimental data of DCA and MCA profiles. The study found a piecewise quadratic relationship between off-design total pressure loss coefficient, off-design incidence angle and inlet Mach number. The derived correlation took the form of Equation (2.3.21) and is graphically represented in Figure 13:

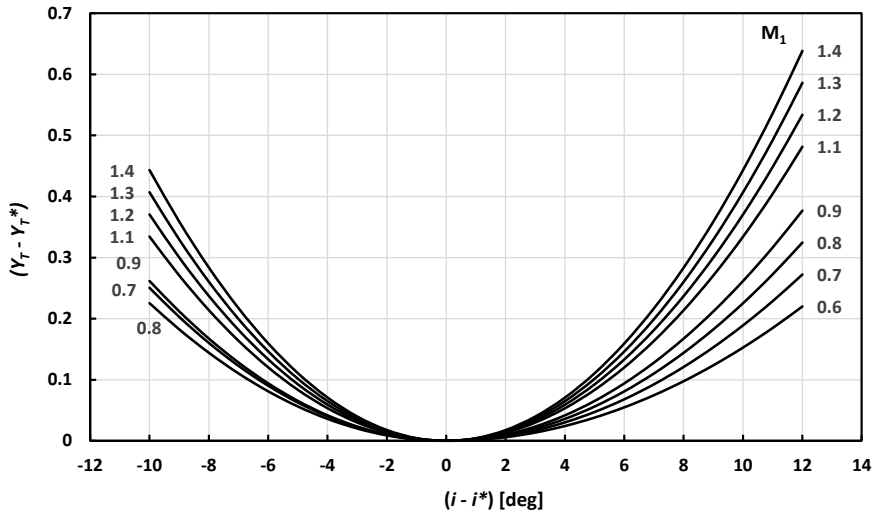

Figure 13: Çetin's off-design total pressure loss correlation [10]

$$Y_T - Y_T^* = c_m \left(i - i^*\right)^2 \tag{2.3.21}$$

In Equation (2.3.21), Y_T^* and i^* represent the design-point total pressure loss coefficient and incidence angle, respectively, and c_m is a function of inlet Mach number. The value of c_m is calculated from Table 2:

Table 2: Calculation of c_m for Çetin's total pressure loss correlation [10]

Blade type	$(\mathbf{i} - \mathbf{i}^*)$	$\mathbf{c_m}$
MCA	< 0	$0.02845M_1 - 0.01741$
	> 0	$0.00363M_1 - 0.00065$
DCA	< 0	$0.05336M_1 - 0.02937$
	> 0	$0.005M_1 - 0.00075$

It is evident that Cetin's method represents a loss bucket similar to that in Figure 12, however with its width already calibrated and without the need to determine individual loss sources. This therefore reduces the amount of calculation and number of calibration factors required, making it a favourable alternative to the other aforementioned methods, particularly for one-dimensional modelling where the total pressure loss coefficient is of greatest concern.

2.4 Shock treatment

As discussed in the previous section, the formation of shock structures in transonic blade rows causes entropy generation which is typically represented as a shock pressure loss included in the overall calculation of total pressure loss coefficient. Determining the specific passage shock structures and their resultant entropy generation has typically been informed from experimental data. Common shock models, such as those of Koch and Smith [8] and König et al. [22] include combinations of both oblique and normal shock structures at various positions along the blade's suction surface. Koch and Smith [8] assumed that an oblique shock structure is responsible for the reduction of inlet Mach number to sonic or subsonic conditions. König et al. [22] assumed that there is a normal shock structure at the passage exit, and either a normal or oblique shock structure at the passage inlet, depending on blade pre-compression characteristics [19]. The derivation of oblique shock treatment is relatively lengthy compared to normal shock and requires a comparatively large number of inputs and assumptions. For this reason, the derivation is omitted from this work. However, since normal shock structures are prevalent in many shock treatment models [19], the normal shock derivation is discussed below.

The one-dimensional normal shock model assumes that, in the presence of supersonic inlet flows, the resultant shock structure forms in a plane perpendicular to the direction of flow, illustrated in Figure 14.

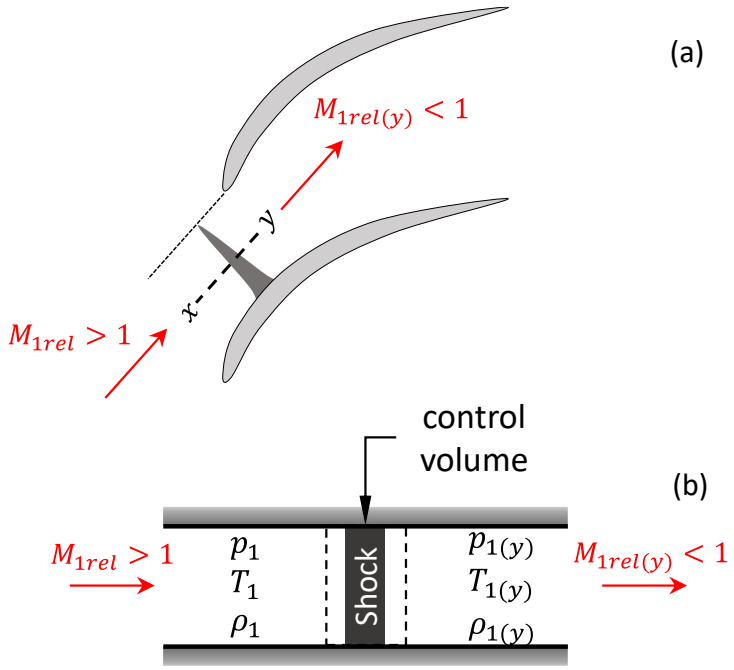

Figure 14: One-dimensional normal shock model through (a) a blade inlet passage, and (b) an arbitrary 1D pipe – Adapted from [40]

The normal shock model allows one to determine the flow characteristics at the shock exit (y) as functions of those at the shock inlet (x), by employing the compressible ideal gas equations. The model assumes that if the inlet flow is supersonic, dissipation and entropy generation over the shock will result in a subsonic flow at its exit, illustrated in Figure 14. One can calculate the shock-exit Mach number, static pressure, velocity and density, respectively using Equations (2.4.1)-(2.4.4) below:

$$M_{1y} = \sqrt{\frac{M_{1x}^2 + \frac{2}{\gamma - 1}}{\left(\frac{2\gamma}{\gamma - 1}\right) M_{1x}^2 - 1}} \tag{2.4.1}$$

$$p_{1y} = p_{1x}\left(1 + \frac{2\gamma}{\gamma + 1}\left(M_{1x}^2 - 1\right)\right) \tag{2.4.2}$$

$$c_{1y} = c_{1x}\left(\frac{(\gamma + 1) M_{1x}^2}{2 + (\gamma - 1) M_{1x}^2}\right)^{-1} \tag{2.4.3}$$

$$\rho_{1y} = \rho_{1x} \frac{c_{1x}}{c_{1y}} \tag{2.4.4}$$

The above equations demonstrate the normal shock model's simplicity. However, Kidikian [3] noted that the exit Mach number resulting from the normal shock treatment alone does not represent exit Mach numbers encountered in an axial compressor.

2.5 Rotating stall and surge prediction

One of the greatest areas of concern to the gas turbine operator is compressor stall and surge. At mass flow rates notably lower than the operating point on any rotor speed line, the effects of high incidence-induced boundary layer separation will result in a phenomenon known as rotating stall. Rotating stall is a highly complex, transient condition whereby, instead of all blades stalling together, isolated groups of blades stall, causing variations in flow obstruction and incidence in blades on either side of the stalled region. This is illustrated in Figure 15.

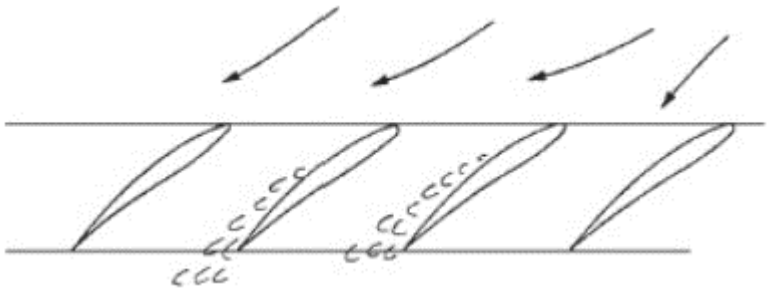

Figure 15: Graphical representation of rotating stall cell propagation – Taken from [2]

As Figure 15 demonstrates, the high incidence angle induced on the left of the stalled region will cause that region to enter a stalled condition, thus causing the stalled region to propagate to the left. There may exist more than one stalled cell around a blade row's annulus. Rotating stall is considered a highly undesirable condition of operation as cyclic loading and unloading of stalled blade cells may lead to dangerous levels of noise and vibration which can cause damage to the machine [2].

If mass flow rate is reduced further, the compressor will enter a condition known as compressor surge, which is characterised by oscillation of mass flow in the axial direction. This too results in unsafe vibration, and the cyclic occurrence of reverse flow within the compressor can cause incomplete combustion in the downstream combustion chamber.

Modelling of rotating stall and compressor surge is a complex exercise. It is therefore of greater concern to plant operators that the compressor does not approach unsafe operation at off-design.

Therefore, it is important that operators are able to predict the onset of stall. Understanding the envelope of safe compressor operation will help define the instability line, as illustrated in Figure 4.

Several studies in the literature have attempted to formulate empirical or semi-empirical correlations for predicting the onset of stall in mean-line analyses. Citing the similarities in function between compressors and diffusers, Koch [24] defined the maximum static-pressure-rise coefficient of an axial compressor stage using a method analogous to the stall-prediction method for two-dimensional diffusers presented by Reneau et al. [25]. Similar to Reneau's method, Koch defined the stalling pressure rise coefficient as a function of the ratio of mean-line diffusion length to blade-passage exit area. Koch found application of the criteria to be consistent with performance data of two-dimensional diffusers. Li et al. [26] improved on Koch's diffuser-analogy method by including of varying flow angles on the non-dimensional diffusion length.

One of the most notable and widely cited methods of stall prediction is that of Lieblein et al. [4], [5]. Lieblein formulated a means of determining whether a blade row has neared instability through calculation of a single parameter, now widely known as the diffusion factor. Derived from theory of diffusion and maximum blade suction-surface velocity, the diffusion factor represents the amount of diffusion through a blade row as a function of relative velocity ratio, flow turning, and solidity. The mean-line diffusion factor for rotor and stator rows is expressed in Equations (2.5.1) and (2.5.2) respectively. Lieblein noted that suction-surface boundary layer separation was typically observed at diffusion factors greater than 0.6 [5].

$$DF_R = 1 - \frac{w_2}{w_1} + \frac{|c_{1\theta} - c_{2\theta}|}{2w_1\sigma} \tag{2.5.1}$$

$$DF_S = 1 - \frac{c_2}{c_1} + \frac{|c_{1\theta} - c_{2\theta}|}{2c_1\sigma} \tag{2.5.2}$$

A simpler alternative method of predicting the onset of surge is by use of the relative velocity ratio criterion, also known as the De Haller number [2]. The De Haller criterion recommends that the velocity ratio c_2/c_1 should be no less than 0.72 for safe operation.

Veres [16] employed a combination of both diffusion factor and relative velocity ratio criteria to predict the onset of stall in their mean-line code validation. Veres's findings confirmed that the stall point occurred at a rotor diffusion factor of approximately 0.6. However, Veres found that the stall point corresponded to a rotor relative velocity ratio of around 1.90, which was notably higher than De Haller's recommended cut-off value. Kidikian [3] argued that the De Haller number of 0.72 was based on blade profiles other than the more modern MCA types, and therefore could not be employed in modern applications.

Noting several shortfalls and inadequacies in the commonly employed methods, Kidikian [3] developed a new engineering-based surge criterion which predicted stall to occur at the point where the rotor mid-span exit absolute axial velocity c_{3x} is less than or equal to the rotor mid-span exit absolute tangential velocity, $c_{3\theta}$. Kidikian found good agreement of the method with experimental data. However, Kidikian's method relied on use the performance modelling methods developed in their own work, possibly limiting the method's universal applicability in applications where different methods are used.

2.6 Choked flow prediction

Choked flow refers to the condition when mass flow becomes restricted at some maximum, critical value due to compressible flow effects. Conventionally, it is assumed that choke occurs at the point of minimum cross-sectional area, also known as the throat area (A_t), illustrated in Figure 16. The restriction of mass flow significantly affects compressor performance and efficiency and is an important factor to consider for compressor designers and plant operators. The choke limit is therefore a critical element of a compressor performance map, as it determines the upper limit of mass flow for safe operation at a particular rotor speed, as illustrated in Figure 4.

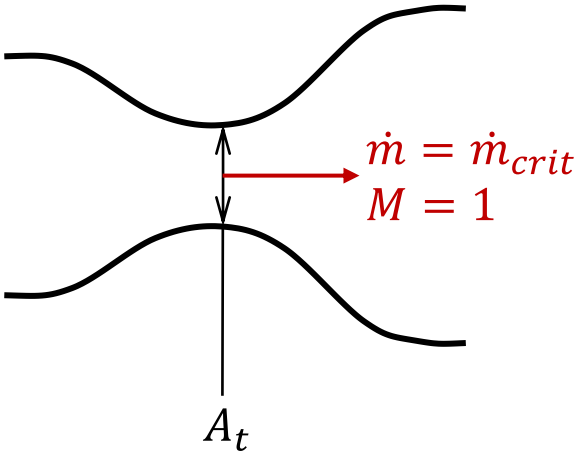

Figure 16: Simple representation of one-dimensional choked flow

Traditionally, choke is defined as occurring when the Mach number through the throat area reaches unity ($M = 1$), after which the mass flow cannot be increased without changing flow geometry or inlet conditions. To determine the mass flow at which choke occurs, the traditional definition of the nondimensional mass flow rate, or capacity, is employed, derived from the compressible ideal gas relationships [2]:

$$\frac{\dot{m}\sqrt{c_p T_0}}{A p_0} = \frac{\gamma}{\sqrt{\gamma - 1}} M \left(1 + \frac{\gamma - 1}{2} M^2\right)^{-\frac{1}{2}\left(\frac{\gamma+1}{\gamma-1}\right)} \tag{2.6.1}$$

Using the conventional definition of choke, the critical mass flow rate at which choke will occur can be determined by substituting $M = 1$ and setting A to the minimum cross-sectional area, A_t:

$$\dot{m}_{crit} = \frac{A_t p_0}{\sqrt{c_p T_0}} \cdot \frac{\gamma}{\sqrt{\gamma - 1}} \left(\frac{\gamma + 1}{2} \right)^{-\frac{1}{2}\left(\frac{\gamma+1}{\gamma-1}\right)} \tag{2.6.2}$$

Several other definitions of choke have however been described in the literature. Barbosa [27] defined choke as occurring when the speed-lines of a compressor performance map become vertical, or when pressure ratio decreases without any change in mass flow rate. However, Kidikian [3] found that this definition did not hold true for a range of test cases. Veres [16] determined the choke condition at the point where their COMDES code could not converge on rotor exit velocity triangles. Kidikian [3] however noted that choke could occur in either the rotor or stator rows of a compressor stage. Cadrecha et al. [28] argued that the conventional definition of choke is only applicable for isentropic flows, and that the actual critical Mach number may be less than unity when losses are taken into account. Arguing that there is a general ambiguity surrounding the conventional definition of choke, Kidikian [3] developed a new set of pressure-based criteria for determining choke without the need for any semi-empirical formulae or correlations. Kidikian's method was defined by comparing the static pressure at the stator exit to those at the rotor and stator inlets and correlated the maximum attainable mass flow to the maximum achievable diffusion by the stator. In most test cases, Kidikian found good agreement between their method and experimental data.

Despite the developments described above, it must be noted that in certain cases, the conventional definition of choke occurring at a throat Mach number of unity is unavoidable and is often the best estimate of the choked condition, even in modern applications. This is especially true when subsonic solvers are employed, of which the defined choke point is that occurring at the critical Mach number of 1. In such cases, the predefined choke limit must be accepted, and resultant shortfalls must be accounted for in other ways.

2.7 Model tuning and calibration factors

To obtain better agreement between predicted compressor performance and experimental data, several authors have employed calibration and tuning factors in their modelling methodologies. These may be applied to any one element, or a combination of the performance modelling techniques described in previous sections. As previously mentioned, Petrovic et al. [11] included calibration factors for calculating reference incidence and deviation angles. Through experimentation, Veres [16] determined a single value of slip for determining rotor deviation angle that resulted in reasonable agreement with test data. Other tuning factors may include, for example, the coefficient k for determining deviation angle due to axial velocity ratio in Equation (2.3.18), the width parameter W in Equation (2.3.20), or those included in calculating the individual loss contributions in Equation (2.3.20). Various other studies not discussed here have included correction factors for effects such as Reynolds number. Several authors have also included blockage factors which describe the degree of flow area contraction of blade passages due to boundary layer formation. Veres [16] assumed constant values of rotor aerodynamic blockage for different validation cases. Kidikian [3] modified the mean-line method to include blockage factors at both rotor and stator inlet and outlets. It is notable that the definition of aerodynamic blockage varies between studies, and therefore their use within mean-line calculation is not consistent. Application of blockage factors is also not a universal practise, with many authors omitting this method altogether and rather accounting for other physical phenomena or tuning other factors in their calculations. Trends in the literature show that an author may choose to account for as much of the physical phenomena in their simulation as possible, or instead incorporate a number of tuning factors which compensate for the physics that have not been modelled.

Having reviewed over sixty years' worth of loss modelling methods in the literature, Kidikian [3] argued that there has not been a definitive continuity of loss and deviation models over the course of their development, with each author selecting their own set of loss and deviation criteria, and then applying their own unique correction factors for model validation. On this basis, Kidikian developed a mean-line methodology which omitted correlations of loss and deviation altogether, and rather employed a tuning scheme which treated loss, deviation and blockage factors as tuning factors, each being non-constant at off-design. The author achieved a near-exact match between predicted values and test data by tuning both rotor and stator loss and deviation angle, as well as the rotor and stator blockage factors at their respective inlets and exits. Kidikian's process involved tuning these factors manually until both the velocity triangles and predicted compressor performance agreed with the experimental data.

Although Kidikian's method achieved very good agreement with experimental data, it posed several obstacles. Firstly, the notable number of tuning factors included in the method would have compounded the time and complexity to complete the tuning operation over the range of conditions considered. Over and above this, Kidikian found several co-dependencies between tuning factors. For example, adjusting rotor and stator blockage factors would require a subsequent retuning of their respective losses. Furthermore, the tuning process relied on knowledge of the flow vectors reported in the experimental data. Kidikian did develop correlations for the above correction factors from the calibrated tuning factors, and these performed well in another validation exercise, however the deduced correlations added several levels of complexity to the overall calculation.

2.8 Observed trends

Having reviewed the literature, two common, arguably conflicting, approaches to compressor performance modelling are identified. The first is to model performance using semi-empirical physics-based correlations. This includes determining off-design total pressure loss and deviation as the sum of their individual sources. The second approach is motivated by simpler calculation methodologies and includes employing the idealised loss bucket and assumption of constant deviation angle. It tends to be more common for authors performing two-dimensional throughflow simulations to use the sum-of-contributions method for off-design loss and deviation, since this allows for the calculation of span-wise variations in these parameters and is thus useful in the compressor design context. For mean-line analysis however, employing the loss bucket and constant deviation method has tended to make more sense, as 1) the average total pressure loss coefficients are of greatest importance for determining the overall stage performance characteristics, and 2) it has allowed for an overall simpler calculation. In addition, the simpler method generally requires fewer geometric inputs.

One may argue that the first approach is more correct, as it accounts for as much of the actual physics observable in the compressor, and that the latter is not truly based on the underlying physics. However, one may also argue that it is not uncommon to make modelling assumptions which allow for less intensive calculations. This is especially true in the case of large, high-level analyses.

The above arguments may be extended to model tuning and calibration. As has been discussed, it is common practise for authors to apply calibration factors on top of their base methodology to achieve better agreement between predicted and experimental results. One extreme case of this is Kidikian's method [3], which treated losses, deviation angles and area blockage factors all as tuning factors. One may argue that the method is questionable, as it seems to remove most of the underlying physics from the calculation. However, as the model was built for incorporating it into a

larger gas turbine analysis software, its method is arguably no less valid than the first approach, in context of what is ultimately to be achieved.

What has generally not been addressed however, is the large number of tuning factors typically required for proper model calibration. As was observed in Kidikian's method, the application of a large number of tuning factors can result in interdependencies between them, and thus compound the complexity of the calibration process. It is therefore needed to address this issue by determining a method that requires as few tuning factors as possible, and thus achieve a robust model that is simple in calculation.

3. Methodology

This chapter describes the one-dimensional, diffuser-analogy-based modelling methodology developed in this study. Firstly, the various sources of geometric and operational inputs are outlined. Following this, the diffuser analogy model is discussed in detail. A design-point calibration process is then outlined, which will demonstrate the application of the mean-line method in this study. The off-design analysis model developed in Flownex will then be described in detail. Lastly, the chosen models of total pressure loss and deviation angle employed in this study are discussed and motivated.

3.1 Minimum-input sources

Before proceeding, it is important to identify the necessary information required to perform the analysis. Doing so will inform proper development of the modelling methodology. To achieve the study's aims, a minimal set of input sources must be selected. Based on preliminary studies and observations from the open literature, four input sources were identified that were considered as obtainable. These are described below.

Measurable and observable geometry

This set of inputs arises from what is assumed to be observable by plant operators, or measurable using common measurement tools. These inputs include blade thickness-distribution, blade chord-length, and the number of blades in the rotor and stator rows.

Basic 2D layout drawings

It is assumed that plant operators have access to basic dimensioned 2D layout drawings of the compressor assembly, such as that illustrated in Figure 17. Such drawings allow the analyst to determine the rotor tip, hub and mean-line radii.

Known design-point operational parameters

Certain compressor operating parameters are assumed to be known by plant operators. These include rotor RPM, and stage total temperature ratio or total pressure ratio. In the case of multi-stage compressors where only the overall compressor performance is known, one may employ assumptions, such as the normal repeating stage assumption and equal reaction ratio per stage, to deduce these parameters for a single stage.

Industry knowledge

In absence of any of the abovementioned inputs, one can make assumptions from accumulated industry knowledge. For instance, if the design-point stage total temperature is not known, then one can assume a common value of stage loading (as discussed in Section 2.1.2), and then calculate the total temperature ratio using Equation (2.1.7). Another assumption required is that of the inlet guide vane angle, or stator exit angle. In the absence of an inlet guide vane, the pre-swirl angle (α_1) can be assumed to be zero. Furthermore, industry knowledge can inform assumptions of design-point pre-swirl. Multi-stage compressor test data from Steinke [29] illustrated one case in which the pre-swirl angle is equal to zero at design-point. The test data also indicated that the normal repeating stage assumption had been made, in which the pre-swirl angle was the same at the inlet of each rotor.

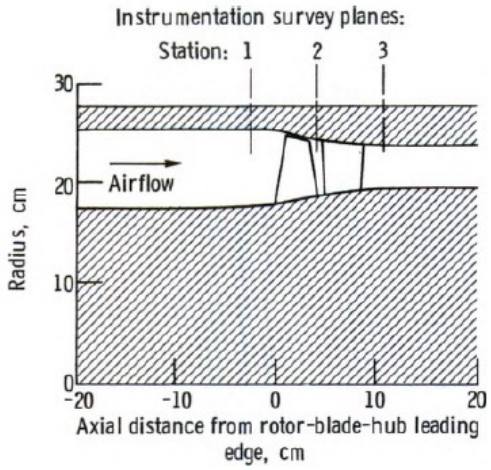

Flow path coordinates

Inner		Outer	
Axial distance, cm	Radius, cm	Axial distance, cm	Radius, cm
-22.860	17.526	-22.860	25.654
-15.400	17.526	-15.400	25.654
-7.620	17.526	-7.620	25.654
-2.568	17.539	-2.568	25.643
0	17.780	0	25.400
1.854	18.255	.632	25.247
4.137	18.714	1.854	24.925
4.859	18.821	1.974	24.882
6.566	19.035	3.282	24.511
8.890	19.279	4.445	24.285
10.640	19.380	4.859	24.232
12.700	19.431	6.538	24.145
15.400	19.431	8.628	24.011
		8.890	23.993
		10.640	23.851
		12.700	23.749
		15.400	23.749

Figure 17: NASA Stage 35 basic 2D layout drawing with flow path coordinates – Taken from [33]

3.2 Diffuser analogy

The theory and development of the diffuser analogy is largely based on those of the Nozzle Flow Analogy by Fuls [1]. Fuls's model was developed to simulate gas and steam turbines under off-design and abnormal operating conditions. Similarly, Fuls aimed to develop an axial turbine simulation tool which required limited geometric and operational inputs, which are typically withheld by OEMs. The mean-line-based method achieved this by analogising the stator and rotor rows of a turbine stage to two one-dimensional nozzles in series, with a simple "bucket" component to represent the work extracted in the rotor. The model only required calibration of the nozzle areas, and thus did not require detailed information of flow path geometry.

In a similar manner to the Nozzle Flow Analogy, the diffuser analogy method models the rotor and stator rows in an axial compressor stage as two one-dimensional diffusers in series. The moving rotor diffuser experiences the relative inlet and exit conditions, while the stationary stator diffuser sees the absolute conditions. Since a diffuser cannot perform work on the working fluid, a simple one-dimensional work-input component is included. The diffuser analogy method is illustrated in Figure 18(b), with accompanying velocity triangles and Mollier diagram in Figure 19, respectively. The mean-line calculation procedure involving the velocity triangles and thermodynamic processes is demonstrated in the following section.

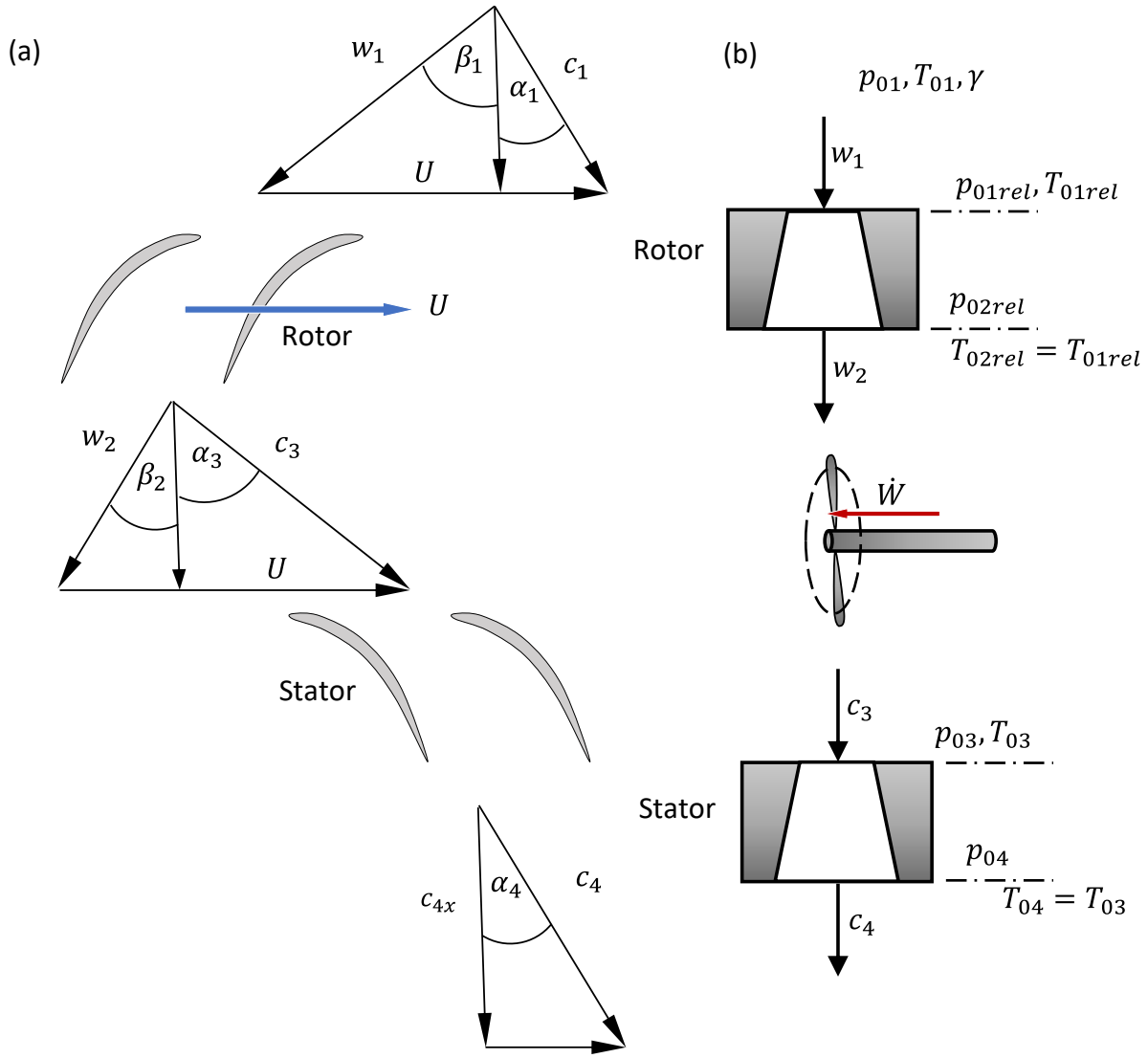

Figure 18: (a) Mean-line method velocity triangles, and (b) Graphical representation of the diffusor analogy

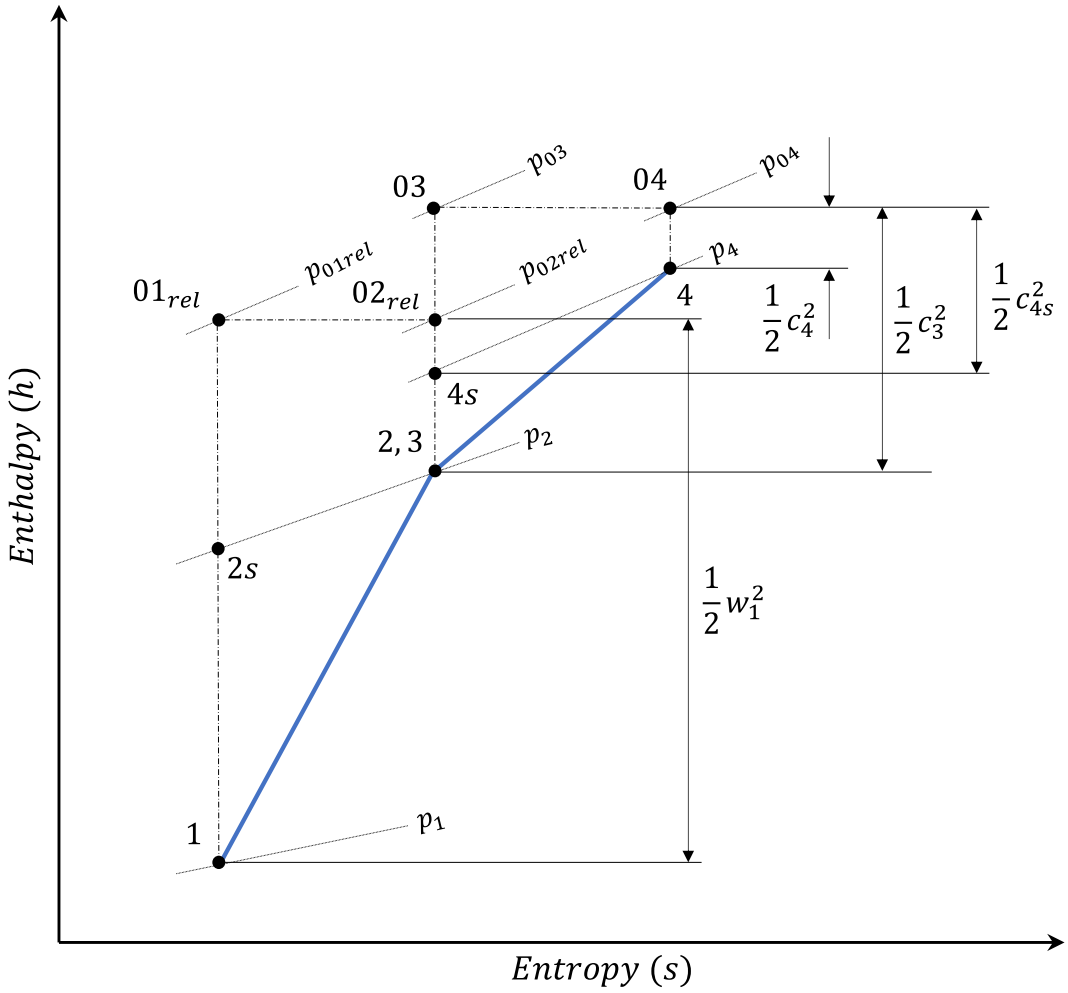

Figure 19: Mollier diagram of diffuser analogy

The study adopted various assumptions that are conventional to other mean-line codes as well. Firstly, it was assumed that the meridional angle over a single stage was negligible, and therefore a constant mean-line radius through the stage was assumed. Secondly, it was assumed that heat transfer between the blades and casing and the working fluid was negligible in both rotor and stator rows. Based on these two assumptions and the conservation of rothalpy, it could be assumed that the relative total enthalpy (and therefore total temperature) through the rotor diffuser, and the absolute total enthalpy through the stator diffuser both remained constant. This is illustrated in Figure 18(b) and Figure 19. Therefore, conservation of energy in the calculation was handled through Equations (2.2.1) and (2.2.2) for the absolute and relative frames, respectively.

3.3 Design-point calibration

In order to perform off-design compressor analysis, one requires knowledge of the various flow path areas to calculate the velocity triangles and thermodynamic properties at the blade-row inlets and exits. Furthermore, knowledge of the incidence and deviation angles is needed to determine off-design losses and blade-exit velocity triangles. However, as indicated in Equations (2.1.1) and (2.1.2), the inlet and exit blade angles are required to determine incidence and deviation.

Knowledge of three specific flow-passage areas is required to perform the mean-line analysis. These are: the effective inlet area $A_{in_{eff}}$, effective exit area $A_{ex_{eff}}$, and passage throat area A_{throat}. The definitions of these areas are indicated in Figure 20 below. The figure illustrates the areas belonging to a single blade passage, and therefore the total of each flow area through a blade row is equal to the sum of their respective areas through a single passage.

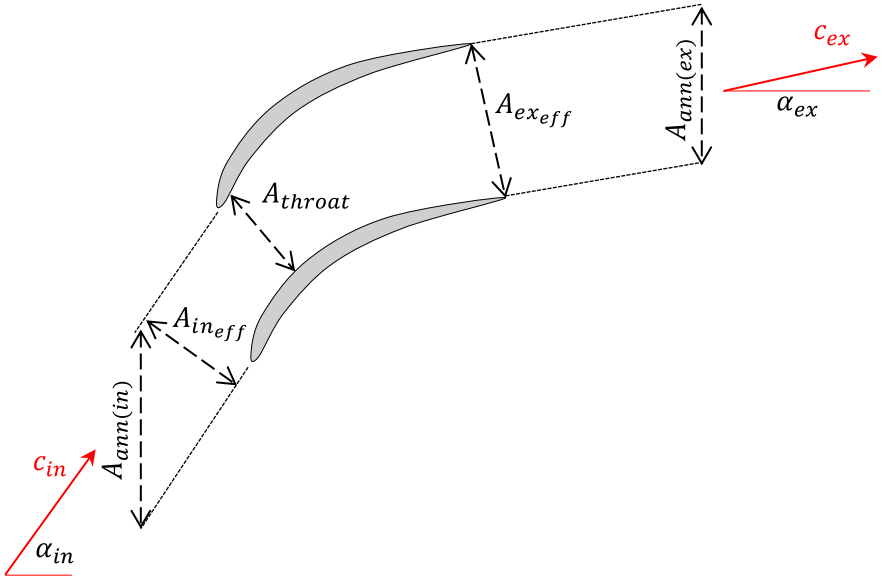

Figure 20: Definitions of flow-passage areas through a blade row

It is assumed that the passage throat area is a characteristic of physical blade geometry, and therefore does not vary at off-design. This is also true for the inlet and exit annulus areas, $A_{ann(in)}$ and $A_{ann(ex)}$. However, the effective inlet and exit areas will vary significantly at off-design due to changes in incidence and deviation. As illustrated in Figure 20, the effective inlet and exit areas are functions of their respective annulus areas and flow angles, and are determined using Equations (3.3.1) and (3.3.2):

$$A_{in_{eff}} = A_{ann(in)} \times \cos(\alpha_{in}) \tag{3.3.1}$$

$$A_{ex_{eff}} = A_{ann(ex)} \times \cos(\alpha_{ex}) \tag{3.3.2}$$

It is therefore evident that one can calculate the necessary flow-passage areas if the physical annulus areas are known.

Analysis is greatly limited in cases where knowledge of the above geometries is withheld by OEMs, and therefore a method is required to estimate the various flow-passage areas and blade angles through the compressor stage. This section outlines the process in which knowledge and assumptions of design-point operation are used to estimate the flow-path areas and blade angles in a geometry calibration exercise. The calibrated geometries can then be used as inputs in off-design analysis, which will be discussed in later sections. The complete analytical calculation is found in Appendix A.

3.3.1 Inputs and assumptions

The various design-point inputs needed for flow calibration are summarised in Table 3 to Table 6 below.

Table 3: Design-point calibration operational inputs

Input	Description
$\dot{m}_D$	Design-point mass flow rate
ω_D	Design-point rotor RPM

Table 4: Design-point calibration fluid property inputs

Input	Description
T_{01}	Stage-inlet total temperature
p_{01}	Stage-inlet total pressure
c_p	Specific heat at constant pressure
R	Gas constant
γ	Ratio of specific heats

Table 5: Design-point calibration basic blade dimension inputs

Input	Description
N_R, N_S	Number of rotor and stator blades
l_R, l_S	Rotor, stator mean-line chord lengths
r_h	Rotor hub radius
r_t	Rotor tip radius
$t_{\max(R)}$, $t_{\max(S)}$	Rotor, stator maximum blade thicknesses
Rotor and stator blade types	MCA, DCA, NACA etc.
a_R, a_S	Distance of max. camber from leading edge for rotor and stator

Table 6: Design-point calibration performance inputs

Input	Description
T_D	Design-point stage total temperature ratio
α_1	Stage absolute inlet flow angle
Π_D	Total pressure ratio

The operational inputs in Table 3 were assumed to be known by plant operators and are otherwise measurable. The inlet total temperature and pressure in Table 4 are also assumed to be easily measurable, and fluid properties can be determined from available data. It was assumed that the number of rotor and stator blades, blade chord lengths and thickness distributions are easily measurable by plant operators.

For blade type, one can make an assumption from industry knowledge of modern compressors. As discussed in Section 3.1, the analyst can make an assumption of the stage absolute inlet flow angle, or stage pre-swirl.

Before commencing the mean-line analysis, the stage inlet annulus area and rotor and stator solidities needed to be calculated. First, the mean-line radius was estimated as the average of the rotor hub and tip radii:

$$r_m = \frac{r_h + r_t}{2} \tag{3.3.3}$$

The stage inlet annulus area was then estimated as:

$$A_{inlet} = \pi\left(r_t^2 - r_h^2\right) \tag{3.3.4}$$

Using the mean-line radius, number of rotor and stator blades and their respective mean-line chord lengths, the rotor and stator mean-line solidities were determined using Equation (2.1.5).

3.3.2 Rotor-inlet calculation

The mean-line calculation begins with determining the static conditions and velocity triangle at the rotor inlet. Since only information of the inlet total properties are known, three unknowns needed to be determined simultaneously: the rotor-inlet axial velocity c_{1x}, static pressure p_1, and static temperature T_1. A simple root-solving scheme is employed to solve the following three equations simultaneously:

$$c_{1x} = \dot{m}\frac{RT_1}{p_1}\cdot\frac{1}{A_{inlet}} \tag{3.3.5}$$

$$p_1 = p_{01}\cdot\left(\frac{T_{01}}{T_1}\right)^{-\frac{\gamma}{\gamma-1}} \tag{3.3.6}$$

$$T_1 = T_{01} - \frac{c_{1x}^2}{2c_p} \tag{3.3.7}$$

The rotor mean-line blade speed is calculated as:

$$u = \omega_D r_m \tag{3.3.8}$$

Knowing p_1 and T_1, the rotor-inlet density could be calculated. The velocity triangles at the rotor inlet and all other stations were defined using standard vector algebra to maintain the defined angle sign convention. Therefore, some velocity vector $\bar{V}$ could be determined knowing its magnitude v and angle α:

$$\bar{V} = \begin{pmatrix} v\cdot\cos(\alpha) \\ v\cdot\sin(\alpha) \end{pmatrix} \tag{3.3.9}$$

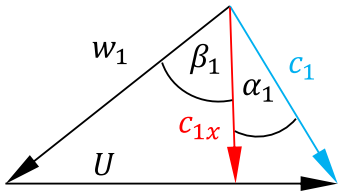

Figure 21: Rotor-inlet velocity triangle

Having calculated c_{1x} and assuming a value for α_1, the magnitude of the rotor-inlet absolute velocity is determined using Equation (3.3.10).

$$c_1 = \frac{c_{1x}}{\cos(\alpha_1)} \tag{3.3.10}$$

Following calculation of magnitude c_1, the rotor-inlet absolute velocity vector $\bar{C}_1$ is calculated using Equation (3.3.9). The rotor blade speed vector $\bar{U}$ is calculated in the same manner, assuming a vector angle of 90°. The rotor-inlet relative velocity vector $\bar{W}_1$ is then determined vectorially using Equation (3.3.11), and thus completely defining the rotor-inlet velocity triangle. The rotor relative inlet flow angle and Mach number can then be determined using Equations (3.3.12) and (3.3.13), respectively.

$$\bar{W}_1 = \bar{C}_1 - \bar{U} \tag{3.3.11}$$

$$\beta_1 = \arctan\left(\frac{\bar{W}_{1\theta}}{\bar{W}_{1x}}\right) \tag{3.3.12}$$

$$M_{1rel} = \frac{\left|\bar{W}_1\right|}{\sqrt{\gamma R T_1}} \tag{3.3.13}$$

Finally, the rotor-inlet relative total temperature and density is calculated using Equations (3.3.14) and (3.3.15), respectively:

$$T_{01rel} = T_1 + \frac{\left|\bar{W}_1\right|^2}{2c_p} \tag{3.3.14}$$

$$\rho_1 = \frac{p_1}{RT_1} \tag{3.3.15}$$

3.3.3 Design-point shock treatment

As discussed in the literature review, shock in blade rows due to supersonic flow can be treated as a source of pressure loss which contributes to the row's total pressure loss coefficient. However, as will be justified in later sections, this study chose to treat shock phenomena using the derivations of shock wave thermodynamics instead of explicitly determining a unique shock pressure loss coefficient. For the purpose of computational simplicity, and thus in line with the study's aims, shock is treated as a single normal shock structure occurring at the blade inlet passage, as illustrated in Figure 14. Furthermore, it was assumed that a shock structure could only occur at the inlet of the rotor row, since 1) the highest velocity would always be observed at the rotor inlet, 2) the Mach number at the exit of a shock structure is subsonic, and 3) both rotor and stator rows diffuse the flow in their respective frames of reference, and thus increases in Mach number beyond unity cannot occur at any point after the shock structure.

The equations for normal shock treatment, discussed in Section 2.4, are reproduced here for the rotor relative frame of reference:

$$M_{1rel(y)} = \sqrt{\frac{{M_{1rel}}^2 + \frac{2}{\gamma - 1}}{\left(\frac{2\gamma}{\gamma - 1}\right){M_{1rel}}^2 - 1}} \tag{3.3.16}$$

$$w_{1(y)} = \left|\bar{W}_1\right|\left[\frac{(\gamma + 1){M_{1rel}}^2}{2 + (\gamma - 1){M_{1rel}}^2}\right]^{-1} \tag{3.3.17}$$

$$p_{1(y)} = p_1\left[1 + \frac{2\gamma}{\gamma + 1}\left({M_{1rel}}^2 - 1\right)\right] \tag{3.3.18}$$

$$T_{1(y)} = T_{01rel} - \frac{w_{1(y)}^2}{2c_p} \tag{3.3.19}$$

$$\rho_{1(y)} = \frac{\rho_1\left|\bar{W}_1\right|}{w_{1(y)}} \tag{3.3.20}$$

The ultimate purpose of the shock treatment is to determine the actual relative total pressure after the rotor-inlet shock. Since it is assumed that the normal shock only occurs when inlet Mach numbers are above unity, a condition must therefore be defined to determine the relative total pressure based on the rotor inlet relative Mach number. The condition included in the method is shown in Equation (3.3.21):

$$p_{01rel} = \begin{cases} p_{1(y)} \left(\frac{T_{01rel}}{T_{1(y)}} \right)^{\frac{\gamma}{\gamma-1}}, & M_{1rel} \geq 1 \\ p_1 \left(\frac{T_{01rel}}{T_1} \right)^{\frac{\gamma}{\gamma-1}}, & M_{1rel} < 1 \end{cases} \tag{3.3.21}$$

3.3.4 Rotor energy addition

Establishing a known work input in the design-point method helped to eliminate unknowns that, without knowledge of flow path geometry, would otherwise greatly limit the calculation. It also enabled calculations at the trailing edges of both rotor and stator rows.

The rotor energy addition in the diffuser analogy is represented by a one-dimensional work-input component, observed in Figure 18(b). Following the Mollier diagram in Figure 19, the specific work performed by the rotor is calculated as:

$$\Delta W = h_{03} - h_{01} = c_p \left(T_{03} - T_{01} \right) \tag{3.3.22}$$

In order to determine the rotor-exit total temperature T_{03}, a known design-point stage total temperature ratio T_D is required as an input. T_{03} can then be calculated as:

$$T_{03} = \mathrm{T}_D \times T_{01} \tag{3.3.23}$$

In the case where the stage total temperature ratio is not known, one may estimate T_{03} by assuming a value for stage loading coefficient, as discussed in Section 2.1.2. Rearranging Equation (2.1.7), T_{03} can calculated as:

$$T_{03} = T_{01} + \psi_D \left(\frac{u^2}{c_p} \right) \tag{3.3.24}$$

Finally, the rotor and stator exit total temperatures are defined as equal to their respective inlets, based on the definition of rothalpy discussed in Section 2.2:

$$T_{02rel} = T_{01rel} \tag{3.3.25}$$

$$T_{04} = T_{03} \tag{3.3.26}$$

3.3.5 Stage intermediate-pressure convergence

A challenge many mean-line codes encounter is what has been referred to as "crossing the unbladed region [23]." The unbladed region refers to the space in between the rotor and stator rows. Determining the velocity triangle and thermodynamic properties in this region is made difficult by the fact that it is not possible to obtain experimental measurements in this region due small inter-blade-row clearances. In order to address this, several authors have had to make assumptions of the conditions in this region. For example, Smith [23] made assumptions of rotor axial-velocity density ratio (AVDR) to determine the fluid density in the unbladed region, which could then be used to calculate other properties. However, Smith's method required information of stage flow-passage areas, which the current exercise assumes are unknown at this stage. Therefore, an alternative method was needed to determine the stage intermediate-properties. Based on the above, an iterative Newton–Raphson-based root-finding method was used to converge on the static pressure in the unbladed region, p_2, by calculating both the rotor-exit velocity triangle and thermodynamic properties as functions of rotor-exit static pressure, p_2.

Before beginning the iterative solver, the rotor-exit relative flow angle, β_2, is estimated using Equation (2.1.9). It is also required at this point to determine the rotor-exit relative total pressure. This is achieved by assuming a rotor total pressure loss coefficient Y_R and then rearranging Equation (2.3.19) for p_{02rel}, as shown in Equation (3.3.27).

$$p_{02rel} = p_{01rel} - Y_R\left(p_{01rel} - p_1\right) \tag{3.3.27}$$

The pressure loss coefficient assumption can be based on typical loss coefficients seen in literature or calculated using one of the various design base loss models. In either case, after the total pressure at the stator exit has been calculated at the end of the process, the total pressure ratio can be checked with the design condition Π_D . Further small adjustments to the loss coefficient are then made until the calculated total pressure ratio agrees with the design input.

The calculation steps of the iterative program are outlined below, and the program is visualised in the flow diagram in Figure 23.

Firstly, having determined p_{02rel}, the stage intermediate static temperature can be calculated as:

$$T_2 = T_{02rel}\left(\frac{p_{02rel}}{p_2}\right)^{-\frac{\gamma-1}{\gamma}} \tag{3.3.28}$$

The rotor-exit relative velocity is then determined from the definition of total enthalpy:

$$w_2 = \sqrt{2c_p\left(T_{02rel} - T_2\right)} \tag{3.3.29}$$

The rotor-exit absolute velocity is calculated in a similar manner, knowing that T_3 is equal to T_2:

$$c_3 = \sqrt{2c_p\left(T_{03} - T_3\right)} \tag{3.3.30}$$

The rotor-exit absolute velocity using from the velocity triangle and a simple rearrangement of the cosine rule is given as:

$$c_3 = \sqrt{w_2^2 + u^2 + 2w_2 u \sin\left(\beta_2\right)} \tag{3.3.31}$$

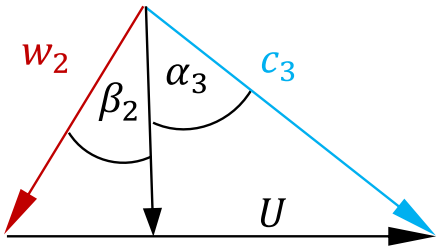

Figure 22: Rotor-exit velocity triangle

It is clear that solving Equations (3.3.28) to (3.3.31) requires a known p_2, and therefore the objective of the root-solving program is to determine the value of p_2 at which Equations (3.3.30) and (3.3.31) are equal (within a predefined tolerance).

Having determined the intermediate static pressure, only the rotor-exit/stator-inlet velocity triangle needs to be completed. This is done in a similar manner to the rotor-inlet velocity triangle. Knowing w_2, the rotor-exit relative velocity vector $\bar{W}_2$ is calculated using Equation (3.3.9). The rotor-exit/stator-inlet absolute velocity vector $\bar{C}_3$ and its related angle are then determined vectorially using Equations (3.3.32) and (3.3.33), respectively.

$$\bar{C}_3 = \bar{W}_2 + \bar{U} \tag{3.3.32}$$

$$\alpha_3 = \arctan\left(\frac{\bar{C}_{3\theta}}{\bar{C}_{3x}}\right) \tag{3.3.33}$$

Finally, the rotor-exit relative Mach number, stator-inlet Mach number and density are calculated from the ideal gas equations. This completes the unbladed region calculation.

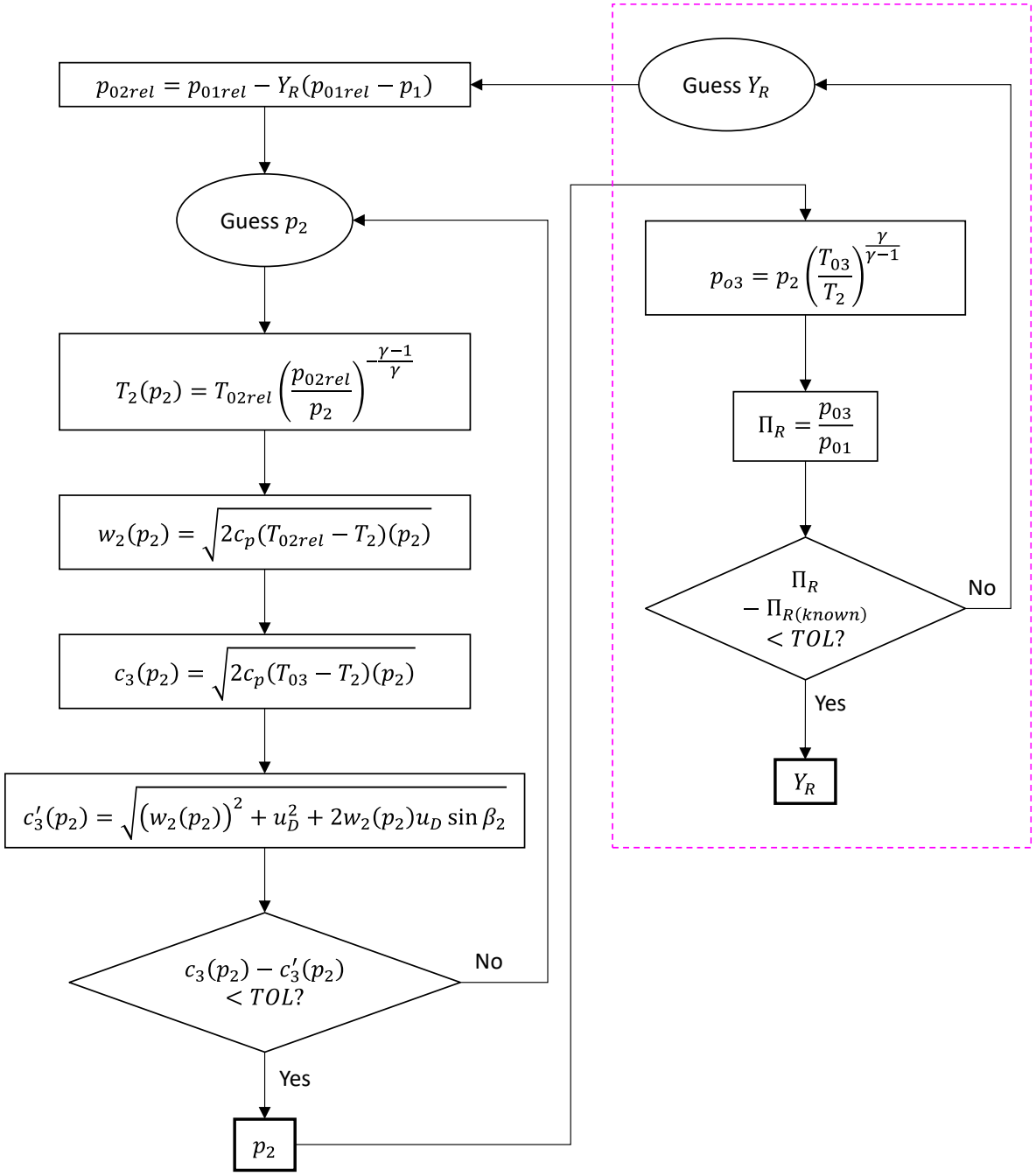

Figure 23: Flow diagram of stage intermediate pressure convergence program

3.3.6 Stator-exit calculation

Knowing the stator-exit total temperature T_{04}, determining the velocity triangle and thermodynamic properties at the stator exit is a simple task. This is achieved using the normal repeating stage assumption, which states that the axial velocity through the stage remains constant, and the stator-exit absolute flow angle is equal to the rotor-inlet absolute flow angle:

$$c_{4x} = c_{1x} \tag{3.3.34}$$

$$\alpha_4 = \alpha_1 \tag{3.3.35}$$

Using this assumption, the stator-exit velocity vector $\bar{C}_4$ is determined using Equation (3.3.9), with c_4 calculated from Equation (3.3.36).

$$c_4 = \frac{c_{4x}}{\cos(\alpha_4)} \tag{3.3.36}$$

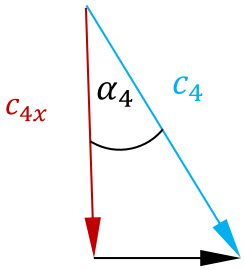

Figure 24: Stator-exit velocity triangle

The stator-exit total pressure is calculated using the stator total pressure loss coefficient Y_S. As is necessary for the rotor, the loss coefficient is either assumed based on typical stator loss parameters, or calculated using correlations, and then adjusted to achieve the design-point stage pressure ratio.

$$p_{04} = p_{03} - Y_S\left(p_{03} - p_3\right) \tag{3.3.37}$$

Finally, the stator-exit static temperature and static pressure, Mach number and density are determined using Equations (3.3.38) and (3.3.39), respectively. The stator-exit Mach number and density are calculated from the ideal gas equations. This completes the design-point mean-line calculation.

$$T_4 = T_{04} - \frac{c_4^2}{2c_p} \tag{3.3.38}$$

$$p_4 = p_{04}\left(\frac{T_{04}}{T_4}\right)^{-\frac{\gamma}{\gamma-1}} \tag{3.3.39}$$

3.3.7 Flow-area calculation

Having determined the components and angles in all velocity triangles, as well as the static fluid properties, it is now possible to calculate the stage flow-passage areas. This is achieved by using mass-flow conservation to first determine the various diffuser inlet and exit areas, as well as the stage inlet area. The annulus and throat areas are then calculated from the diffuser areas and their respective flow angles. The method is summarised for all stations below:

Stage inlet

$$A_{inlet} = \frac{\dot{m}_D}{c_1\rho_1} \tag{3.3.40}$$

Rotor inlet

$$A_{R(in)} = \frac{\dot{m}_D}{w_1\rho_1} \tag{3.3.41}$$

$$A_{ann(R)_{in}} = \frac{A_{R(in)}}{\cos(\beta_1)} \tag{3.3.42}$$

Rotor exit

$$A_{R(ex)} = \frac{\dot{m}_D}{w_2\rho_2} \tag{3.3.43}$$

$$A_{ann(R)_{ex}} = \frac{A_{R(ex)}}{\cos(\beta_2)} \tag{3.3.44}$$

Stator inlet

$$A_{S(in)} = \frac{\dot{m}_D}{c_3\rho_3} \tag{3.3.45}$$

$$A_{ann(S)_{in}} = \frac{A_{S(in)}}{\cos(\alpha_3)} \tag{3.3.46}$$

Stator exit

$$A_{S(ex)} = \frac{\dot{m}_D}{c_4\rho_4} \tag{3.3.47}$$

$$A_{ann(S)_{ex}} = \frac{A_{S(ex)}}{\cos(\alpha_4)} \tag{3.3.48}$$

3.3.8 Blade-angle estimation

Having calculated all design-point flow angles from the velocity triangles, all physical blade angles can be determined by estimating the incidence and deviation angles for both rotor and stator. Correlations of design-point incidence and deviation are employed in order to complete this task.

Based on results from preliminary studies and its general popularity in the open literature, the modified NASA 2D method by Çetin et al. [5], [10] was employed for the design-point incidence angle. The method was also selected due to its inclusion of compressibility effects, which were not included in Lieblein's original method [5]. Furthermore, Cetin's updated method included correlations for MCA bladings, which are more typical in modern, transonic compressor stages. Preliminary studies showed good agreement between the method's results and validation data. Lieblein's method is restated below [5]:

$$i^*_{2D} = (K)_{sh}(K_i)_t(i_0)_{10} + n\theta \tag{3.3.49}$$

Values for $(K)_{sh}$ are taken from Table 1. $(K_i)_t$, $(i_0)_{10}$ and n are calculated using Falck's correlations [9] from Equations (2.3.4), (2.3.2) and (2.3.3), respectively. It was found adequate to assume a $(K)_{sh}$ value of 0.7 for MCA blades.

For design-point deviation angle, Çetin et al.'s modified Carter's rule [7], [10] was selected due to its relatively simple calculation compared to alternative methods. The unmodified Carter's rule [7], modified Carter's rule [10] and Lieblein's method for reference deviation [5] were all compared in preliminary studies, and results from Cetin's method showed the best agreement with validation data. Carter's rule [7], with function m determined from the correlation stated in Dixon and Hall [2], is rewritten below:

$$\delta^*_{CAR} = \left[0.23\left(2\frac{a}{l}\right)^2 + \frac{\alpha^*_2}{500}\right]\frac{\theta}{\sqrt{\sigma}} \tag{3.3.50}$$

The above equation requires one to know the point of maximum camber on the compressor blading. This may be considered a difficult parameter to measure. However, common assumptions of camber distribution can be made to remove this unknown.

Calculating the design-point incidence and deviation angles from the above two methods is not a trivial task, since both correlations are functions of camber angle, and are therefore themselves functions of inlet and exit blade angles. To address this, a simple successive approximation scheme

is employed, which iteratively calculates the inlet and exit blade angles from guessed values of incidence and deviation until convergence in the calculation is achieved. A flow diagram of the successive approximation program is illustrated in Figure 25. An initial guess of zero for both angles are a suitable place to start.

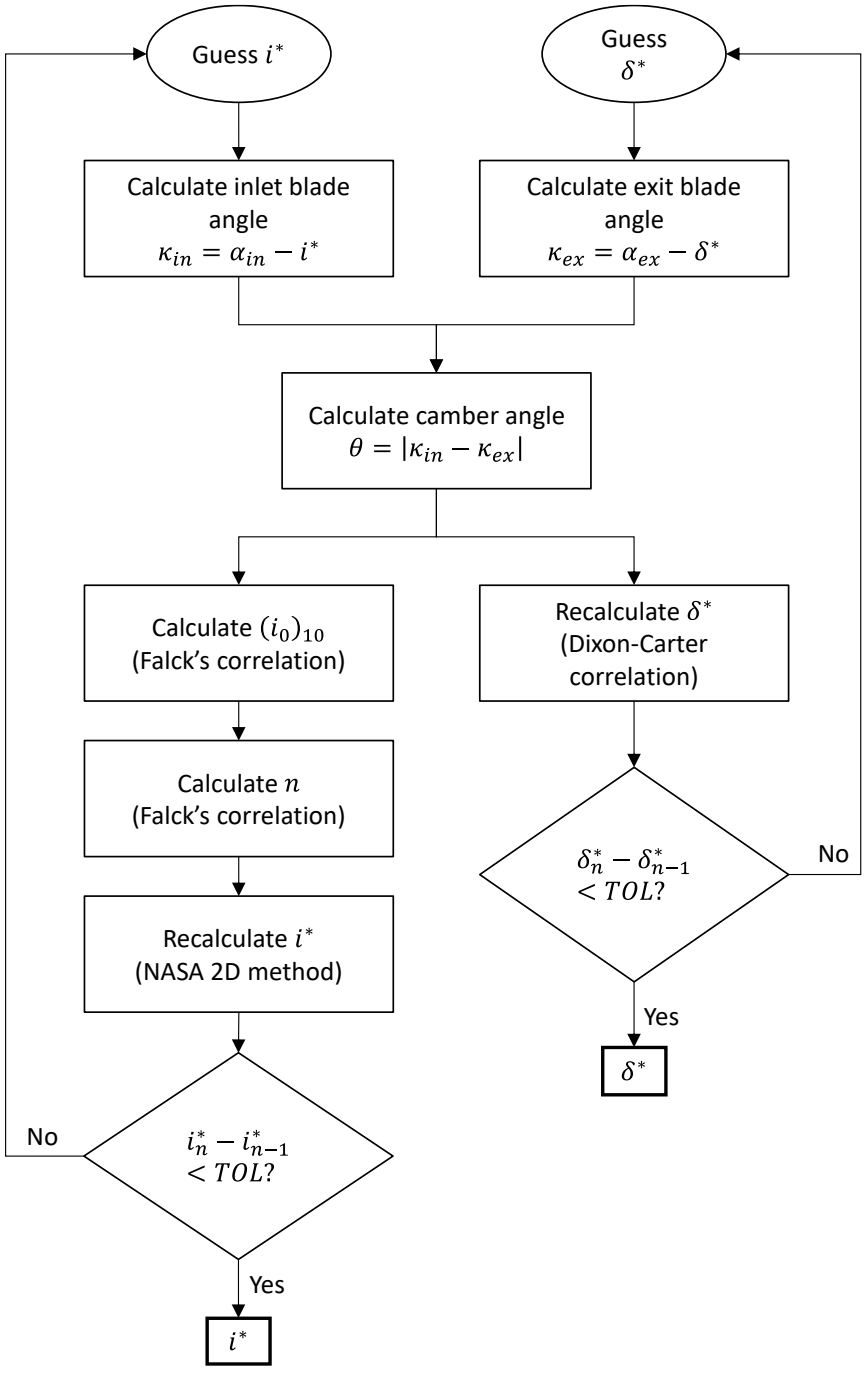

Figure 25: Flow diagram of successive-approximation scheme for estimating design-point incidence and deviation angles

The successive-approximation scheme is performed for both rotor and stator rows. Once the incidence and deviation angles are estimated, Cetin's recommended modifications are applied. The modified design-point incidence angle is calculated from Equation (2.3.5) or (2.3.6), depending on blade type, and the modified deviation angle is calculated from Equation (2.3.9). Once the incidence and deviation angles are known, all blade angles can be defined.

This completes the design-point calibration exercise as knowledge of all the geometric parameters of the blade passages are now known.

3.3.9 Summary of calibrated parameters

Table 7 below summarises all parameters to be used as inputs in the off-design analysis method, discussed in the following chapter.

Table 7: Calibrated geometric and performance inputs for off-design analysis

Parameter	Description
r_m	Mean-line radius
σ_R, σ_S	Rotor and stator solidities
A_{inlet}	Stage inlet area
$A_{ann(R)_{in}}$, $A_{ann(R)_{ex}}$	Rotor inlet and exit annulus areas
$A_{R(in)}$	Rotor inlet (throat) area
$A_{ann(S)_{in}}$, $A_{ann(S)_{ex}}$	Stator inlet and exit annulus areas
$A_{S(in)}$	Stator inlet (throat) area
i_R^*, i_S^*	Rotor and stator design-point incidence angles
δ_R^*, δ_S^*	Rotor and stator design-point deviation angles
κ_1, κ_2	Rotor inlet and exit blade angles
κ_3, κ_4	Stator inlet and exit blade angles
Y_R^*	Rotor design-point total pressure loss coefficient
Y_S^*	Stator design-point total pressure loss coefficient

3.4 Off-design Flownex model

One-dimensional system-level analyses of gas turbines typically involve calculating the thermodynamics and fluid mechanics through each system component, as well as the interactions between them. Such analyses also usually incorporate various calculations of loss and efficiency which determine the operating characteristics of each component, as well as the system as a whole. Simulations grow in complexity as the size of the system being modelled increases, due to the fact that calculations are rarely linear, but rather implicit and nonlinear in nature. This is a common challenge in modelling large thermofluid networks, including open- or combined-cycle gas turbine powerplants, which comprise of a large number of components and piping networks, and in which the compressor is only a single component.

For the above reasons, system analysts often employ commercially-available software packages which are capable of simulating large, complex thermofluid networks. One such example is Flownex SE [30]. Flownex enables large one-dimensional network simulations by simultaneously solving the conservation of mass, momentum and energy equations for each system component with its associated component characteristics. The software includes an extensive built-in library of components which incorporate all relevant physics and can be used for building customised compound components. Scripting components also allow one to include behaviour that are not already included.

For these reasons, it was decided to create the off-design compressor stage model in Flownex, as the software's built-in components could be used to model the compressor stage. Furthermore, since Flownex manages the calculation of all thermodynamic properties and fluid velocities through the network, only the velocity-triangle and loss calculations needed to be incorporated into the model. Lastly, it made sense to build the model in a commercially-available software for future studies in which it would be included in larger gas turbine simulations. This section details the structuring of the Flownex model and how it was built to achieve the study's objectives.

3.4.1 Model overview

Figure 26 shows the developed Flownex model. The model comprises of three primary components and one script: the stage inlet is modelled using a Pipe component, the rotor and stator diffusers are each modelled using a 'Restrictor with Loss Coefficient' component, and lastly, the Main Script component is included to perform the mean-line calculation. In addition, a Results script is included which reads the total pressure and temperature at each component's inlet and exit to calculate the simulated total pressure- and temperature-ratios. The Main Script code is shown in Appendix B.

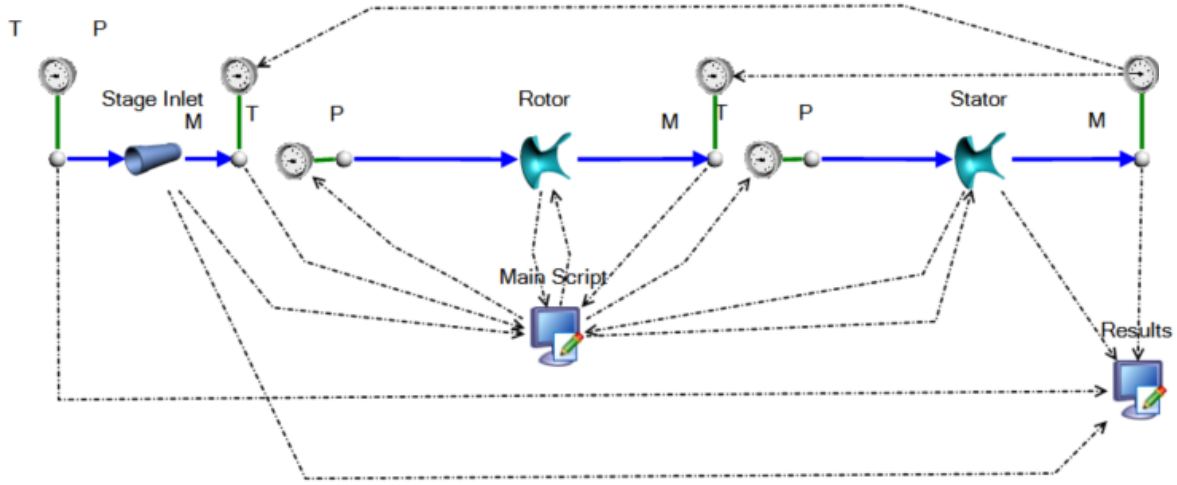

Figure 26: Off-design Flownex compressor-stage model

On its own Flownex cannot convert or differentiate between absolute and relative conditions, which is a crucial part of the mean-line calculation. To address this, the stage inlet, rotor, and stator components were separated, each having their own set of inlet- and exit-boundary conditions. The Main Script would then receive information from one component, perform the mean-line calculations, and return the appropriate boundary conditions to the following component. Figure 27 below shows the boundary conditions set for the rotor and stator, respectively.

The Main Script's other functions are to determine pressure loss coefficients from correlations, as well as calculate the effective upstream and downstream areas for both rotor and stator. The calculation procedure is described in more detail in the following sections.

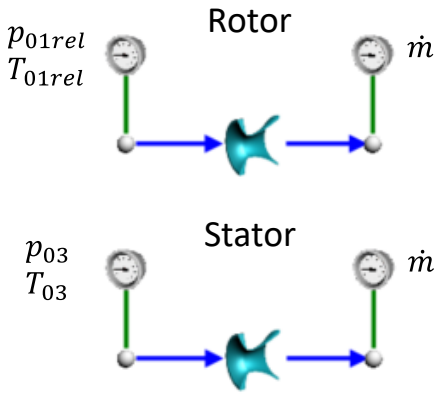

Figure 27: Rotor and stator boundary conditions in Flownex model

3.4.2 Component breakdown

The various Flownex library components used to build the diffuser analogy model are summarised in Table 8 below.

Table 8: Description of Flownex library components – adapted from [31], [32]

Icon	Block symbol	Description
	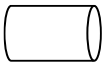	**Pipe:** Used to model fluid flow through a pipe with viscous and secondary losses; has diameter (constant or non-constant), length, and circumference as inputs.
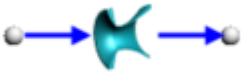		**Restrictor with Loss Coefficient (diffuser):** Used to model flow through a flow element with a distinct throat area, to which total pressure loss is applied; can have varying upstream and downstream areas. These areas, throat area and loss coefficients are inputs.
		**Script:** Used for defining parameters and performing calculations that are otherwise not already included in the Flownex solver. It makes use of C# coding language.
		**Node:** Represents the end-point of a flow element and holds information of the element's upstream or downstream conditions (depending on which end it is placed); can also represent a one-dimensional volume.
		**Boundary Condition:** Specifies the boundary condition at the inlet or exit of a flow element; will typically specify either a combination of pressure and temperature, or a mass source.
		**Data Transfer Link (DTL):** Used to pass information or data from one component to another, or from a component to a Script for use in additional calculations, and vice versa.

The component of greatest significance is the Restrictor with Loss Coefficient. This component was selected for modelling the rotor and stator diffusers as it has three distinct areas and is thus able to simulate conditions at the inlet, throat, and exit of a blade passage. This made the off-design calculation consistent with the design-point model. Furthermore, the restrictor element adopts Flownex's own definition of choked flow, being that occurring at a throat-Mach number of unity, and as such no additional choke model is needed.

Figure 28 below illustrates the correlations drawn between the three areas through a blade passage and those of the restrictor component.

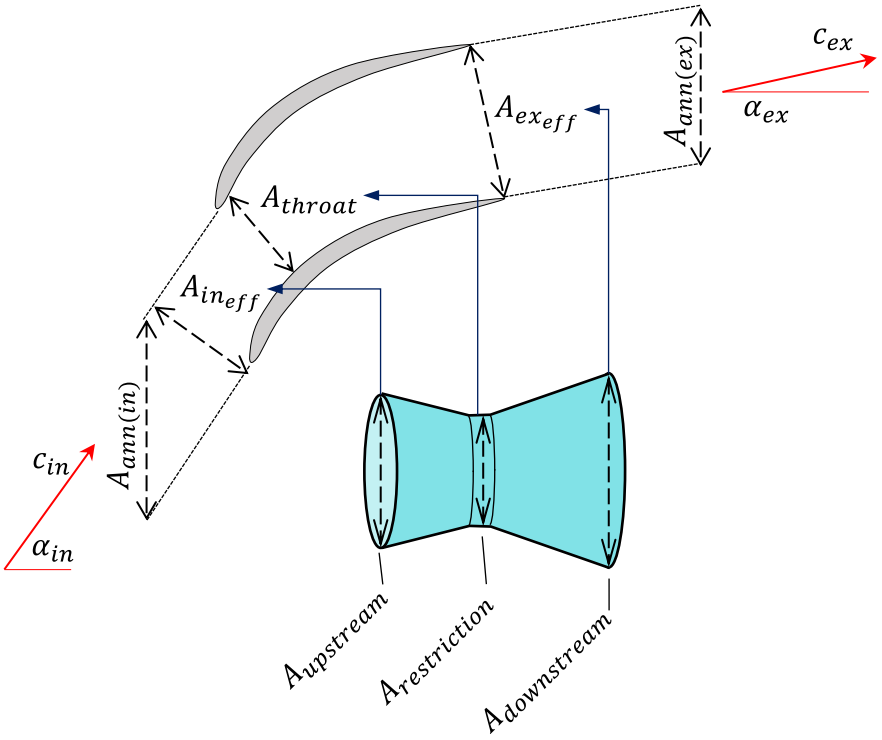

Figure 28: Correlation between areas of a blade passage and those of the Restrictor with Loss Coefficient

As Figure 28 shows, the restrictor upstream area is correlated to the blade passage effective inlet area, the restriction area is correlated to the blade throat area, and the restrictor downstream area is correlated to the blade passage effective exit area.

3.4.3 Off-design inputs

In addition to the geometric and performance inputs listed in Table 7, the off-design Flownex model also requires several operational inputs. These are listed in Table 9 below.

Table 9: Off-design operational inputs

Input	Description
$\dot{m}$	Off-design mass flow rate
ω	Off-design rotor RPM
α_1	Off-design stage inlet angle
Blade type	MCA or DCA
p_{01}	Stage-inlet total pressure
T_{01}	Stage-inlet total temperature

All inputs need to be manually entered into the appropriate fields before beginning simulations. The calibrated geometric and performance inputs of Table 7 are entered through the Main Script's user interface, illustrated in Figure 29. The blade type is entered as 0 for MCA blading, or 1 for DCA blading.

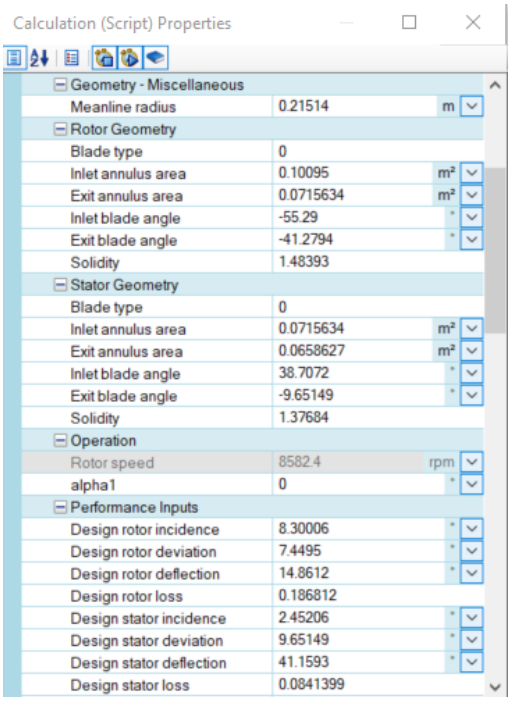

Figure 29: Main Script user-interface for entering calibrated inputs

The rotor and stator throat areas must be entered as the restrictor areas in the user interfaces of their respective components. This interface is shown in Figure 30 below.

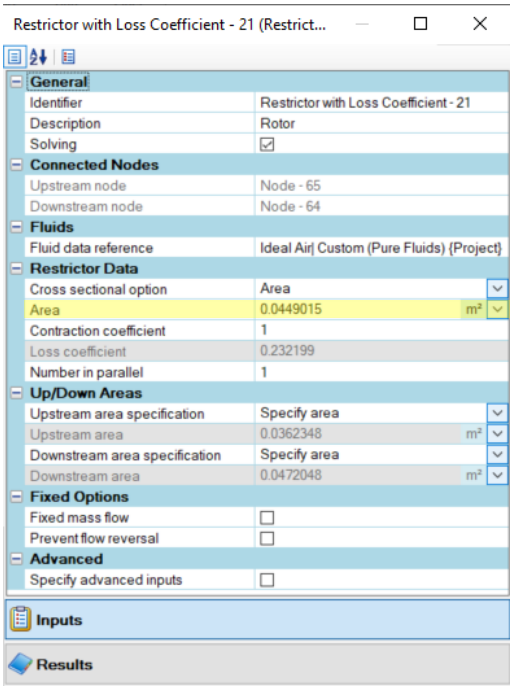

Figure 30: Inputs user-interface of Restrictor with Loss Coefficient

3.4.4 Data-transfer structure

The Flownex model comprises of several data transfer links which deliver the required information between components and the Main Script for use in the mean-line calculations. The Flownex solver achieves convergence of properties between flow elements by solving for the three continuity equations, and thus the stage intermediate-pressure convergence described in Section 3.3.5 does not need to be included in the script. This significantly reduces the scripting complexity.

It is important to understand the network of data transfer links and the information each link carries in order to understand how the mean-line code is incorporated into the Flownex solver. This is outlined below. The model block diagram in Figure 31 shows the various DTLs between components and the Main Script, while Table 10 lists all information transferred through each DTL.

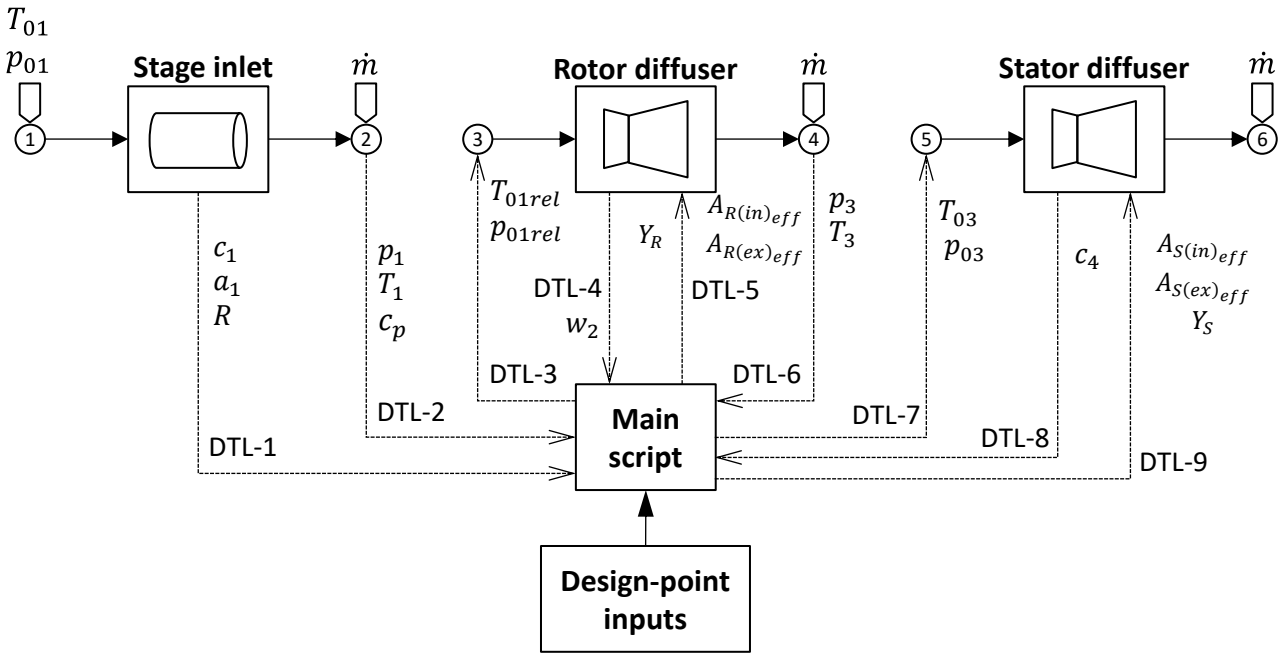

Figure 31: Block diagram of Flownex model

Table 10: Flownex model data transfer structure

Data Transfer Link	From	To	Information transferred
1	Stage inlet	Main script	• Downstream velocity c_1 • Sonic velocity a_1 • Gas constant R
2	Node 2	Main script	• Static pressure p_1 • Static temperature T_1 • Specific heat c_p
3	Main script	Boundary condition 3	• Relative total temperature T_{01rel} • Relative total pressure p_{01rel}
4	Rotor diffuser	Main script	• Downstream velocity w_2
5	Main script	Rotor diffuser	• Upstream area $A_{R(in)_{eff}}$ • Downstream area $A_{R(ex)_{eff}}$ • Loss coefficient Y_R
6	Node 4	Main script	• Static pressure p_3 • Static temperature T_3

Data Transfer Link	From	To	Information transferred
7	Main script	Boundary condition 5	• Absolute total temperature T_{03} • Absolute total pressure p_{03}
8	Stator diffuser	Main script	• Downstream velocity c_4
9	Main script	Stator diffuser	• Upstream area $A_{S(in)_{eff}}$ • Downstream area $A_{S(ex)_{eff}}$ • Loss coefficient Y_S

3.4.5 Off-design mean-line calculation

The off-design mean-line calculation is similar in order to the design-point calculation discussed in Section 3.3. The major difference being that the unbladed region calculation is not performed using design-point assumptions but is rather achieved through convergence of mass flow continuity, performed by the Flownex solver. Rather than describing an analytical model, this section outlines how the transferred information described in Table 10 is used in the main script to perform the mean-line calculation.

Rotor-inlet calculation

Firstly, the rotor speed u is calculated from the off-design rotor RPM and mean-line radius:

$$u = \omega \times r_m \tag{3.4.1}$$

Rotor-inlet vectors $\overline{U}$ and $\bar{C}_1$ are then calculated using Equation (3.3.9), with velocity magnitude c_1 received from DTL 1, and angle α_1 being an input. Following this, the rotor-inlet relative velocity vector $\overline{W}_1$ is determined using Equation (3.3.11), with angle β_1 then calculated from Equation (3.3.12), and velocity magnitude calculated as $|\overline{W}_1|$. The rotor incidence is then calculated from Equation (3.4.2). The negative sign in Equation (3.4.2) ensures conformance with the method's sign convention.

$$i_R = (-1)(\beta_1 - \kappa_1) \tag{3.4.2}$$

Lastly, the rotor-inlet relative total temperature and relative Mach number are determined from Equations (3.3.14) and (3.4.3) , respectively, with a_1, T_1 and c_p received from data transfer links as per Table 10.

$$M_{1rel} = \frac{w_1}{a_1} \tag{3.4.3}$$

Rotor shock-treatment and total-pressure loss

The Flownex solver is strictly subsonic, and therefore any supersonic Mach numbers observed in the system would prohibit solver convergence and cause the simulation to terminate. For this reason, it was decided to perform the shock treatment within the Main Script before the rotor-diffuser calculation.

The study's approach to shock treatment in the Flownex model was identical to that of the design-point method. It was assumed that, in the case of supersonic inlet flows, only a single normal-shock structure would occur in the inlet-passage of the rotor, resulting in flow being subsonic through the rotor-inlet and the rest of the stage. The method thus ensures that the Flownex solver only observes subsonic flows.

As in the design-point case, the rotor-shock is treated through the following procedure: The main script first evaluates whether M_{1rel} is subsonic or supersonic. If it is supersonic, then the post-shock relative velocity $w_{1(y)}$, static pressure $p_{1(y)}$ and static temperature $T_{1(y)}$ are calculated from Equations (3.3.17), (3.3.18) and (3.3.19), respectively. Otherwise, the post-shock static conditions are assumed equal to those at the inlet. The rotor-inlet relative total pressure is then calculated according to the conditions stated in Equation (3.3.21). This method ensures that M_{1rel} is calculated and remains within the main script only, thus ensuring the Flownex solver only perceives subsonic flows. At this point, once the shock treatment is completed, any incidence- or Mach-number-based rotor total pressure losses can be determined and returned to the rotor-diffuser through DTL 5.

Rotor deviation and exit velocity triangle

For the rotor-exit velocity triangle, the rotor deviation angle is first calculated using any chosen correlation or is set as an input. From this, the rotor-exit relative flow angle β_2 is calculated. The rotor-exit relative velocity vector $\bar{W}_2$ is then determined using Equation (3.3.9), with velocity magnitude w_2 received through DTL 4. Following this, the rotor-exit absolute velocity vector $\bar{C}_3$ is calculated vectorially using Equation (3.3.32), with its magnitude c_3 then calculated as $|\bar{C}_3|$, and angle α_3 calculated from Equation (3.3.33). The stator incidence is then calculated as:

$$i_S = \alpha_3 - \kappa_3 \tag{3.4.4}$$

Stator-inlet calculation and total-pressure loss

Having completed the rotor-exit velocity triangle, only the stator inlet total temperature and total pressure need to be determined. In the design-point calculation this was achieved using a known temperature ratio, however in off-design the properties are determined using Equations (3.4.5) and (3.4.6), respectively, with T_3 and p_3 received through DTL 6. The calculated conditions are then returned to Node 5 through DTL 7 to be used as the stator-inlet boundary conditions. Following this, any correlation-based stator total pressure losses can be calculated and then returned to the stator-diffuser through DTL 9. The total pressure p_{03} is also transferred to the Results script for determining the rotor total-pressure ratio, which is calculated using Equation (3.4.7).

$$T_{03} = T_3 + \frac{c_3^2}{2c_p} \tag{3.4.5}$$

$$p_{03} = p_3 \left(\frac{T_{03}}{T_3} \right)^{\frac{\gamma}{\gamma-1}} \tag{3.4.6}$$

$$\Pi_R = \frac{p_{03}}{p_{01}} \tag{3.4.7}$$

Stator-exit calculation

The next step is to determine the velocity triangle and conditions at the stator-exit. First, the stator deviation angle is determined from empirical correlation or is set as an input. From this, the stator-exit flow angle α_4 is determined. The stator-exit velocity vector $\bar{C}_4$ is then calculated using Equation (3.3.9), with velocity vector c_4 received from the stator-diffuser through DTL 8. Finally, the Flownex solver determines the stator-exit total temperature T_{04} and total pressure p_{04}. The stator-exit conditions are then transferred to the Results script for determining the stage total-temperature and total-pressure ratios, which are calculated using Equations (3.4.8) and (3.4.9) respectively.

$$\mathrm{T}_{stage} = \frac{T_{04}}{T_{01}} \tag{3.4.8}$$

$$\Pi_{stage} = \frac{p_{04}}{p_{01}} \tag{3.4.9}$$

Effective flow-area calculation

The final step in the mean-line calculation is to determine the effective flow-path areas at the inlets and exits of both rotor and stator. The flow-path area is a function of both its related annulus area and flow angle. As a result, these areas are sensitive to off-design incidence angle, as well as off-design deviation angle (if it is being modelled). Therefore, the four effective flow-path areas are recalculated at the end of each solver iteration using Equations (3.4.10) to (3.4.13):

$$A_{R(in)_{eff}} = A_{ann(R)_{in}} \times \cos\left(\beta_1\right) \tag{3.4.10}$$

$$A_{R(ex)_{eff}} = A_{ann(R)_{ex}} \times \cos\left(\beta_2\right) \tag{3.4.11}$$

$$A_{S(in)_{eff}} = A_{ann(S)_{in}} \times \cos\left(\alpha_3\right) \tag{3.4.12}$$

$$A_{S(ex)_{eff}} = A_{ann(S)_{ex}} \times \cos\left(\alpha_4\right) \tag{3.4.13}$$

4. Results and Discussion

The final part of the study was to verify and validate the developed methodology. The validation exercise sought to evaluate three major elements of the methodology, being:

1. The accuracy of the design-point-calibration method's predictions of compressor stage geometry.
2. The overall performance of the base mean-line methodology with no specific off-design loss correlations applied.
3. The performance of the model with implementation of an established loss correlation from the open literature.

The first objective was achieved through comparing predicted geometric parameters from the analytical model with those from a published source. The second and third objectives were achieved through validation of four off-design sub-models, each including an additional modelling element from the previous one. With a validated base-methodology, the focus of the validation exercise turned to evaluating methods of performance modelling incorporated into the base-method. This included the evaluation of off-design loss correlations and tuning factors.

Lastly, brief observations of stall-point diffusion factor are made to inform a rule-of-thumb for detecting the stalled condition in the Flownex model.

4.1 Validation cases

The model was validated against four widely-referenced compressor stages from NASA. The four stages considered were the NASA Stage 35 [33], Stage 36 [34], Stage 37 [35], and Stage 38 [36]. Table 11 summaries the design-point performance characteristics for the four NASA stages, against which the Flownex models' predicted values were compared.

Table 11: Design-point performance characteristics of four NASA compressor stages

Stage	Rotor RPM	Mass flow rate [kg/s]	Rotor total pressure ratio	Stage total pressure ratio	Stage total temperature ratio
35	17188.700	20.188	1.865	1.820	1.225
36	17188.700	20.188	1.863	1.820	1.227
37	17188.700	20.188	2.106	2.050	1.270
38	17188.700	20.188	2.105	2.050	1.269

Kidikian [3] motivated the four NASA stages for use in validation as follows:

1. ***Close representation of modern compressors:*** The four NASA stages represent modern compressor stages comparatively well, since none of them contained part-span shrouds; they cover a range of pressure and aspect ratio; they have comparatively high total pressure ratios, and thus high work capacities.
2. ***Time frame:*** All four stages was designed and tested within the same five-year time frame.
3. ***Similarity:*** All four compressor stages were consistent in design and testing methodology, and all had the same design-point rotor speed and mass flow rate.
4. ***Modern blading:*** The four compressors contained MCA blading, which are generally favoured for their better off-design performance in transonic conditions, when compared to other blading such as NACA and DCA profiles.
5. ***Completeness of data:*** The four NASA datasets are the most extensive and complete when compared to alternatives. The datasets included extensive information of spanwise variations in velocity components and thermodynamic properties at the inlet and exits for both rotor and stator, and for every test case investigated. Furthermore, the four reports included complete datasets of rotor and stator aerofoil coordinates, as well as spanwise variations of inlet and exit blade angles. Indeed, the available information of the four NASA compressors far exceeded what is available from other sources in the open literature, which generally only provide compressor maps.

From the above points, it may be argued that successful validation of this study's model against the four NASA stages would allow one to assume that the study's findings are applicable to other modern compressors.

The NASA Stage 35 compressor was used as the primary case for model building, verification, and validation. The additional use of Stages 36 to 38 was for verification of the design-point calibration, as well as for defining correlations of the area correction factor.

It was decided that stage total-pressure ratio would be the main focus in all off-design validation cases, as it was believed that this is the most significant parameter in large system-level thermofluid-network simulations. Therefore, the simulations' performances were primarily evaluated against the compressor maps of stage total-pressure ratio from the experimental data, and all adjustments of total pressure losses and correction factors were made to achieve the known total pressure ratios.

The secondary focus in each validation case was the sensitivity of rotor total-pressure ratio and stage total-temperature ratio to adjustments made for stage total-pressure ratio. Validation cases

therefore includes error analyses of the three performance parameters using statistical methods, in addition to the qualitative assessments of predicted compressor maps.

4.2 Design-point geometry prediction

It was important to first ensure that the design-point calibration method produced accurate predictions of flow-path geometry. The method was applied to the Stage 35 case using the design-point inputs listed in Table 3 to Table 6, and its results were compared with those reported in [33].

Firstly, the predicted design-point mean-line blade angles from the geometry-calibration exercise were compared to the reported values. The predicted and true values are listed in Table 12 below.

Table 12: Comparison of predicted Stage 35 blade angles with true values

Angle	**Predicted [deg]**	**True value [deg]**	**Absolute Error [deg]**
Rotor incidence i_R^*	8.30	5.10	3.20
Rotor deviation δ_R^*	7.45	6.50	0.95
Rotor inlet κ_1	-55.29	-56.16	0.87
Rotor exit κ_2	-41.28	-44.26	2.98
Stator incidence i_S^*	2.45	4.20	1.75
Stator deviation δ_S^*	9.65	6.70	2.95
Stator inlet κ_3	38.71	35.72	2.99
Stator exit κ_4	-9.65	3.11	12.76

The angles reported in Table 12 indicate that the design-point calibration program performed generally well in predicting the Stage 35 blade angles with an average error less than 2.3° (excluding stator exit angle). It is clear from the reported values that the estimated angle of -9.65° for the stator exit angle was produced to ensure a stator-exit flow angle of 0°, by accounting for the stator deviation. This is a consequence of the normal repeating stage assumption, which does not actually apply to Stage 35.

In order to validate the predicted flow passage areas, a three-dimensional CAD model of the Stage 35 compressor was created from the flow path and blade manufacturing coordinates presented in [37]. The various areas were then measured in the CAD model and compared to those predicted by the calibration program, including stage inlet annulus, and the inlet and exit flow areas for both rotor and stator. Figure 32 below illustrates the three-dimensional CAD model with measured flow areas. The measured areas from the CAD model are compared with those predicted from the design point calibration program in Table 13.

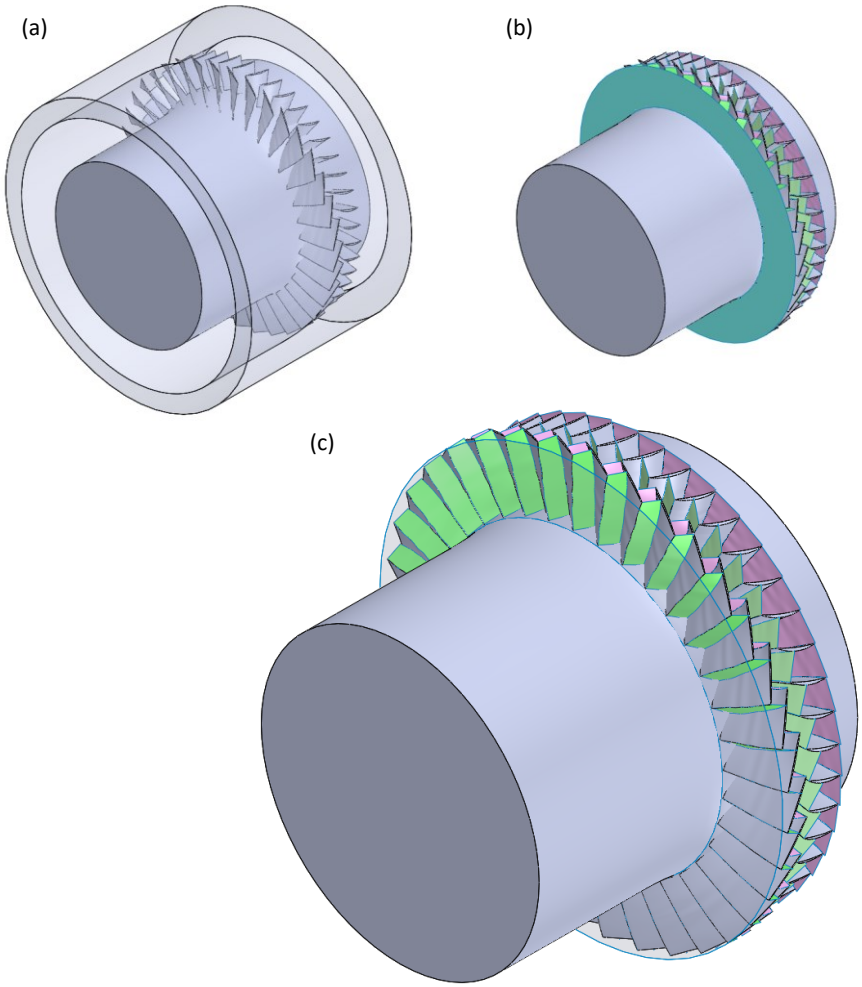

Figure 32: (a) 3D CAD model of Stage 35, (b) measured flow-path areas, and (c) enlarged view of compressor stage areas

Table 13: Comparisons between predicted Stage 35 flow-passage areas and CAD model

Area	Predicted area [cm^2]	CAD model [cm^2]	Absolute relative error [%]
Stage inlet annulus A_{inlet}	1009.50	1033.68	2.339
Rotor inlet $A_{R(in)}$	449.01	518.76	13.446
Rotor exit $A_{R(ex)}$	472.05	531.36	11.162
Stator inlet $A_{S(in)}$	538.79	604.90	10.929
Stator exit $A_{S(ex)}$	658.63	650.808	1.202

It can be observed from Table 13 that the calibration method predicted the stage inlet annulus area with reasonable accuracy, however it underpredicted the rotor-inlet, rotor-exit and stator-inlet flow areas by as much as 13.4%. This underprediction may have been attributed to the placement of the measured areas within the CAD model, thus having not taken into account the thickness distribution of the blades or the actual design-point incidence and deviation angles. Nevertheless, for the purposes of this study, the errors presented were considered acceptable.

It is interesting to note that the stator-exit flow area is predicted with good accuracy despite the large error in predicted stator exit angle presented in Table 12. This may suggest that the normal repeating-stage assumption remains suitable for geometry estimation, even for cases where the actual stage does not present such characteristics. It can therefore be concluded that the design-point calibration methodology was generally successful.

Lastly, the method was applied for the remaining three NASA stages using the preliminary model discussed in Sections 3.3.5 and 3.3.6, in order to determine a suitable range of design-point pressure loss coefficients to be used as assumed inputs. The findings of this brief exercise are listed in Table 14 below.

Table 14: Calibrated design-point losses for Stages 35 to 38

Stage	Rotor total loss Y_R^*	Stator total loss Y_S^*
35	0.187	0.084
36	0.207	0.081
37	0.200	0.082
38	0.194	0.082
Average	0.197	0.082

Based on observations from Table 14, it was deduced that one could reasonably assume values of around 0.2 and 0.08 for rotor and stator design-point total losses, respectively, as inputs for the design-point calibration exercise.

4.3 Model 1 – Flownex model verification

Before method-refinement and investigations of loss-modelling, it was first necessary to verify the developed Flownex model and incorporated mean-line script. Therefore, the model was first applied without incorporation of any specific pressure loss model, in order to specifically verify the base-methodology. Flownex's built-in Designer functionality was employed to calibrate only the rotor total-pressure loss coefficient in order to achieve the known stage total-pressure ratio for each reading of the Stage 35 dataset. The Flownex Designer functionality employs a Newton-Raphson based method to solve a set of non-linear equations resulting from a number of user-inputted independent variables and equality constraints [38]. The Designer iteratively increments and updates the independent variables until changes in these variables are negligible. In this exercise, the stator total-pressure loss coefficient was held constant at a value of 0.02 for all readings. The detailed results of the verification exercise are presented in Appendix C Table 15.

Off-design simulations of Stage 35 were performed using the methods discussed above. The results from these simulations are illustrated in the compressor map of stage total-pressure ratio in Figure 33 below.

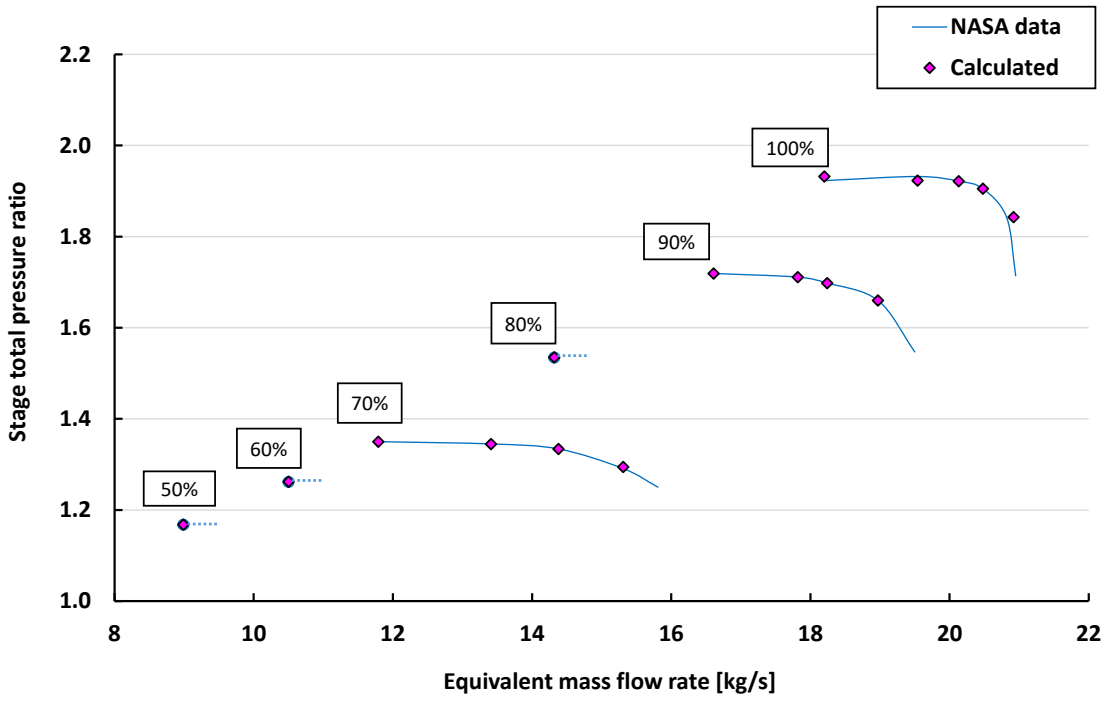

Figure 33: Predicted Stage 35 compressor map using manually tuned rotor total-pressure loss coefficient

It is evident from Figure 33 that the applied methodology was generally successful in predicting the overall compressor map, as good agreement is found between the majority of simulated and experimental data. Furthermore, there is notable agreement between simulated and reported data at the surge-points of all speed-lines. The Flownex solver was however unable to achieve convergence for the recorded choke-points on the 100%, 90%, and 70% speed-lines. It was speculated that the reason for this was due to the model being restricted to Flownex's own definition of choked-flow, which assumes that flow through the restrictor is choked when the critical Mach number of unity is exceeded [31]. As has been discussed by Kidikian [3], the choke point in modern transonic compressors is generally difficult to define, and in many cases the conventional definition of choke at critical Mach number may not apply. It is also believed that the solver's failure to achieve convergence in these cases may be resolved in future through application of several relaxation parameters, and that the solver may have achieved convergence for mass flows slightly lower than the current limits, had they been simulated. Achieving better solver convergence or even implementing an alternative choke criteria was deemed outside the scope and main purpose of this study.

Despite the above, inspection of Figure 33 suggests an overall successful verification of the developed model. However, it was also required to evaluate other significant simulation outputs such as the stage total-temperature ratio, to ensure that the model captured other fundamental physics. Figure 34 shows the relative error distributions of predicted stage total-pressure and total-temperature ratio.

It is clear from Figure 34 that the errors of predicted stage total-pressure ratio are generally low. This was to be expected since this was the primary objective of the Designer, and the remaining error may simply be due to the Designer convergence criteria, which were set to 0.001 in this case.

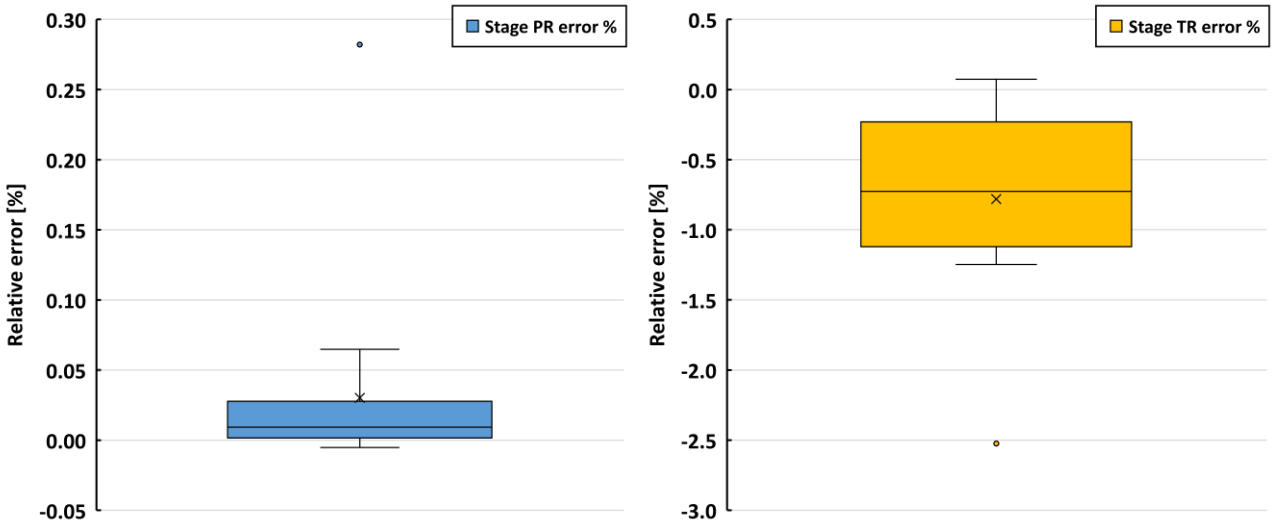

Figure 34: Distribution of relative errors of Model 1 simulated results

The range of relative errors for predicted stage total-temperature ratio were generally low, with a maximum absolute error of around 2.5%. This was despite the parameter not being a focus of calibration. Given the minimal-input nature of the study, this error was considered to be within an acceptable range. Based on this observation, there is initial evidence to suggest that the stage total-temperature ratio is not greatly sensitive to calibrations for stage total-pressure ratio, even when it is not subject to any calibration itself. This is a desirable finding, as it indicates that fewer calibration factors are required in subsequent models.

The above findings presented enough evidence of the base-methodology's general success in predicting off-design compressor behaviour. Furthermore, the design-point stage intermediate pressure predicted by the Flownex solver lay within 0.5-percent of that predicted from the analytical design-point calibration program. However, there was about a 30-percent difference in the predicted design-point rotor losses from the two methods. This was simply attributed to the stator losses being held at a constant value in the Flownex model. Despite this, the general success of the exercise confirmed the base methodology to be adequately verified.

Data of off-design rotor loss vs incidence angle is presented in Figure 35. One would have expected to see the generic loss-bucket in the results, but that is clearly not the case. The reason for this can probably be attributed to the stator total-pressure loss coefficient being held constant at all off-design conditions. The necessity to include an area adjustment factor (as will be described later), may also have contributed to the observed deviation.

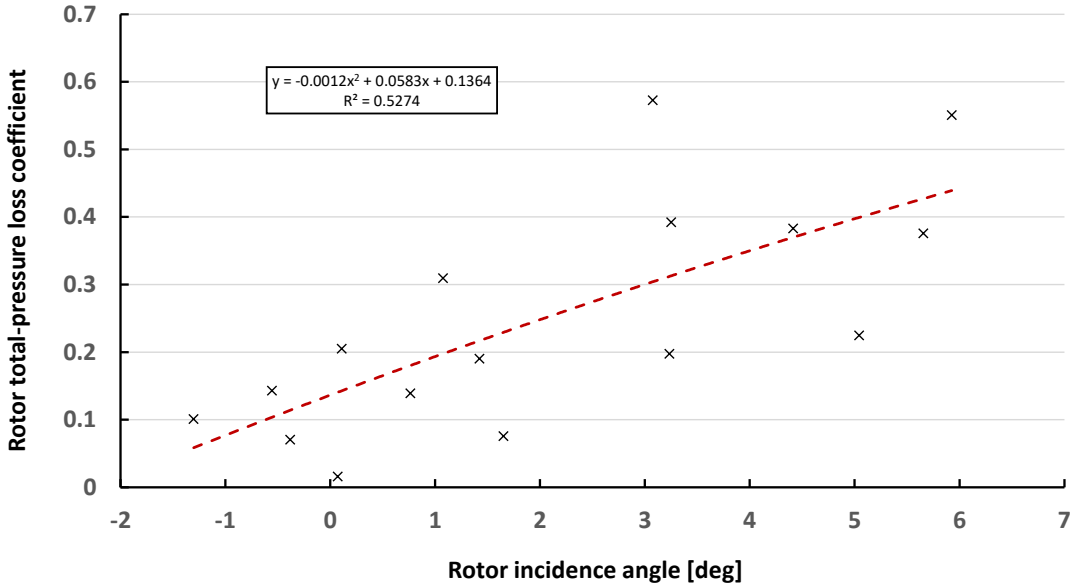

Figure 35: Plotted data of rotor losses vs incidence angle from Model 1 simulations

4.4 Model 2 – Addition of an established loss correlation

Following on from the findings of the previous sub-model, it was desired to investigate the incorporation of an established correlation for determining rotor and stator pressure losses. This would allow for simulation execution without requiring knowledge of true stage total-pressure ratio at off-design conditions. Furthermore, incorporation of a defined loss model would reduce the amount of calibration required, which is a primary objective of this study.

From literature review, it was decided to adopt the loss model of Çetin et al. [10], which calculates the total-pressure loss coefficient as a function of inlet Mach number, design-point total-pressure loss, and design-point incidence angle. The model removes the need to determine individual loss contributions, thus reducing the complexity of calculation, as well as the number of tuning factors required. Furthermore, the loss curves of Çetin's method are already defined through empirical correlation which simplifies the incorporation into a computer model.

The constant deviation angle assumption was made, and therefore no correlations for off-design deviation were investigated. This is based on findings from the literature review which argued that the mean-line deviation angle does not vary significantly at off-design conditions [13]. The assumption also reduced the computational complexity and allowed focus to remain on only pressure-loss characteristics.

It must be noted that the study only partially adopted Cetin's full method [10]. Cetin's full list of recommendations included:

- ✗ Using Koch and Smith's method [8] to determine design-point total pressure losses;
- ✓ Using the modified NASA-2D method [5], [10] for calculating design-point incidence angle;
- ✓ Using the modified Carter's rule [7], [10] for calculating design-point deviation angle;
- ✓ Using Cetin's own developed correlation of off-design total pressure loss coefficient, and
- ✗ Using Creveling and Carmody's method [15] for calculating off-design deviation angle.

This study only adopted three of the five above recommendations, since the design-point total-pressure losses were assumed and calibrated from typical values and off-design deviation angle was not considered.

Figure 36 below shows the predicted compressor map of stage total pressure ratio for the Stage 35 compressor. All simulation data from Model 2 are found in Appendix C, Table 16. The design-point operation was also simulated in Model 2 and all subsequent models for complete verification and validation of the methodology. The errors of all design-point predictions are shown in each model's respective dataset table in Appendix C.

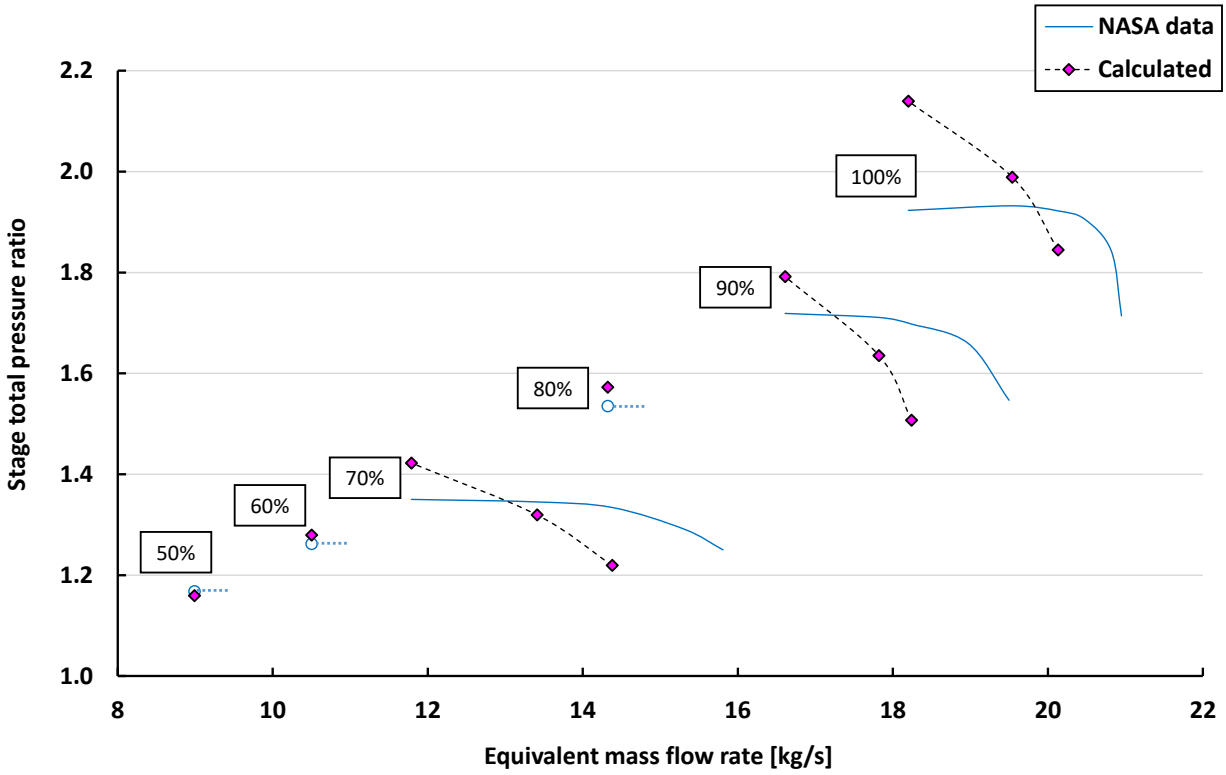

Figure 36: Predicted Stage 35 compressor map using Çetin's method for determining losses

As is evident from Figure 36, the compressor map predicted by the Flownex model appears similar to a generic case. However, the model did not adequately capture the true shape and absolute values of the Stage 35 experimental data, which is characterised by the flattening section towards the surge-point. The Flownex model also overpredicted the surge-point on all speed lines. This overprediction was greatest for the 100% speed-line and decreased as off-design rotor speed decreased. Figure 36 also indicates, as was observed in the previous exercise, that the Flownex solver was unable to achieve convergence for the true choke points of the 100%, 90%, and 70% speed-lines. The causes for this were assumed the same as in the previous section. In addition to poor solver convergence, the observed trends were also likely due to poor prediction of rotor- and stator-inlet Mach numbers, as a result of the diffuser upstream and downstream areas being miscalculated (as will be shown later). Since the estimated losses were made functions of inlet Mach number, this resulted in the solver underpredicting losses at lower mass flow rates, while over predicting losses at higher mass flows. Figure 37 shows the distribution of relative errors for the simulated Model 2 data.

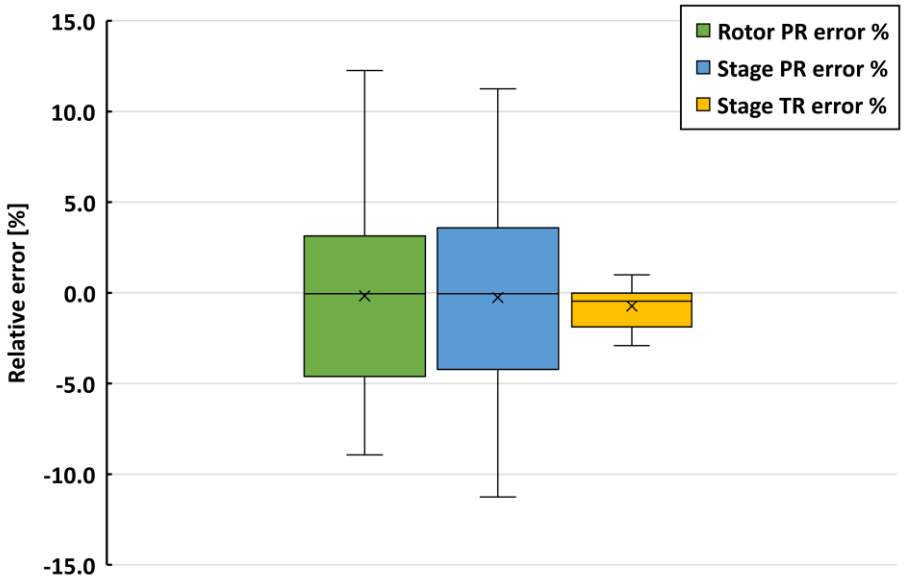

Figure 37: Distribution of relative errors of Model 2 simulated results

Figure 37 indicates that the simulated data produced a large range of relative errors for rotor and stage total-pressure ratio, with maximum absolute errors of around 12% and 11%, respectively. Interestingly, a smaller range of errors is observed for predicted stage total-temperature ratio, with an absolute maximum error of around 2.9%. This may again suggest that the stage total-temperature ratio is relatively insensitive to errors in stage total-pressure ratio.

Assessing Model 2's performance as a whole, one may argue that the errors observed in Figure 37 are still acceptable given the model's minimal-input characteristics. Indeed, the predicted compressor map in Figure 36 appears similar to the generic case often used for thermofluid system modelling. However, poor prediction of the flattened sections in the speed-lines indicates that the model is not suited to modern transonic compressor stages, which often include this feature.

4.5 Model 3 – Addition of a simple area correction factor

The findings from Model 2 posed a significant challenge. Application of Çetin's off-design loss correlation alone did not produce results of acceptable accuracy. This might be attributed to the Flownex solver miscalculating the diffuser upstream- and downstream-areas. Kidikian included different tuned blockage factors [3] for each upstream- and downstream-area to overcome the same kind of error.

Since the aim of this study is to require minimal tuning, it was decided to incorporate a single area correction factor K_A applied to the upstream and downstream areas of both rotor and stator diffusers. Therefore, the calculations of effective flow-passage areas were modified as follows:

$$A_{R(in)_{eff}} = A_{ann(R)_{in}} \times \cos(\beta_1) \times K_A \tag{4.5.1}$$

$$A_{R(ex)_{eff}} = A_{ann(R)_{ex}} \times \cos(\beta_2) \times K_A \tag{4.5.2}$$

$$A_{S(in)_{eff}} = A_{ann(S)_{in}} \times \cos(\alpha_3) \times K_A \tag{4.5.3}$$

$$A_{S(ex)_{eff}} = A_{ann(S)_{ex}} \times \cos(\alpha_4) \times K_A \tag{4.5.4}$$

Unlike Kidikian's blockage factor, the area correction factor could either be greater than, less than, or equal to one, whereas Kidikian's blockage factor was less than one in all cases. This was due to the fact that the area correction was made with reference to the design-point condition, at which the area correction factor was set to one. The area correction factor could therefore be considered as either an area blockage factor, or an area "expansion" factor, depending on the conditions of operation. The four flow-passage areas were calculated in the main script in the same sequence as before.

Adjustments to the diffuser areas would result in corrections to the calculated inlet- and exit- velocities, and therefore their corresponding Mach numbers. This would subsequently result in a recalculation of the rotor and stator total pressure losses and potentially improve the total pressure ratio.

The area correction factor was manually adjusted for each operating case until the absolute relative error of stage total-pressure ratio became less than 0.1% in all off-design cases, where possible. The complete set of Stage 35 simulation data with calibrated area correction factors is found in Appendix C, Table 17. Figure 38 shows the predicted compressor map of stage total-pressure ratio for the Stage 35 compressor using the calibrated area correction factor.

It is immediately clear from Figure 38 that the area correction exercise resulted in a substantially more accurate prediction of stage total-pressure ratio than in the previous attempt. This is especially

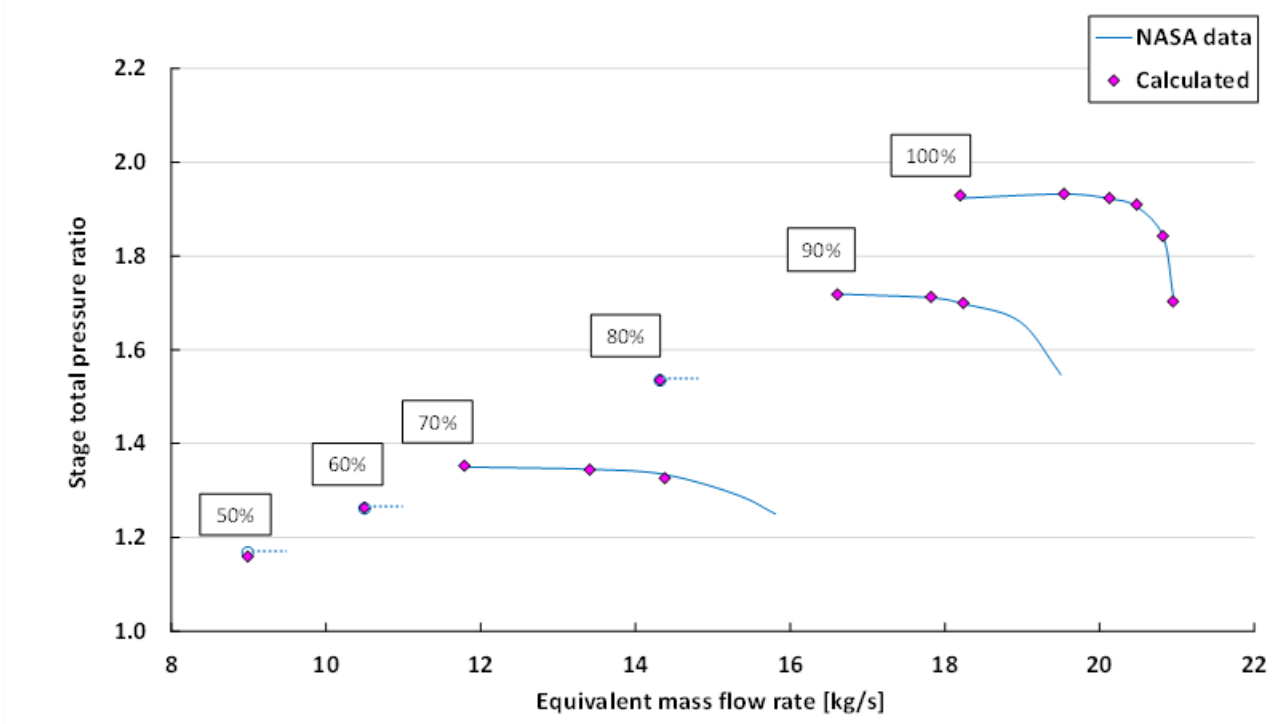

Figure 38: Predicted Stage 35 compressor map using manually tuned area correction factor

true for all operating cases on the 100% speed-line. In addition, the model was able to predict the surge-point on all speed lines with good accuracy. Unfortunately, the model still suffered the same issues of solver stability with regards to convergence at the true choke-points on the 70% and 90% speed lines. Interestingly, however, it is observed that the Flownex solver successfully converged for the true choke-point operation of the 100% speed line. It is believed that the solver may have been able to determine the true choke point by simply selecting mass flow rates slightly less than the values reported in the published data and/or making adjustments to the solver iteration process.

Figure 39 compares the relative errors from Model 3 simulations of Stage 35 to those of the previous model. It is clear from Figure 39 that Model 3 resulted in a notable improvement in prediction of rotor total-pressure ratio over Model 2. This is a favourable outcome, especially since this parameter was not the focus of calibration. As expected, there was a significant reduction in the overall error,

and distribution thereof, for stage total-pressure ratio from Model 2 to Model 3. There is also a slight improvement to the average error of stage total-temperature ratio for the Model 3.

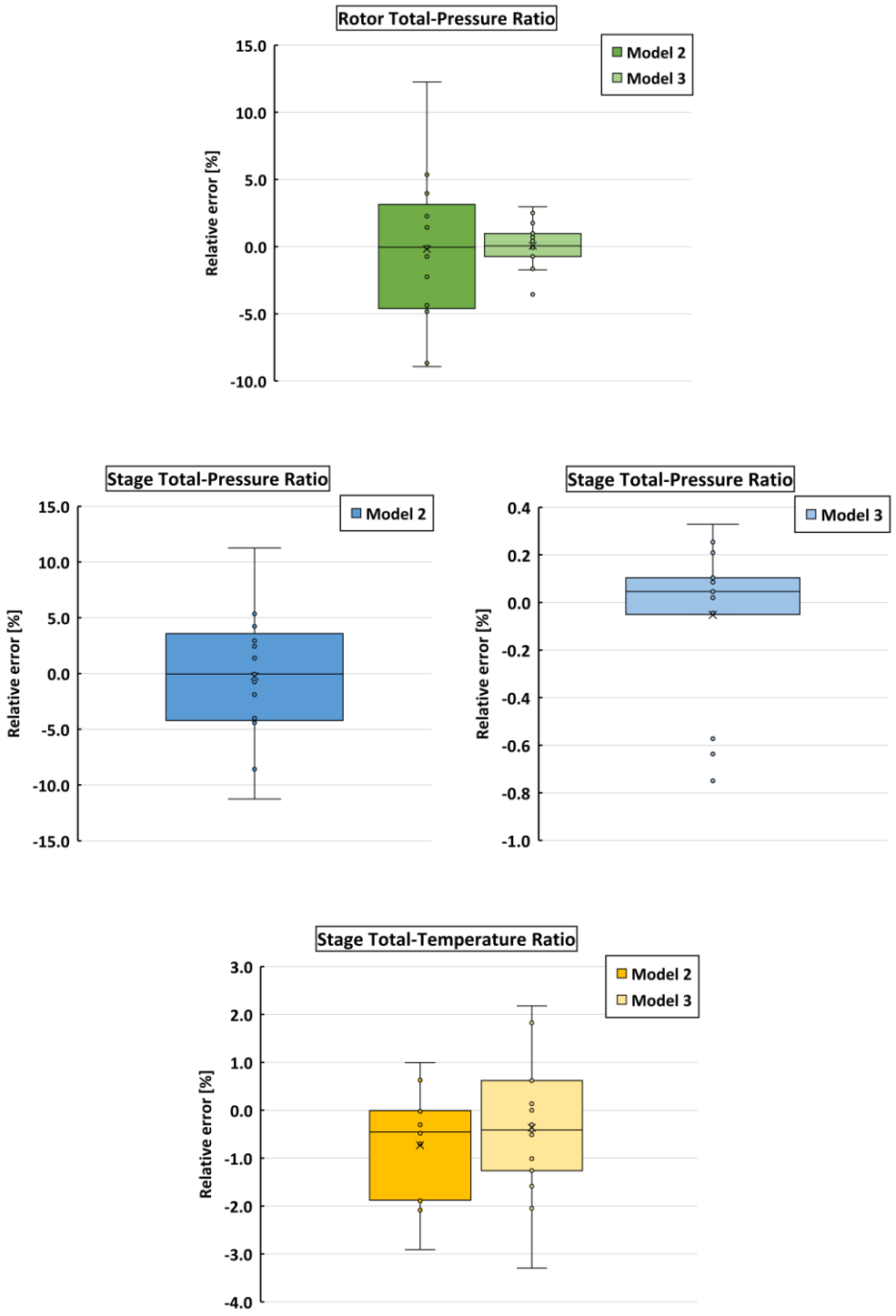

Figure 39: Comparisons of error distributions for Model 2 and Model 3 simulations of Stage 35

The above exercise was repeated for NASA Stages 36, 37, and 38 in order to further validate the area-correction method, as well as to identify any potential correlations of area correction factor. Figure 40 to Figure 42 show the predicted compressor maps of stage total-pressure ratio for Stages 36, 37, and 38, respectively. The full datasets of simulated results for the three stages are found in Appendix C Table 18, Table 19, and Table 20, respectively.

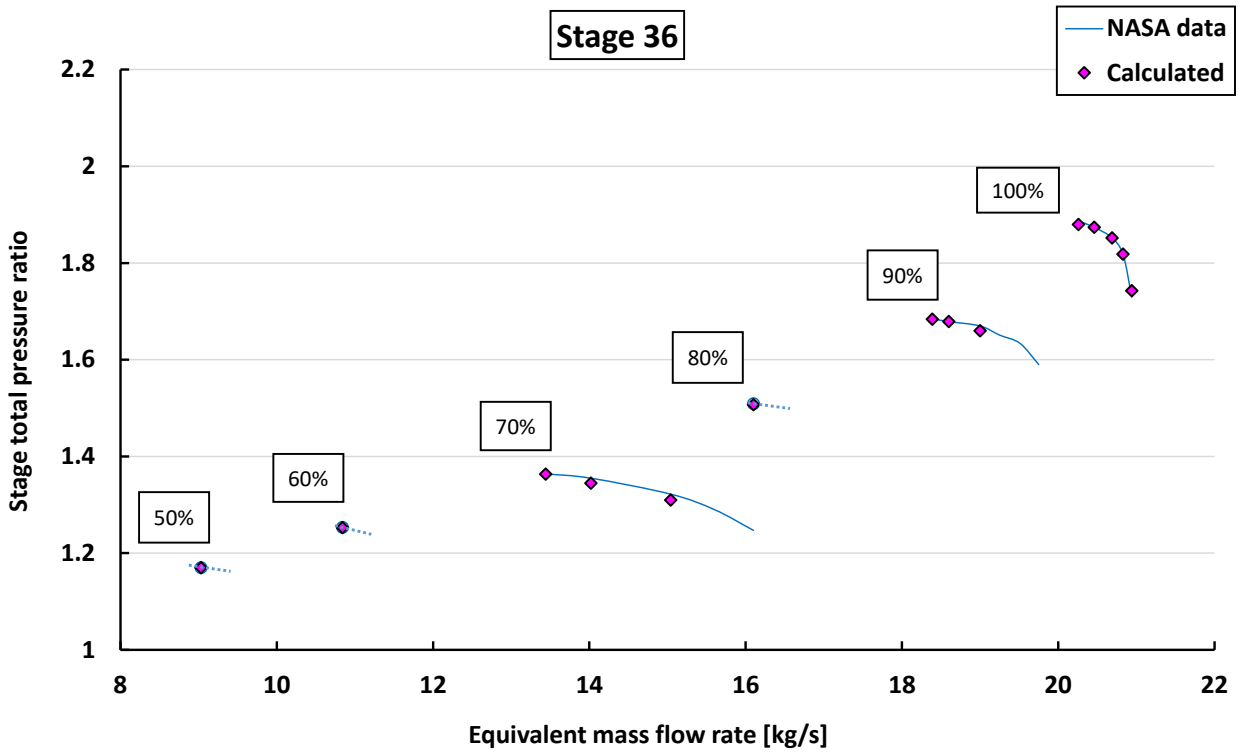

Figure 40: Predicted Stage 36 compressor map using manually-tuned area correction factor

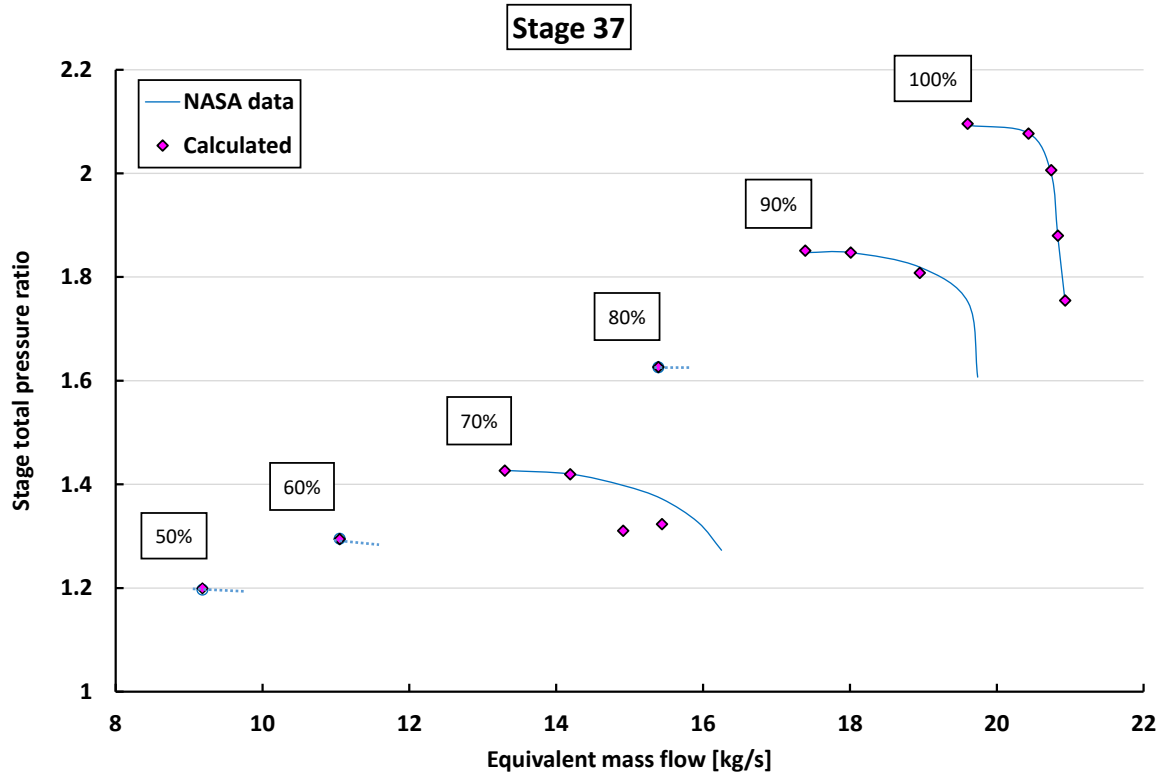

Figure 41: Predicted Stage 37 compressor map using manually-tuned area correction factor

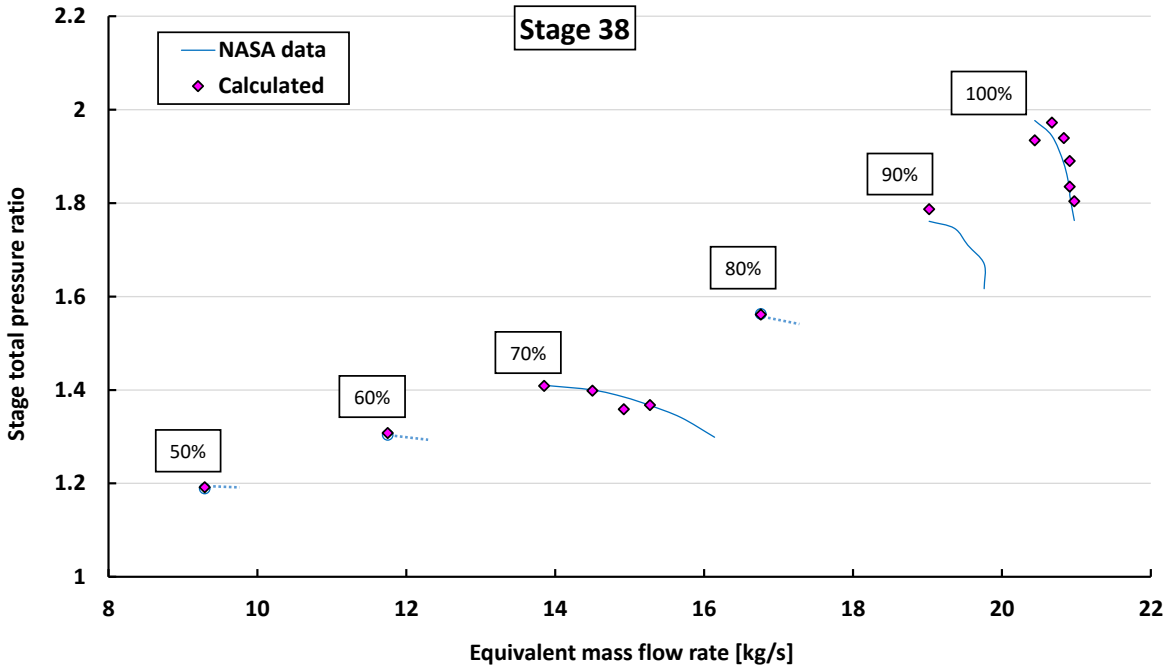

Figure 42: Predicted Stage 38 compressor map using manually-tuned area correction factor

Similar observations are made for Stages 36 to 38 to those of Stage 35. Firstly, the model was able to predict all operating points on the 100% speed-lines of all three stages with acceptable accuracy, with a few exceptions in Stage 38. Secondly, the model was able to accurately predict the surge-points of all speed-lines of all three stages. However, as was observed for Stage 35, the Flownex solver was unable to achieve convergence for the true choke points on the 70% and 90% speed lines of all three stages. This was again attributed to solver stability. Furthermore, several other exceptions in model accuracy are observed in the above figures, notably on the 70% speed-line of Stage 37, and the 90% speed-line of Stage 38, where the model was only able to predict the surge-point. This too was attributed to solver stability.

Figure 43 compares the error distributions of Model 3 simulations for the four NASA stages. It is evident from Figure 43 that the Flownex model predicted the rotor total-pressure ratios of Stages 35, 36, and 37 with fairly good agreement, with maximum relative errors of 3.6%, 2.0%, and 6.7%, respectively. However, significantly higher errors are observed for Stage 38 predictions, with a maximum absolute error of 16%. Despite this, the maximum errors of rotor total-pressure ratio for Stage 35 to 37 are considered acceptable.

The Flownex model predicted stage total-pressure ratio with good accuracy for all four stages, with maximum relative errors of 0.75%, 0.93%, 6.3% and 2.1%[2] for stages 35 to 38, respectively. Again, this was expected since this was the parameter of focus in model calibration. The average error of stage total-pressure predictions remained below 1% for all four stages. Although the absolute maximum error for Stage 37 was significantly higher than the other three stages, the overall range of errors is considered acceptable in context of this study's aims.

Lastly, it is evident that the Flownex model's predictions provided reasonably accurate results of stage total-temperature ratio. The greatest range of errors is observed from Stage 38, with a maximum relative error of around 5.25% and an average relative error of around 1.93%. Nevertheless, the overall range of errors in stage total-temperature ratio for all four stages is considered acceptable.

It can be concluded from Figure 43 that the Flownex model generally performed the poorest for Stage 38. The reason for this is not completely clear to the author. It was speculated that this may have been due to the Stage 38 having both the higher rotor aspect ratio and stage total-pressure ratio, and thus a higher stage loading. This however could not be confirmed due to the constrained amount of available test data. Nevertheless, the findings discussed above confidently demonstrate the model's overall success.

[2] Absolute values.

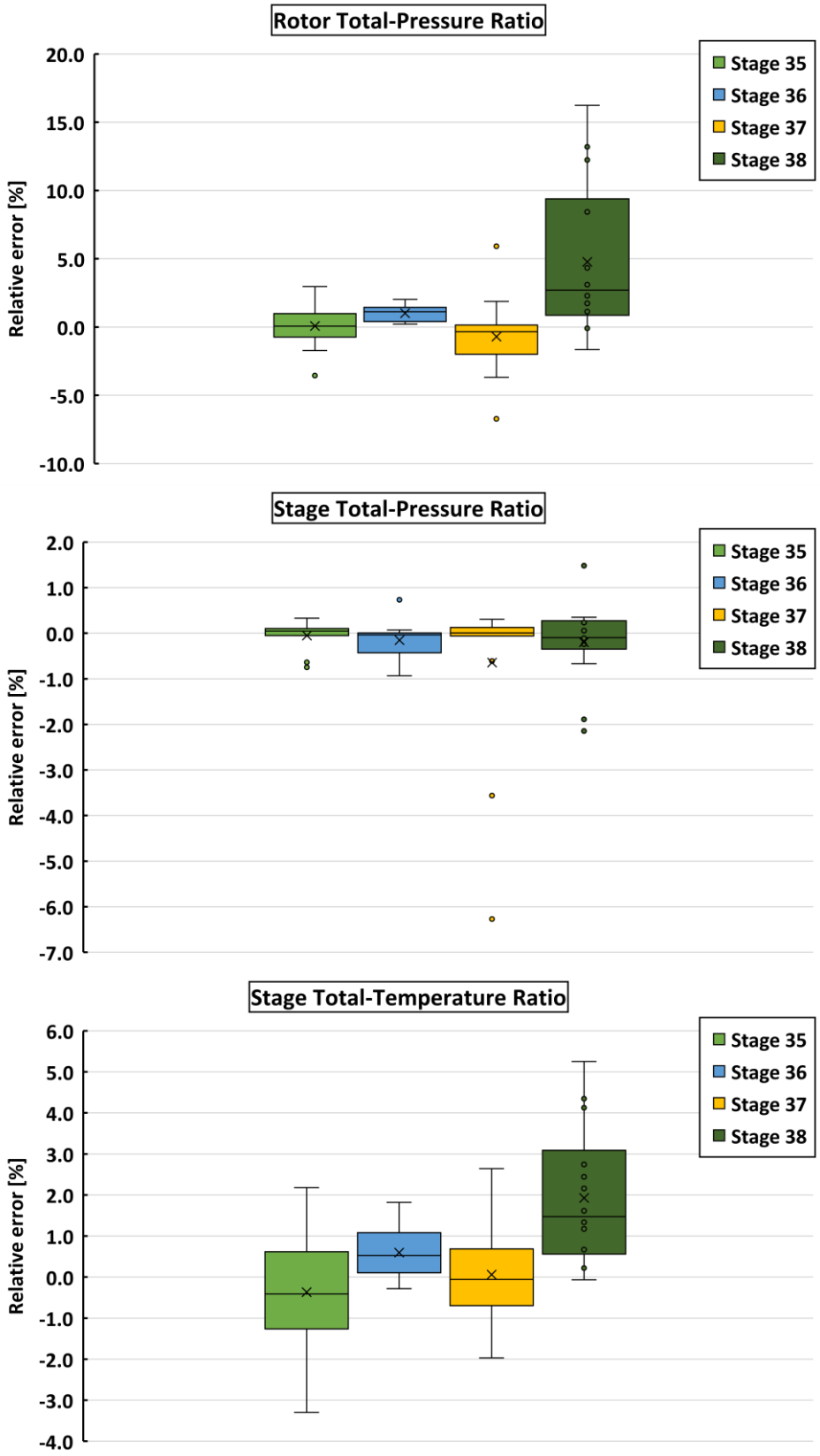

Figure 43: Comparisons of error distributions of Model 3 simulations for Stages 35 to 38

The final objective of the Model 3 exercise was to identify any potential trends in area correction factor from the four stages. To achieve this, the area correction factors from all successful simulations were compared and plotted. This is illustrated in Figure 44 below.

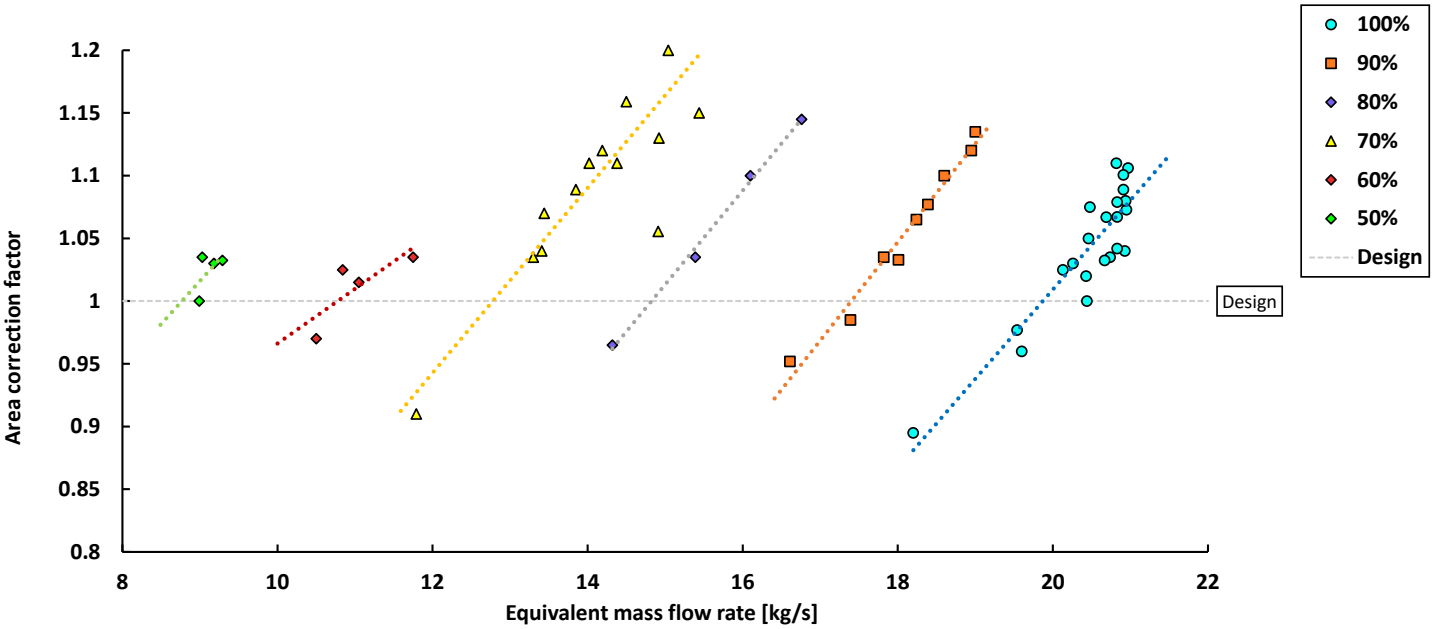

Figure 44: Correlations of manually-tuned area correction factors for Stages 35 to 38

Several important observations can be made from Figure 44. Firstly, area correction factors appear to group on positive-sloping lines of rotor speed. Secondly, all speed-lines appear to have similar gradients, with the exception of the 50% and 60% speed lines. A multiple-regression study was performed to determine the mathematical correlation between the parameter. The resultant correlation is shown in Equation (4.5.5). The correlation returned an adjusted R-squared value of 0.807, showing it to be relatively strong.

$$K_A = 0.07538(\dot{m}) - 9.9912\times10^{-5}(RPM) + 1.227 \tag{4.5.5}$$

It is also noticeable that the area correction factor is less than 1 closer to the surge point, while it tends to increase to well above 1 as mass flow rate increases, for a particular rotor speed. Several factors attributing to these trends were speculated: the area contraction observed near surge in Figure 44 may be attributed to boundary-layer thickening as incidence angle increases and flow separation ensues. This phenomenon may also be exacerbated by an increase in deviation angle near the surge condition, resulting from increased flow separation. If this is the case, then the area correction method would have captured the effects due to off-design deviation angle, without explicitly including it in the calculation. Furthermore, the increasing area correction, and thus increasing degree of flow-area widening with increasing mass flow rate may be attributed to boundary-layer thinning at lower- or negative-incidence angles. However, Mach number effects are

not as easily observed, as interactions between shock-structures and blade suction-surface boundary layer are known to occur at high Mach numbers. It is generally difficult to assess the effects of different physical phenomena on the observed trends separately since a single area correction factor was applied to all flow-path areas, and this may need to be considered in future studies.

Recall that the passage areas predicted by the design-point method resulted in an under-prediction of the physical passage areas by about 10% (see section 4.2). The design point for these compressor stages is at quite a low mass flow, hence one would expect a large blockage factor. This blockage is effectively incorporated into the design-point area result, which means the true physical area should be larger than what was calculated. As the mass flow increases, so the blockage decreases, which means at a high mass flow, one should observe areas closer to the physical area. It is interesting to note that the area correction factor at high mass flows for the 100% speed line is about 1.1, i.e. 10% larger than the design-point condition. There is thus some form of relationship between the blockage factor and the area correction factor. The true meaning of the area correction factor, and what physics it describes is a topic for future studies.

4.6 Model 4 – Implementation of the area correction correlation

The final objective of this study was to evaluate the performance of the area correction correlation derived in the previous section. Successful validation of the method would ultimately achieve the study's aim of developing a mean-line methodology which requires a minimal number of required calibration factors. The validation was performed by applying the derived correlation in the Flownex model of the NASA Stage 35 compressor. Figure 45 compares the area correction factors calculated for Stage 35 using Equation (4.5.5) to those manually tuned in the previous exercise. The full set of simulated data of Model 4 is found in Appendix C Table 21.

Figure 45 indicates that values of area correction factor calculated from the derived empirical correlation generally agree well with the manually-tuned values. The average difference between predicted and manually-tuned values was found to be -0.424%, with the empirical correlation underpredicting the area correction in the majority of cases. The difference between the two values was greatest for the 50% speed-line, with an absolute maximum difference of 4.71%. Both of these metrics indicate good reliability of the derived correlation.

Figure 46 shows the predicted Stage 35 compressor performance map of stage total-pressure ratio from applying the derived correlation. It is evident from Figure 46 that the Model 4 methodology performed generally well in predicting the compressor's off-design behaviour. However, the model underpredicted the surge-points of the 100%, 90%, and 80% speed-lines by around 4%, 2.7%, and

3.4%, respectively. It was postulated that the anomalies in gradient of the 50% and 60% speed lines observed in Figure 44 could have affected the accuracy of the empirical correlation. Additional studies attempted to recalculate the empirical correlation by omitting these speed lines from the data, however little improvement in the predicted surge points was observed. Furthermore, the updated model still suffered issues of solver convergence at the true choke points on the 70% and 90% speed lines.

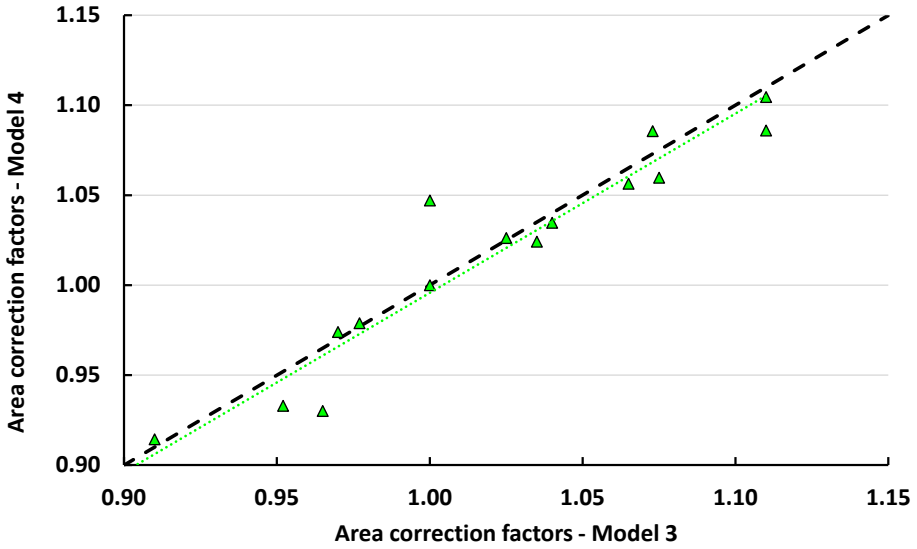

Figure 45: Comparison of area correction factors determined in Models 3 and 4 for Stage 35

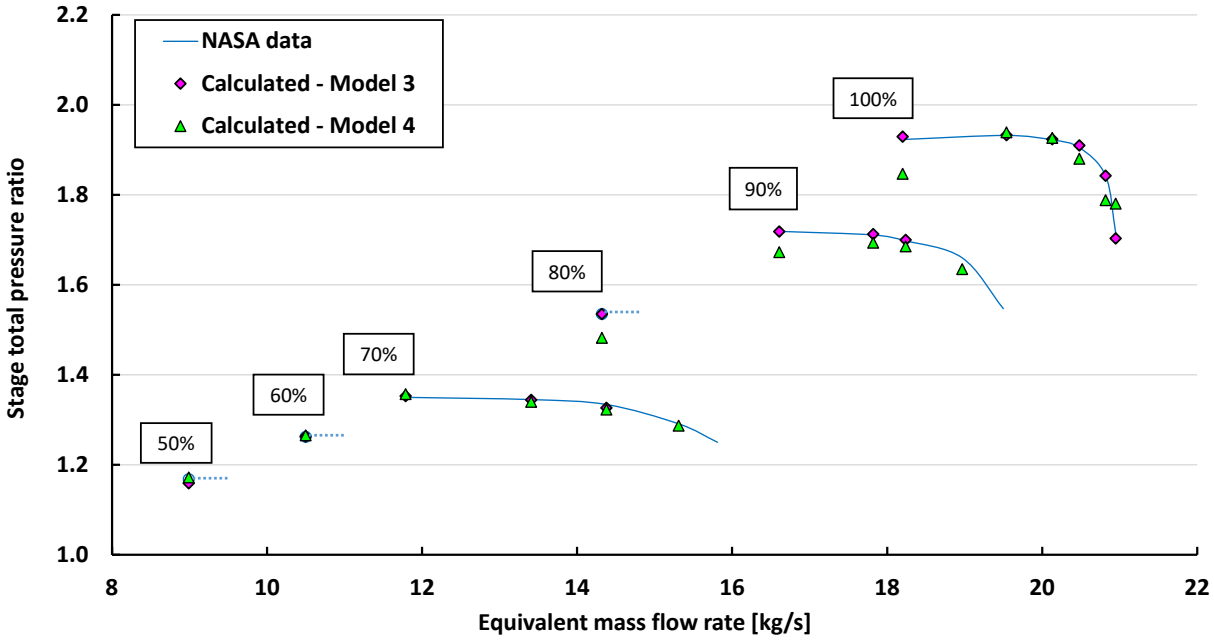

Figure 46: Predicted Stage 35 compressor map using derived empirical correlation of area correction factor

Despite the above, the model was able to accurately predict the surge-points of the remaining speed-lines and performed notably well in predicting most of the 70% speed-line. Overall, these initial observations of the predicted compressor map indicate a general success of the Model 4 methodology.

From the presented findings, it is believed that the Model 4 methodology was an overall success, despite slight increases in error observed from the previous sub-model. For the sake of this study's aims, the range of errors observed in the Model 4 methodology are considered acceptable, especially considering the reduction of required calibration factors achieved through this method.

4.7 Surge-point prediction

The remaining component of a mean-line code is its ability to accurately predict the onset of surge for safe compressor operation. As discussed in the literature review, surge and stall modelling is very complex, and so it is much more convenient to employ a set of easily calculated criteria which warn of the onset of stall. Indeed, this makes more sense for implementation in the Flownex model, as a simple warning message for the onset of stall is sufficient to understand the limits of off-design operation.

Surge-point prediction was not a primary objectives of the current study, and so no warning mechanisms were incorporated into the Flownex model. However, it is still desirable to identify trends in surge behaviour for implementation in later studies. From the literature review, it was found that one of the simplest methods of surge-point prediction was that of Lieblein's diffusion factor [5]. Veres [16] employed the diffusion factor method for predicting the surge-point in their mean-line methodology, and found that the surge-point would typically occur at a rotor diffusion factor of around 0.6. This agreed well with the criteria originally presented by Lieblein. Due to the method's simplicity, it was decided to investigate trends of surge-point diffusion factor in the simulated data for surge-point prediction.

Since the Model 3 methodology predicted surge-point with the greatest accuracy, data of rotor and stator average surge-point diffusion factors calculated using this model was compared for all four NASA stages. Averages were calculated from data of surge-point diffusion factors on all speed lines. The average surge-point rotor and stator diffusion factor calculated for Stage 35 using the Model 4 methodology were also compared for completion. The calculated average surge-point diffusion factors are illustrated in Figure 47 below.

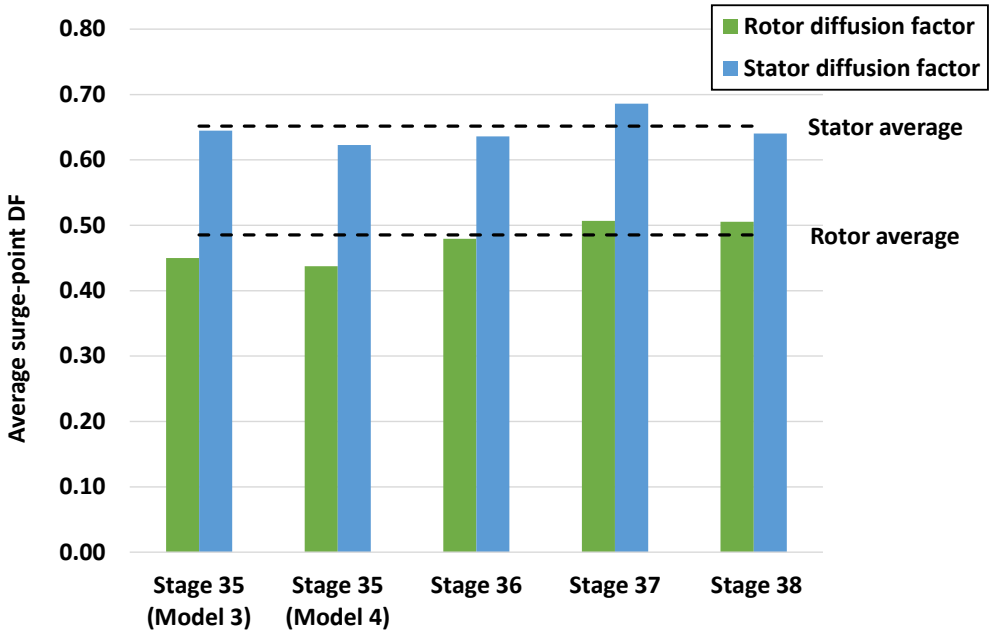

Figure 47: Calculated average rotor and stator surge-point diffusion factors for four NASA stages

Contrary to Veres's findings, the average rotor surge-point diffusion factor calculated from Model 3 was found to be significantly lower than 0.6, with a value of 0.49. Those calculated using Model 4 deviated even further, with an average value of 0.44. However, values of surge-point stator diffusion factor appeared more consistent with Veres's findings, with averages of 0.65 and 0.62 for Models 3 and 4, respectively.

The above findings suggest that it would make sense for this study to adopt a surge-point criteria based on stator diffusion factor. However, a criteria based on rotor diffusion factor is ultimately more logical considering the comparatively higher blade loadings of rotor blades in modern compressors. It may have been beneficial to also investigate trends in axial velocity ratio as Veres did, however this was not done for the present study. Therefore, the above findings are considered inconclusive given the limited extent of investigations, but for the sake of the current study, the surge-point can be related to a rotor diffusion factor of between 0.44 and 0.49.

5. Conclusions and Recommendations

5.1 Conclusions

This study sought to develop and validate a one-dimensional methodology for modelling a transonic axial compressor stage, which requires a minimal number of geometric inputs and tuning factors, as well as minimal knowledge of the compressor's operation. The study also sought to identify a set of appropriate performance models which would ensure adequate accuracy of the methodology, while still conforming to the study's aforementioned aims. Achieving this would ultimately enable compressor operators or analysts to gain greater insight into the machine's off-design operation, without requiring the usually unavailable OEM data.

To achieve the study's aims, a simple modified mean-line method was developed using a diffuser analogy, which modelled the rotor and stator rows in a compressor stage as two one-dimensional diffusers in series, with the rotor diffuser experiencing the relative frame of reference, and the stator diffuser experiencing the absolute frame. The simplified model allowed for compressor performance prediction of acceptable accuracy, while reducing the required knowledge of flow-path geometry.

A design-point calibration method was first developed which required limited knowledge of compressor design-point operation. The design-point calibration exercise served to determine the various flow-passage areas through the compressor stage. These would then be set as inputs to the off-design model. In addition, rotor and stator blade angles were estimated using a successive-approximation scheme, which included a range of widely-referenced correlations from the open literature. The design-point model was able to predict the blade angles of the validation dataset with an average error of less than 2.3°, with exception of the stator exit angle. Creation of a three-dimensional CAD model of the NASA Stage 35 compressor also assisted in validating flow-passage area predictions.

An off-design model was developed in Flownex SE using the Restrictor with Loss Coefficient component to model the rotor and stator diffusers. A scripting component was included to perform the mean-line calculation. The Flownex model was validated against four well-documented single-stage compressors from NASA. Stage 35 was the primary focus for all model building and final model validation.

Extensive review of the open literature showed that the most appropriate compressor loss model for off-design modelling that would result in the simplest calculation was that of Çetin. In addition, an off-design deviation angle model was omitted to reduce required calibration efforts.

Further validation exercises showed that use of Çetin's method alone returned results of poor accuracy, with strong overprediction of surge-point on most speed-lines. This was mostly attributed to the Flownex solver miscalculating the diffuser upstream- and downstream-areas, resulting in miscalculation of total pressure losses. To address this, a single area correction factor was applied to all upstream- and downstream-areas of both rotor and stator diffusers. The method yielded far more accurate results of stage total-pressure ratio compared to the previous sub-model. In addition, improved accuracy was observed for rotor total-pressure ratio, while good prediction accuracy was found for stage total-temperature ratio, despite these not being the primary parameters of focus in model calibration.

A strong multiple-linear correlation was found between the manually-tuned area correction factor, off-design mass flow rate and rotor RPM. The correlation predicted similar correction factors to the manually-tuned values within an average difference of around 0.4%, and a maximum difference less than 5%. Application of the empirical correlation within the Flownex model showed generally acceptable agreement with the Stage 35 data. The model was able to predict rotor total-pressure ratio and stage total-temperature ratio within acceptable limits.

Perhaps the greatest shortfall in the developed methodology was the Flownex solver's inability to achieve convergence at the true choke points in most cases, and in all sub-model iterations. This was predominantly attributed to poor solver stability, which would have likely been improved through use and calibration of relaxation parameters. Furthermore, it was believed that the solver would have likely accomplished convergence at mass flow rates slightly lower than those at the reported choke points. However, this was not investigated further.

Despite the abovementioned shortfalls, the developed model achieved the study's primary aim of providing a simple means of accurately predicting compressor stage performance while requiring a limited knowledge of compressor geometry and design-point operation. Furthermore, the study was able to improve model accuracy by employing only a single tuning factor of flow-passage areas, thus greatly reducing the complexity of model calibration when compared to previous studies.

5.2 Recommendations

Based on assessment of the study's shortfalls, the following opportunities for future studies are identified:

- Improvements to the model's choke-point prediction should be pursued. This will most likely involve investigations of improving solver stability.
- Observed trends of area correction factor in the Model 3 exercise could not be related to their underlying physics. Future studies should place focus on determining which underlying physics contribute to the observed variations in area correction factor, and whether the coefficients for the correlation could possibly be determined from physical compressor parameters.
- Lastly, the current work was unable to determine an appropriate set of surge-point prediction criteria. Since only a diffusion factor-based criterion was assessed in this study, future works should investigate alternative criteria such as axial-velocity ratio and stalling pressure rise capability.

References

[1] W. F. Fuls, “Accurate stage-by-stage modelling of axial turbines using an appropriate nozzle analogy with minimal geometric data,” *Appl. Therm. Eng.*, vol. 116, pp. 134–146, 2017, doi: 10.1016/j.applthermaleng.2017.01.048.

[2] S. L. Dixon and C. A. Hall, *Fluid mechanics and thermodynamics of turbomachinery, 7th edition*. 2013.

[3] J. Kidikian, “An Off-Design Mean-Line Methodology to Predict the Missing Data of Single-Stage Transonic Axial Compressor Tests,” Polytechnique Montreal, 2019.

[4] S. Lieblein, F. C. Schwenk, and R. L. Broderick, “Diffusion Factor for Estimating Losses and Limiting Blade Loading in Axial-Flow-Compressor Blade Elements,” *Natl. Advis. Comm. Aeronaut.*, 1953.

[5] S. Lieblein, “Experimental Flow in Two-Dimensional Cascades,” in *Aerodynamic Design of Axial-Flow Compressors*, National Aeronautics and Space Administration, 1965, pp. 183–226.

[6] S. Lieblein, “Loss and Stall Analysis of Compressor Cascades,” *J. Basic Eng.*, vol. 81, no. 3, pp. 387–397, 1959, doi: 10.1115/1.4008481.

[7] A. D. S. Carter, “The Low Speed Performance Of Related Aerofoils In Cascades,” *Aeronaut. Res. Counc.*, vol. NGTE-R55, no. 19, pp. 1–20, 1950.

[8] C. C. Koch and L. H. Smith, “Loss sources and magnitudes in axial-flow compressors,” *J. Eng. Gas Turbines Power*, vol. 98, no. 3, pp. 411–424, 1976, doi: 10.1115/1.3446202.

[9] N. Falck, “Axial Flow Compressor Mean Line Design,” Lund University, 2008.

[10] M. Çetin, A. S. Ucer, C. Hirsch, and G. K. Serovy, “Application of modified loss and deviation correlations to transonic axial compressors,” *AGARD Rep. No.745*, pp. 1–75, 1987.

[11] M. V. Petrovic, A. Wiedermann, and M. B. Banjac, “Development and validation of a new universal through flow method for axial compressors,” *Proc. ASME Turbo Expo*, vol. 7, no. PART A, pp. 579–588, 2009, doi: 10.1115/GT2009-59938.

[12] A. D. S. Carter, “The Calculation of Optimum Incidences for Aerofoils,” *Aeronaut. Res. Counc.*, no. 646, pp. 1–21, 1961.

[13] K. M. Boyer, “An Improved Streamline Curvature Approach for Off-Design Analysis of Transonic Compression Systems,” Virginia Polytechnic Institute and State University, 2001.

[14] I. A. Johnsen and R. O. Bullock, “Aerodynamic Design of Axial-Flow Compressors,” *NASA SP-36*, 1965.

[15] H. F. Creveling and R. H. Carmody, “Axial Flow Compressor Computer Program For Calculating Off-Design Performance,” *NASA CR-72427*, no. 10873, pp. 1–21, 1968.

[16] J. P. Veres, “Axial and centrifugal compressor mean line flow analysis method,” *47th Aerosp. Sci. Meet.*, vol. AIAA-2009-, 2009, doi: 10.2514/6.2009-1641.

[17] P. I. Wright and D. C. Miller, “An improved compressor performance prediction model,” 1992.

[18] W. M. König, D. K. Hennecke, and L. Fottner, “Improved Blade Profile Loss and Deviation Angle

Models for Advanced Transonic Compressor Bladings: Part I - A Model for Subsonic Flow," in *Proceedings of the ASME International Gas Turbine and Aeroengine Congress and Exposition*, 1994, pp. 1–9.

[19] M. Manfredi and F. Fontaneto, "Transonic Axial Compressors Loss Correlations: Part I - Analysis and Update of Loss Models," *Proc. ASME Turbo Expo 2020 Turbomach. Tech. Conf. Expo.*, vol. 2A: Turbo, pp. 1–14, 2020.

[20] G. Crutzen, "Loss Sources and Magnitudes Breakdown in an Axial Low Pressure Compressor Blade Row," Liège University, 2020.

[21] G. R. Miller, G. W. Lewis, and M. J. Hartmann, "Shock losses in transonic compressor blade rows," *J. Eng. Gas Turbines Power*, vol. 83, no. 3, pp. 235–241, 1961, doi: 10.1115/1.3673182.

[22] W. M. König, D. K. Hennecke, and L. Fottner, "Improved Blade Profile Loss and Deviation Angle Models for Advanced Transonic Compressor Bladings: Part II - A Model for Supersonic Flow," *J. Turbomach.*, vol. 117, pp. 81–87, 1996.

[23] S. L. Smith, "1-D Mean Line Code Technique to Calculate Stage-by-Stage Compressor Characteristics," The University of Tennessee, 1999.

[24] C. C. Koch, "Stalling Pressure Rise Capability of Axial Flow Compressor Stages.," *Am. Soc. Mech. Eng.*, vol. 103, no. 81-GT-3, pp. 645–656, 1981.

[25] L. R. Reneau, J. P. Johnston, and S. J. Kline, "Performance and design of straight, two-dimensional diffusers," *J. Fluids Eng. Trans. ASME*, vol. 89, no. 1, pp. 141–150, 1967, doi: 10.1115/1.3609544.

[26] J. Li, J. Teng, M. Ferlauto, M. Zhu, and X. Qiang, "An improved stall prediction model for axial compressor stage based on diffuser analogy," *Aerosp. Sci. Technol.*, vol. 127, 2022, doi: 10.1016/j.ast.2022.107692.

[27] J. R. Barbosa, "A Streamline Curvature Computational Programme for Axial Compressor Performance Prediction," Cranfield Institute of Technology, 1986.

[28] D. Cadrecha, J. M. Chaquet, R. Corral, and V. P. Timon, "Robust method to solve meanline equations for choked flows," in *Proceedings of the ASME Turbo Expo*, 2018, vol. 2C-2018, doi: 10.1115/GT201875362.

[29] R. J. Steinke, "Design of 9.271-pressure-ratio 5-stage compressor and overall performance for first 3 stages.," *NASA Tech. Pap. 2597*, pp. 1–32, 1986.

[30] "Flownex Simulation Environment." [Online]. Available: https://flownex.com/.

[31] "Flownex Library Manual," 2021. www.flownex.com.

[32] A. C. Marx and W. F. Fuls, "Determining appropriate loss coefficients for use in the nozzle-model of a stage-by-stage turbine model," University of Cape Town, 2019.

[33] L. Reid and R. D. Moore, "Performance of Single-Stage Axial-Flow Transonic Compressor With Rotor and Stator Aspect Ratios of 1.19 and 1.26, Respectively, and With Design Pressure Ratio of 1.82," 1978. [Online]. Available: https://ntrs.nasa.gov/citations/19790001889.

[34] R. D. Moore and L. Reid, "Performance of Single-Stage Axial-Flow Transonic Compressor With Rotor and Stator Aspect Ratios of 1.63 and 1.78, Respectively, and With Design Pressure Ratio of 1.82.," 1982. [Online]. Available: https://ntrs.nasa.gov/citations/19820011348.

[35] R. D. Moore and L. Reid, “Performance of Single-Stage Axial-Flow Transonic Compressor With Rotor and Stator Aspect Ratios of 1.19 and 1.26, Respectively, and With Design Pressure Ratio of 2.05,” 1980. [Online]. Available: https://ntrs.nasa.gov/citations/19800012840.

[36] R. D. Moore and L. Reid, “Performance of Single-Stage Axial-Flow Transonic Compressor With Rotor and Stator Aspect Ratios of 1.63 and 1.77, Respectively, and With Design Pressure Ratio of 2.05,” 1982. [Online]. Available: https://ntrs.nasa.gov/citations/19820014395.

[37] L. Reid and R. D. Moore, “Design and Overall Performance of Four Highly Loaded, High-Speed Inlet Stages for an Advanced High-Pressure-Ratio Core Compressor,” *NASA Tech. Pap. 1337*, no. 1337, pp. 1–119, 1978, [Online]. Available: https://ntrs.nasa.gov/citations/19780025165.

[38] “Flownex SE 18 General User Manual,” 2021. https://flownex.com/.

[39] X. Yu, Z. Zhang, and B. Liu, “The evolution of the flow topologies of 3D separations in the stator passage of an axial compressor stage,” *Exp. Therm. Fluid Sci.*, vol. 44, pp. 301–311, 2013, doi: 10.1016/j.expthermflusci.2012.07.002.

[40] G. Bar-Meir, *Fundamentals of Compressible Fluid Mechanics*, 0.5.0. Chicago, 2021.

Appendix A. Design-point analytical calculation

Design Prediction

This model makes use of minimal information that would typically be availabe, as well as some common design assumptions to estimae the blade angles and areas

Operating conditions (Reid & Moore, 1978):

Design-point mass flow rate : $m'_D := 20.188 \frac{kg}{s}$

Design-point rotor speed : $\omega_D := 17188.70 rpm = 1800 \frac{1}{s}$

Inlet conditions:

Inlet total pressure : $p_{01} := 101.4 \cdot kPa$

Inlet total temperature : $T_{01} := 15\ ℃$

General fluid properties:

Specific heat of air at constant pressure : $c_p := 1.004 \frac{kJ}{kg \cdot K}$

Air specific heat ratio : $\gamma_a := 1.400$

Air gas constant : $R_a := \frac{c_p \cdot (\gamma_a - 1)}{\gamma_a} = 0.287 \cdot \frac{kJ}{kg \cdot K}$

Geometry:

Hub radius : $r_h := 17.78 \cdot cm$

Tip radius : $r_t := 25.4 \cdot cm$

from p77

Mean-line radius $r_m := \frac{r_t + r_h}{2} = 0.216\,m$

Inlet passage area : $A_{inlet} := \pi \cdot \left(r_t^{\,2} - r_h^{\,2} \right) = 1033.68 \cdot cm^2$

Inlet flow angle : $\alpha_1 := 0°$

Performance

Total temperature ratio : $T_{RD} := 1.225$ *same as enthalpy ratio* $\frac{h_{03}}{h_{01}}$

Loss constants

Average rotor total pressure loss coefficient : $Y_R \equiv 0.187$

Average statot total pressure loss coefficient : $Y_S \equiv 0.084$

Validation parameters

Meridional inlet velocity : $c_{1x(exp)} := 205.255 \frac{m}{s}$

Relative rotor inlet Mach number : $M_{1rel(exp)} := 1.347$

Meridional stator inlet velocity : $c_{3x(exp)} := 184 \cdot \frac{m}{s}$

Stator inlet Mach number : $M_{3(exp)} := 0.7289$

Stator exit Mach number : $M_{4(exp)} := 0.6085$

Stage total pressure ratio : $\Pi_D := 1.82$

Areas from CAD model : $A_{inlet(CAD)} := 1033.68\ cm^2$

$A_{Rin(CAD)} := 518.76\ cm^2$

$A_{Rex(CAD)} := 531.36\ cm^2$

$A_{Sin(CAD)} := 604.9\ cm^2$

$A_{Sex(CAD)} := 650.808\ cm^2$

Blade angles from data : $\kappa_{1(exp)} := -55.860°$

$\kappa_{2(exp)} := -44.419°$

$\kappa_{3(exp)} := 33.871°$

$\kappa_{4(exp)} := 3.114°$

Power input from detail model : $W'_{D(exp)} := 1359.704 \cdot kW$

Calculated inlet static conditions

Mean blade speed : $u_D := \omega_D \cdot r_m = 388.619 \frac{m}{s}$

guess : $T_1 := T_{01}$ $p_1 := p_{01}$ $c_{1x} := 0.5 \cdot u_D$

Given

$$m'_D = \frac{p_1}{R_a \cdot T_1} \cdot c_{1x} \cdot A_{inlet} \qquad p_1 = p_{01} \cdot \left(\frac{T_{01}}{T_1} \right)^{-\frac{\gamma_a}{\gamma_a - 1}} \qquad T_1 = T_{01} - \frac{c_{1x}^2}{2 \cdot c_p}$$

$$\begin{pmatrix} c_{1x} \\ T_1 \\ p_1 \end{pmatrix} := Find\left(c_{1x}, T_1, p_1\right)$$

$c_{1x} = 185.611 \frac{m}{s}$

$p_1 = 81.795 \cdot kPa$

$T_1 = -2.157 \cdot ℃$

$\rho_1 := \frac{p_1}{R_a \cdot T_1} = 1.052 \frac{kg}{m^3}$

Estimated dimensionless design parameters :

Inlet total enthalpy : $h_{01} := c_p \cdot T_{01} = 289.303 \cdot \frac{kJ}{kg}$

Outlet total temperature : $T_{03} := T_{01} \cdot \tau_{RD} = 79.834 \cdot ℃$

Outlet total enthalpy : $h_{03} := c_p \cdot T_{03}$

Mean-line stage loading : $\psi_D := \frac{h_{03} - h_{01}}{u_D^2} = 0.431$

Mean-line rotor-inlet flow coefficient : $\phi_D := \frac{c_{1x}}{u_D} = 0.478$

Additional functions:

$$\angle(mag, ang) := \begin{pmatrix} mag \cdot cos(ang) \\ mag \cdot sin(ang) \end{pmatrix}$$

$x := 0 \qquad \theta := 1$

Design-point flow angles:

$$\beta_2 := -atan\left(\frac{1-\psi_D}{\phi_D} - tan(\alpha_1)\right) = -49.99 \cdot °$$

Rotor-inlet velocity triangle:

$$U := u_D \angle (90°) = \begin{pmatrix} 0 \\ 388.619 \end{pmatrix} \frac{m}{s}$$

$$c_{1x} := \phi_D \cdot |U| = 185.611 \frac{m}{s}$$

$$\frac{|c_{1x(exp)} - c_{1x}|}{c_{1x(exp)}} = 9.57 \cdot \%$$

$$c_1 := \frac{c_{1x}}{cos(\alpha_1)} = 185.611 \frac{m}{s}$$

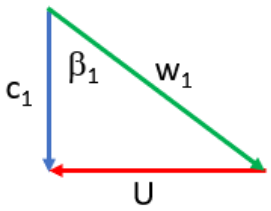

$$C_1 := c_1 \angle \alpha_1 = \begin{pmatrix} 185.611 \\ 0 \end{pmatrix} \frac{m}{s}$$

$$W_1 := C_1 - U = \begin{pmatrix} 185.611 \\ -388.619 \end{pmatrix} \frac{m}{s}$$

$$w_1 := |W_1| = 430.67 \frac{m}{s}$$

$$\beta_1 := atan2\left(W_{1_x}, W_{1_\theta}\right) = -64.47 \cdot °$$

$$M_{1rel} := \frac{w_1}{\sqrt{\gamma_a \cdot R_a \cdot T_1}} = 1.305$$

$$\frac{|M_{1rel(exp)} - M_{1rel}|}{M_{1rel(exp)}} = 3.083 \cdot \%$$

Rotor total inlet properties:

$$h_1 := c_p \cdot T_1$$

$$h_{01rel} := h_1 + 0.5 w_1^{\,2} = 364.815 \cdot \frac{kJ}{kg}$$

$$T_{01rel} := T_1 + \frac{w_1^{\,2}}{2 c_p} = 90.212 \cdot ℃$$

$$p_{01rel} := p_1 \cdot \left(\frac{T_{01rel}}{T_1} \right)^{\left(\frac{\gamma_a}{\gamma_a - 1} \right)} = 228.328 \cdot kPa$$

Treatment of pressure shock :

Conditions after shock

$$M_{1rel\_y} := \sqrt{\frac{M_{1rel}^{\,2} + \frac{2}{\gamma_a - 1}}{\left(\frac{2 \cdot \gamma_a}{\gamma_a - 1} \right) \cdot M_{1rel}^{\,2} - 1}} = 0.783$$

$$w_{1\_y} := w_1 \cdot \left[\frac{\left(\gamma_a + 1 \right) \cdot M_{1rel}^{\,2}}{2 + \left(\gamma_a - 1 \right) \cdot M_{1rel}^{\,2}} \right]^{-1} = 282.363 \frac{m}{s} \qquad w_1 = 430.67 \frac{m}{s}$$

$$p_{1\_y} := p_1 \cdot \left[1 + \frac{2 \cdot \gamma_a}{\gamma_a + 1} \cdot \left(M_{1rel}^{\,2} - 1 \right) \right] = 149.001 \cdot kPa \qquad p_1 = 81.795 \cdot kPa$$

$$T_{1\_y} := T_{01rel} - \frac{w_{1\_y}^{\,2}}{2 \cdot c_p} = 50.506 \cdot ℃$$

$$\rho_{1\_y} := \frac{\rho_1 \cdot w_1}{w_{1\_y}} = 1.605 \frac{kg}{m^3}$$

$$p_{01rel\_y} := p_{1\_y} \cdot \left(\frac{T_{01rel}}{T_{1\_y}} \right)^{\left(\frac{\gamma_a}{\gamma_a - 1} \right)} = 223.399 \cdot kPa \qquad p_{01rel} = 228.328 \cdot kPa$$

Rotor total pressure drop:

$$p_{02rel} := p_{01rel\_y} - Y_R \cdot \left(p_{01rel\_y} - p_{1\_y}\right) = 209.487 \cdot kPa$$

Rotor exit total temperature:

$$h_{02} := h_{01} \qquad h_{02rel} := h_{01rel}$$

$$T_{02} := T_{01} \qquad T_{02rel} := T_{01rel}$$

Convergance of rotor-exit / stator-inlet properties:

Guess stage intermediate pressure: $p_2 := p_1$

$$T_2(p_2) := T_{02rel} \cdot \left(\frac{p_{02rel}}{p_2}\right)^{-\left(\frac{\gamma_a - 1}{\gamma_a}\right)}$$

$$w_2(p_2) := \sqrt{2 \cdot c_p \cdot \left(T_{02rel} - T_2(p_2)\right)}$$

$$c_3(p_2) := \sqrt{2 \cdot c_p \cdot \left(T_{03} - T_2(p_2)\right)}$$

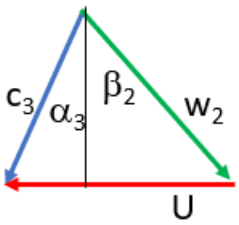

$$c'_3(p_2) := \sqrt{\left(w_2(p_2)\right)^2 + \left(U_\theta\right)^2 + 2 \cdot \left(w_2(p_2)\right) \cdot U_\theta \cdot \sin\left(\beta_2\right)}$$

$$p_2 := root\left(c'_3(p_2) - c_3(p_2), p_2\right) = 137.019 \cdot kPa$$

Stage intermediate properties:

$$w_2 := w_2(p_2) = 288.697\frac{m}{s}$$

$$W_2 := w_2 \angle \beta_2 = \begin{pmatrix} 185.611 \\ -221.121 \end{pmatrix}\frac{m}{s}$$

$$C_3 := W_2 + U = \begin{pmatrix} 185.611 \\ 167.498 \end{pmatrix}\frac{m}{s} \qquad c_3 := |C_3| = 250.014\frac{m}{s}$$

$$\alpha_3 := atan\left(\frac{C_{3_\theta}}{C_{3_x}}\right) = 42.064\cdot°$$

$$T_2 := T_2(p_2) = 48.705\cdot℃$$

$$h_2 := c_p\cdot T_2 = 323.142\cdot\frac{kJ}{kg}$$

$$\rho_2 := \frac{p_2}{R_a\cdot T_2} = 1.484\frac{kg}{m^3} \qquad \rho_3 := \rho_2$$

$$h_3 := h_2 = 323.142\cdot\frac{kJ}{kg}$$

$$T_3 := T_2 = 48.705\cdot℃$$

$$p_3 := p_2$$

$$p_{03} := p_3\cdot\left(\frac{T_{03}}{T_3}\right)^{\left(\frac{\gamma_a}{\gamma_a - 1}\right)} = 189.283\cdot kPa$$

$$M_{2rel} := \frac{w_2}{\sqrt{\gamma_a\cdot R_a\cdot T_2}} = 0.803$$

$$M_3 := \frac{c_3}{\sqrt{\gamma_a\cdot R_a\cdot T_3}} = 0.695$$

$$\frac{|M_{3(exp)} - M_3|}{M_{3(exp)}} = 4.595\cdot\%$$

Stator exit properties:

Stator pressure drop:

$p_{04} := p_{03} - Y_S \cdot \left(p_{03} - p_3\right) = 184.893 \cdot kPa$ $\quad \frac{p_{04}}{p_{01}} = 1.823$

$T_{04} := T_{03} = 79.834 \cdot ℃$

$h_{04} := h_{03}$

Assume repeating stage $\quad c_{4x} := c_{1x} \quad \alpha_4 := \alpha_1$

$c_4 := \frac{c_{4x}}{\cos\left(\alpha_4\right)} = 185.611 \frac{m}{s}$

$h_4 := h_{04} - 0.5 \cdot {c_4}^2$

$T_4 := \frac{h_4}{c_p} = 62.677 \cdot ℃$

$p_4 := p_{04} \cdot \left(\frac{T_{04}}{T_4}\right)^{-\left(\frac{\gamma_a}{\gamma_a - 1}\right)} = 155.304 \cdot kPa$

$C_4 := c_4 \angle \alpha_4 = \begin{pmatrix} 185.611 \\ 0 \end{pmatrix} \frac{m}{s} \quad c_4 := \left|C_4\right| = 185.611 \frac{m}{s}$

$\rho_4 := \frac{p_4}{R_a \cdot T_4} = 1.612 \frac{kg}{m^3}$

$M_4 := \frac{c_4}{\sqrt{\gamma_a \cdot R_a \cdot T_4}} = 0.505$

$\frac{\left|M_{4(exp)} - M_4\right|}{M_{4(exp)}} = 16.941 \cdot \%$

Summary of kinematics:

Rotor inlet velocity triangle:

$$C_1 = \begin{pmatrix} 185.611 \\ 0 \end{pmatrix} \frac{m}{s} \qquad \alpha_1 = 0 \cdot °$$

$$W_1 = \begin{pmatrix} 185.611 \\ -388.619 \end{pmatrix} \frac{m}{s} \qquad \beta_1 = -64.47 \cdot °$$

$$U = \begin{pmatrix} 0 \\ 388.619 \end{pmatrix} \frac{m}{s} \qquad M_{1rel} = 1.305$$

$$\frac{\left| c_{1x(exp)} - c_{1x} \right|}{c_{1x(exp)}} = 9.57 \cdot \%$$

Rotor exit / stator inlet velocity triangle:

$$C_3 = \begin{pmatrix} 185.611 \\ 167.498 \end{pmatrix} \frac{m}{s} \qquad \alpha_3 = 42.064 \cdot °$$

$$W_2 = \begin{pmatrix} 185.611 \\ -221.121 \end{pmatrix} \frac{m}{s} \qquad \beta_2 = -49.99 \cdot °$$

$$U = \begin{pmatrix} 0 \\ 388.619 \end{pmatrix} \frac{m}{s} \qquad M_3 = 0.695$$

$$M_{2rel} = 0.803$$

$$\frac{\left| M_{3(exp)} - M_3 \right|}{M_{3(exp)}} = 4.595 \cdot \%$$

$$C_{3_x} = 185.611 \frac{m}{s}$$

$$\frac{\left| c_{3x(exp)} - C_{3_x} \right|}{c_{3x(exp)}} = 0.876 \cdot \%$$

Stator exit velocity triangle:

$$C_4 = \begin{pmatrix} 185.611 \\ 0 \end{pmatrix} \frac{m}{s} \qquad \alpha_4 = 0 \cdot °$$

$$M_4 = 0.505$$

$$\frac{\left| M_{4(exp)} - M_4 \right|}{M_{4(exp)}} = 16.941 \cdot \%$$

Model calibration check:

Stage total pressure ratio:

$$\Pi_{stage} := \frac{p_{04}}{p_{01}} = 1.823$$

$$\frac{\Pi_D - \Pi_{stage}}{\Pi_D} = -0.187 \cdot \%$$

adjust loss coefficients until convergence is acieved

Estimated diffuser areas and diameters:

$$A_{inlet} := \frac{m'_D}{c_1 \cdot \rho_1} = 0.10337 \cdot m^2$$

$$\frac{A_{inlet} - A_{inlet(CAD)}}{A_{inlet(CAD)}} = 3.151 \times 10^{-4} \cdot \%$$

$$A_{Rin} := \frac{m'_D}{w_1 \cdot \rho_1} = 0.04455 \cdot m^2 \qquad A_{annR(in)} := \frac{m'_D}{w_1 \cdot \rho_1 \cdot \cos(\beta_1)} = 0.10337 \cdot m^2$$

$$\frac{A_{Rin} - A_{Rin(CAD)}}{A_{Rin(CAD)}} = -14.122 \cdot \%$$

$$A_{Rex} := \frac{m'_D}{w_2 \cdot \rho_2} = 0.04712 \cdot m^2 \qquad A_{annR(ex)} := \frac{m'_D}{w_2 \cdot \rho_2 \cdot \cos(\beta_2)} = 0.073\, m^2$$

$$\frac{A_{Rex} - A_{Rex(CAD)}}{A_{Rex(CAD)}} = -11.324 \cdot \%$$

$$A_{Sin} := \frac{m'_D}{c_3 \cdot \rho_3} = 0.05441 \cdot m^2 \qquad A_{annS(in)} := \frac{m'_D}{c_3 \cdot \rho_3 \cdot \cos(\alpha_3)} = 0.07329 \cdot m^2$$

$$\frac{A_{Sin} - A_{Sin(CAD)}}{A_{Sin(CAD)}} = -10.052 \cdot \%$$

$$A_{Sex} := \frac{m'_D}{c_4 \cdot \rho_4} = 0.06747 \cdot m^2 \qquad A_{annS(ex)} := \frac{m'_D}{c_4 \cdot \rho_4} \cdot \frac{1}{\cos(\alpha_4)} = 0.067\, m^2$$

$$\frac{A_{Sex} - A_{Sex(CAD)}}{A_{Sex(CAD)}} = 3.666 \cdot \%$$

$$\frac{W' - W'_{D(exp)}}{W'_{D(exp)}} = -3.354 \cdot \%$$

$$DesignAngles\left(\alpha_{in}, \alpha_{ex}, blade, blade\_type, t/l, C_i, C_\delta\right) :=$$

$sign \leftarrow Sign(blade)$

$\alpha_{1.} \leftarrow \left|\frac{\alpha_{in}}{deg}\right|$

$blade\_type \leftarrow$ "DCA" if $blade\_type \neq$ "DCA" $\vee$ $blade\_type \neq$ "NACA65" $\vee$ $blade\_type \neq$ "C-Series"

$$K_{sh} \leftarrow \begin{cases} 0.7 & \text{if } blade\_type = \text{"DCA"} \\ 1.0 & \text{if } blade\_type = \text{"NACA65"} \\ 1.1 & \text{if } blade\_type = \text{"C-Series"} \end{cases}$$

$$K_{it} \leftarrow -0.0214 + 19.17 \cdot (t/l) - 122.3\,(t/l)^2 + 312.5\,(t/l)^3$$

$$K_{\delta t} \leftarrow 0.0142 + 6.172(t/l) + 36.61\,(t/l)^2$$

$$\sigma \leftarrow \begin{cases} \sigma_R & \text{if } blade = \text{"R"} \\ \sigma_S & \text{if } blade = \text{"S"} \end{cases}$$

$$i_{010} \leftarrow (0.0325 - 0.0674\sigma) + (-0.002364 + 0.0913\sigma)\cdot\alpha_1 + \left(1.64\cdot10^{-5} - 2.38\cdot10^{-4}\sigma\right)\cdot\alpha_1^{\,2}$$

$$n \leftarrow (-0.063 - 0.02274\sigma) + (-0.0035 + 0.0029\sigma)\cdot\alpha_1 - \left(3.79\cdot10^{-5} + 1.11\cdot10^{-5}\sigma\right)\cdot\alpha_1^{\,2}$$

$$\delta_{010} \leftarrow (-0.0443 + 0.1057\sigma) + (0.0209 - 0.0186\sigma)\cdot\alpha_1 + (-0.0004 + 0.00076\sigma)\cdot\alpha_1^{\,2}$$

$$b \leftarrow 0.9655 + 2.538\cdot10^{-3}\cdot\alpha_1 + 4.221\cdot10^{-5}\cdot\alpha_1^{\,2} - 1.3\cdot10^{-6}\alpha_1^{\,3}$$

$$m_{\delta'} \leftarrow \begin{cases} \left[0.17 - 3.33\cdot10^{-4}\cdot\left(1.0 - 0.1\alpha_1\right)\cdot\alpha_1\right] & \text{if } blade\_type = \text{"NACA65"} \\ \left(0.249 + 7.4\cdot10^{-4}\alpha_1 - 1.32\cdot10^{-5}\cdot\alpha_1^{\,2} + 3.16\cdot10^{-7}\alpha_1^{\,3}\right) & \text{otherwise} \end{cases}$$

$$m_\delta \leftarrow \frac{m_{\delta'}}{\sigma^{\,b}}$$

$i_{ref} \leftarrow 0$

$\delta_{ref} \leftarrow 0$

$iter \leftarrow 0$

$err_i \leftarrow 1000$

$err_\delta \leftarrow 1000$

while $err_i > 0.001 \wedge err_\delta > 0.001 \wedge iter < 50$

$iter \leftarrow iter + 1$

$i_{old} \leftarrow i_{ref}$

$\delta_{old} \leftarrow \delta_{ref}$

$$\kappa_1 \leftarrow \frac{\alpha_{in}}{deg} - sign\cdot\left(i_{ref}\right)$$

$$\kappa_2 \leftarrow \frac{\alpha_{ex}}{deg} - sign\cdot\left(\delta_{ref}\right)$$

$\theta \leftarrow \left|\kappa_1 - \kappa_2\right|$

$$i_{ref} \leftarrow K_{sh}\cdot K_{it}\cdot i_{010} + n\cdot\theta + \frac{C_i}{deg}$$

$$\delta_{ref} \leftarrow K_{sh}\cdot K_{\delta t}\cdot\delta_{010} + m_\delta\cdot\theta + \frac{C_\delta}{deg}$$

$$err_i \leftarrow \frac{\left|i_{ref} - i_{old}\right|}{\left|i_{ref}\right|}$$

$$err_\delta \leftarrow \frac{\left|\delta_{ref} - \delta_{old}\right|}{\left|\delta_{ref}\right|}$$

$i_D \leftarrow i_{ref}$

$\delta_D \leftarrow \delta_{ref}$

$$\begin{pmatrix} i_D \\ \delta_D \\ err_i \\ err_\delta \\ iter \end{pmatrix}$$

Appendix B. Flownex model main script code

```
public class Script: IPS.Scripting.IComponentScript
{

    public static double CetinLoss(int blade_type, double inc, double inc_design, double Y_design, double M_in)
    {
        double c_m = 0;
        double diff = (inc * 180 / Math.PI) - (inc_design * 180 / Math.PI);

        if (blade_type == 0)    // Corresponding to blade type MCA
        {
            if (diff <= 0)
            {
                c_m = (0.02845 * M_in) - 0.01741;
            }
            else if (diff > 0)
            {
                c_m = (0.00363 * M_in) - 0.00065;
            }
        }
        else if (blade_type == 1)    // Corresponding to blade type DCA
        {
            if (diff <= 0)
            {
                c_m = (0.05336 * M_in) - 0.02937;
            }
            else if (diff > 0)
            {
                c_m = (0.005 * M_in) - 0.00075;
            }
        }
        return Y_design + (c_m * Math.Pow(diff, 2.0));

    }

}

double Iter;
//do pre simulation initialisation here
public override void Initialise()
{
}

//do post simulation cleanup here
public override void Cleanup()
{
}

//script main execution function - called every cycle
public override void Execute(double Time)
{
  // if (Iter > 10)
   {
      // Fluid properties:
      double k = cp / (cp - R);
```

```
// Rotor inlet velocity triangle:
u.Value = r * rpm;
double[] U = {u * Math.Cos(Math.PI / 2), u * Math.Sin(Math.PI / 2)};
double[] C1 = {c1 * Math.Cos(alpha1), c1 * Math.Sin(alpha1)};
double[] W1 = {C1[0] - U[0], C1[1] - U[1]};
w1.Value = Math.Sqrt(Math.Pow(W1[0], 2) + Math.Pow(W1[1], 2));
beta1.Value = Math.Atan2(W1[1], W1[0]);
inc_R.Value = (-1) * (beta1 - kappa1);

// Rotor inlet properties:
double T01rel = T1 + (Math.Pow(w1, 2)) / (2 * cp);
T02rel.Value = T01rel;
M1rel.Value = w1 / a1;
// Handle normal shock if exists:
if (M1rel > 1)
{
    p1_y.Value = p1 * (1 + 2 * k / (k + 1)*(M1rel * M1rel - 1));
    w1_y.Value = w1 / ((k + 1) * M1rel * M1rel / (2 + (k - 1) * M1rel * M1rel));
    double T1_y = T02rel - w1_y * w1_y / (2 * cp);
    p01rel.Value = p1_y * Math.Pow(T02rel / T1_y, k / (k - 1));
}
else
{
    p1_y.Value = p1;
    p01rel.Value = p1_y * Math.Pow(T02rel / T1, k / (k - 1));
}

// Calculate rotor total pressure loss coefficient:
double Y_R_old = Y_R;
double Y_R_new = CetinLoss(typeR, inc_R, optInc_R, Y_R_design, M1rel) + Y_R_add;
Y_R.Value = Y_R + Relax_R * (Y_R_new - Y_R);
if ((Y_R <= 0) || (Y_R >= 1))
{
    Y_R.Value = Y_R_old;
}

// Rotor deviation angle:
devR.Value = devR_design;

// Rotor exit/stator inlet velocity triangle:
beta2.Value = kappa2 - devR;

double[] W2 = {w2 * Math.Cos(beta2), w2 * Math.Sin(beta2)};

double[] C3 = {W2[0] + U[0], W2[1] + U[1]};
c3.Value = Math.Sqrt(Math.Pow(C3[0], 2) + Math.Pow(C3[1], 2));
alpha3.Value = Math.Atan2(C3[1], C3[0]);
inc_S.Value = alpha3 - kappa3;
```

```
        // Stator inlet properties:
        T03.Value = T3 + Math.Pow(c3, 2) / (2 * cp);
        p03.Value = p3 * Math.Pow(T03 / T3, k / (k-1));

        // Calculate stator total pressure loss coefficient:
        double Y_S_old = Y_S;
        double Y_S_new = CetinLoss(typeS, inc_S, optInc_S, Y_S_design, M3) + Y_S_add;
        Y_S.Value = Y_S + Relax_S * (Y_S_new - Y_S);
        if ((Y_S <= 0) || (Y_S >= 1))
        {
            Y_S.Value = Y_S_old;
        }

        devS.Value = devS_design;

        // Stator exit velocity triangle:
        alpha4.Value = kappa4 + devS;
        double[] C4 = {c4 * Math.Cos(alpha4), c4 * Math.Sin(alpha4)};

        // Normal inlet flow area with relaxation:
        double A_Rin_eff_new =  Math.Abs(A_ann_Rin * Math.Cos(beta1)) * Area_Scale;
        A_Rin_eff.Value = A_Rin_eff + Relax_Area * (A_Rin_eff_new - A_Rin_eff);

        double A_Rex_eff_new = Math.Abs(A_ann_Rex * Math.Cos(beta2)) * Area_Scale;
        A_Rex_eff.Value = A_Rex_eff + Relax_Area * (A_Rex_eff_new - A_Rex_eff);

        double A_Sin_eff_new = Math.Abs(A_ann_Sin * Math.Cos(alpha3)) * Area_Scale;
        A_Sin_eff.Value = A_Sin_eff + Relax_Area * (A_Sin_eff_new - A_Sin_eff);

        double A_Sex_eff_new = Math.Abs(A_ann_Sex * Math.Cos(alpha4)) * Area_Scale;
        A_Sex_eff.Value = A_Sex_eff + Relax_Area * (A_Sex_eff_new - A_Sex_eff);

        // Normal exit flow area with relaxation:

        // Stage performance:
        DF_R.Value = 1 - (w2 / w1) + Math.Abs(C3[1] - C1[1]) / (2 * w1 * sol_R);
        DF_S.Value = 1 - (c4 / c3) + Math.Abs(C4[1] - C3[1]) / (2 * c1 * sol_S);
    }
    Iter = Iter + 1;
 }
//any processing you want to do before steady state
public override void ExecuteBeforeSteadyState()
{
    //IPS.Task.ConsoleSolverOutputProvider.GetConsoleOutputWindow().AddTextLine("Initialize");
    IPS.Task.ConsoleSolverOutputProvider.GetConsoleOutputWindow().Clear();
    A_Rin_eff.Value = A_ann_Rin;
    A_Sin_eff.Value = A_ann_Sin;
    A_Rex_eff.Value = A_ann_Rex;
    A_Sex_eff.Value = A_ann_Sex;
    Y_R.Value = Y_R_design;
    Y_S.Value = Y_S_design;
    devR.Value = devR_design;
    devS.Value = devS_design;

    Iter = 1;
}
```

Appendix C. Simulation data

Table 15: Model 1 simulation data for NASA Stage 35

Reading	RPM	$\dot{m}$ [kg/s]	Y_R	Y_S	Iterations	Π_{stage}	Π_{stage} error [%]	T_{stage}	T_{stage} error [%]	M_R	M_S	i_R [deg]
4004 (100%)	17220.2	20.95	-	-	-	-	-	-	-	-	-	-
3978 (100%)	17119.1	20.92	0.101	0.02	37	1.8432	0.0648	1.2175	-0.6159	0.9581	0.7242	-1.303
3977 (100%)	17125.1	20.48	0.143	0.02	17	1.9056	0.0324	1.2308	-1.0641	0.8340	0.6559	-0.555
3974 (100%)	17196.8	20.13	0.205	0.02	17	1.9219	-0.0028	1.2389	-1.1224	0.7746	0.6286	0.109
3975 (100%)	17224.5	19.54	0.3096	0.02	17	1.9233	0.0136	1.2467	-2.5248	0.7123	0.6019	1.076
3976 (100%)	17218.5	18.2	0.5728	0.02	17	1.9322	0.0112	1.2629	-0.0093	0.6159	0.5391	3.076
3979 (90%)	15451.3	19.5	-	-	-	-	-	-	-	1	1	-
3982 (90%)	15477.7	18.97	0.0705	0.02	97	1.6599	-0.0052	1.1697	-1.0429	0.9308	0.7064	-0.382
3983 (90%)	15467.9	18.24	0.139	0.02	17	1.6981	0.0049	1.1823	-1.1445	0.7849	0.6317	0.763
3984 (90%)	15473.4	17.82	0.19047	0.02	17	1.7112	0.0097	1.1886	-1.1131	0.7363	0.6004	1.422
3985 (90%)	15474.3	16.61	0.39233	0.02	17	1.7192	0.0090	1.2028	-1.2478	0.6354	0.5411	3.251
3987 (80%)	13774.4	14.32	0.3831	0.02	22	1.5352	0.0101	1.1591	-0.7615	0.5932	0.5001	4.415
3995 (70%)	12074.9	15.81	-	-	-	-	-	-	-	1	1	-
3994 (70%)	12074.5	15.31	0.0159	0.01	152	1.2946	0.2821	1.0795	-0.6915	0.8890	0.7019	0.070
3993 (70%)	12073.2	14.38	0.07584	0.02	17	1.3340	0.0002	1.0943	-0.6076	0.7266	0.5943	1.651
3990 (70%)	12040.8	13.41	0.19758	0.02	17	1.3451	0.0041	1.1046	-0.3108	0.6330	0.5303	3.235
3989 (70%)	12022.9	11.79	0.55079	0.02	17	1.3501	0.0084	1.1208	0.0741	0.5167	0.4569	5.927
3997 (60%)	10453.2	10.5	0.376	0.02	17	1.2625	0.0395	1.0878	-0.1060	0.4941	0.3224	5.655
4000 (50%)	8582.4	8.99	0.22464	0.02	12	1.1680	0.0009	1.0549	-0.2030	0.4510	0.3629	5.043

Table 16: Model 2 simulation data for NASA Stage 35

Reading	RPM	$\dot{m}$ [kg/s]	Iterations	Π_R	Π_R error [%]	Π_{stage}	Π_{stage} error [%]	T_{stage}	T_{stage} error [%]	Rotor choke	Stator choke	i_R [deg]	Y_R	DF_R	i_S [deg]	Y_S	DF_S
Design	17188.7	20.188	32	1.864	-0.043	1.819	-0.046	1.225	0.006	FALSE	FALSE	8.298	0.187	0.456	2.433	0.084	0.564
4004 (100%)	17220.2	20.95	-	-	-	-	-	-	-	FALSE	TRUE	-	-	-	-	-	-
3978 (100%)	17119.1	20.82	-	-	-	-	-	-	-	FALSE	TRUE	-	-	-	-	-	-
3977 (100%)	17125.1	20.48	-	-	-	-	-	-	-	FALSE	TRUE	-	-	-	-	-	-
3974 (100%)	17196.8	20.13	27	1.889	-4.834	1.845	-4.014	1.229	-1.892	FALSE	FALSE	8.409	0.187	0.467	3.326	0.086	0.586
3975 (100%)	17224.5	19.54	17	2.060	2.273	1.989	2.945	1.257	-0.481	FALSE	FALSE	9.431	0.192	0.541	9.262	0.173	0.724
3976 (100%)	17218.5	18.2	17	2.286	12.262	2.139	11.254	1.292	0.994	FALSE	FALSE	11.534	0.228	0.636	16.761	0.484	0.921
3979 (90%)	15451.3	19.5	-	-	-	-	-	-	-	TRUE	TRUE	-	-	-	-	-	-
3982 (90%)	15477.7	18.97	-	-	-	-	-	-	-	FALSE	TRUE	-	-	-	-	-	-
3983 (90%)	15467.9	18.24	37	1.575	-8.930	1.507	-11.250	1.161	-2.910	FALSE	FALSE	9.164	0.189	0.377	-3.344	0.127	0.408
3984 (90%)	15473.4	17.82	32	1.672	-4.372	1.635	-4.420	1.180	-1.866	FALSE	FALSE	9.852	0.195	0.439	1.656	0.085	0.554
3985 (90%)	15474.3	16.61	17	1.852	3.972	1.792	4.233	1.212	-0.454	FALSE	FALSE	11.755	0.228	0.551	10.642	0.198	0.783
3987 (80%)	13774.4	14.32	22	1.607	2.321	1.572	2.441	1.163	-0.410	FALSE	FALSE	12.986	0.252	0.523	8.887	0.144	0.760
3995 (70%)	12074.9	15.81	-	-	-	-	-	-	-	TRUE	TRUE	-	-	-	-	-	-
3994 (70%)	12074.5	15.31	-	-	-	-	-	-	-	FALSE	TRUE	-	-	-	-	-	-
3993 (70%)	12073.2	14.38	32	1.227	-8.671	1.220	-8.577	1.078	-2.085	FALSE	FALSE	10.160	0.196	0.252	-12.138	0.019	0.274
3990 (70%)	12040.8	13.41	22	1.326	-2.236	1.319	-1.897	1.100	-0.705	FALSE	FALSE	11.790	0.218	0.379	-2.214	0.025	0.493
3989 (70%)	12022.9	11.79	22	1.449	5.361	1.422	5.350	1.127	0.628	FALSE	FALSE	14.559	0.283	0.535	10.095	0.155	0.815
3997 (60%)	10453.2	10.5	22	1.293	1.433	1.280	1.387	1.089	-0.023	FALSE	FALSE	14.291	0.260	0.476	5.752	0.095	0.701
4000 (50%)	8582.4	8.99	17	1.165	-0.734	1.159	-0.750	1.054	-0.302	FALSE	FALSE	13.675	0.232	0.406	0.371	0.054	0.563

Table 17: Model 3 simulation data for NASA Stage 35

Reading	RPM	$\dot{m}$ [kg/s]	Iterations	Π_R	Π_R error [%]	Π_{stage}	Π_{stage} error [%]	T_{stage}	T_{stage} error [%]	Rotor choke	Stator choke	i_R [deg]	Y_R	DF_R	i_S [deg]	Y_S	DF_S	K_A
Design	17188.7	20.188	192	1.864	-0.043	1.819	-0.048	1.225	0.006	FALSE	FALSE	8.298	0.187	0.456	2.433	0.084	0.564	1.000
4004 (100%)	17220.2	20.95	502	1.790	2.966	1.703	-0.637	1.224	2.179	FALSE	TRUE	6.988	0.222	0.458	2.034	0.085	0.510	1.073
3978 (100%)	17119.1	20.82	22	1.922	2.511	1.842	0.024	1.247	1.826	FALSE	FALSE	7.087	0.217	0.532	7.836	0.139	0.648	1.110
3977 (100%)	17125.1	20.48	17	1.990	1.768	1.910	0.254	1.252	0.619	FALSE	FALSE	7.705	0.194	0.541	8.761	0.160	0.679	1.075
3974 (100%)	17196.8	20.13	22	1.984	-0.067	1.924	0.085	1.247	-0.512	FALSE	FALSE	8.409	0.187	0.517	7.167	0.127	0.664	1.025
3975 (100%)	17224.5	19.54	17	1.981	-1.644	1.933	0.046	1.243	-1.586	FALSE	FALSE	9.431	0.192	0.500	6.192	0.111	0.664	0.977
3976 (100%)	17218.5	18.2	22	1.964	-3.556	1.929	0.328	1.237	-3.297	FALSE	FALSE	11.534	0.228	0.474	4.871	0.095	0.677	0.895
3979 (90%)	15451.3	19.5	-	-	-	-	-	-	-	TRUE	FALSE	-	-	-	-	-	-	-
3982 (90%)	15477.7	18.97	-	-	-	-	-	-	-	FALSE	TRUE	-	-	-	-	-	-	-
3983 (90%)	15467.9	18.24	22	1.746	0.979	1.700	0.104	1.196	-0.001	FALSE	FALSE	9.164	0.189	0.502	6.204	0.108	0.639	1.065
3984 (90%)	15473.4	17.82	27	1.755	0.417	1.713	0.097	1.196	-0.486	FALSE	FALSE	9.852	0.195	0.499	6.214	0.108	0.652	1.035
3985 (90%)	15474.3	16.61	17	1.750	-1.728	1.718	-0.045	1.193	-2.046	FALSE	FALSE	11.755	0.228	0.480	5.364	0.098	0.673	0.952
3987 (80%)	13774.4	14.32	22	1.560	-0.707	1.535	0.020	1.153	-1.262	FALSE	FALSE	12.986	0.252	0.477	5.459	0.097	0.686	0.965
3995 (70%)	12074.9	15.81	-	-	-	-	-	-	-	TRUE	TRUE	-	-	-	-	-	-	-
3994 (70%)	12074.5	15.31	-	-	-	-	-	-	-	FALSE	TRUE	-	-	-	-	-	-	-
3993 (70%)	12073.2	14.38	22	1.351	0.616	1.326	-0.573	1.108	0.664	FALSE	FALSE	10.160	0.196	0.432	1.199	0.080	0.524	1.110
3990 (70%)	12040.8	13.41	22	1.365	0.693	1.344	-0.050	1.110	0.136	FALSE	FALSE	11.790	0.218	0.435	2.010	0.084	0.572	1.040
3989 (70%)	12022.9	11.79	17	1.368	-0.518	1.353	0.209	1.109	-1.010	FALSE	FALSE	14.559	0.283	0.421	1.783	0.083	0.627	0.910
3997 (60%)	10453.2	10.5	22	1.276	0.059	1.263	0.096	1.085	-0.412	FALSE	FALSE	14.291	0.260	0.442	3.203	0.085	0.644	0.970
4000 (50%)	8582.4	8.99	22	1.165	-0.734	1.159	-0.750	1.054	-0.302	FALSE	FALSE	13.675	0.232	0.406	0.371	0.054	0.563	1.000

Table 18: Model 3 simulation data for NASA Stage 36

Reading	RPM	$\dot{m}$ [kg/s]	Iterations	Π_R	Π_R error [%]	Π_{stage}	Π_{stage} error [%]	T_{stage}	T_{stage} error [%]	Rotor choke	Stator choke	i_R [deg]	Y_R	DF_R	i_S [deg]	Y_S	DF_S	K_A
Design	17188.7	20.188	142	1.867	0.201	1.823	0.182	1.228	0.055	FALSE	FALSE	8.435	0.207	0.462	2.594	0.081	0.577	1.000
4273 (100%)	17191.5	20.94	242	1.802	2.023	1.743	0.734	1.229	1.820	FALSE	FALSE	7.129	0.242	0.472	2.866	0.081	0.556	1.080
4272 (100%)	17191.7	20.83	57	1.876	1.203	1.818	0.070	1.240	1.036	FALSE	FALSE	7.326	0.232	0.502	5.250	0.096	0.613	1.079
4271 (100%)	17187.6	20.69	37	1.911	1.202	1.852	0.006	1.243	0.628	FALSE	FALSE	7.569	0.222	0.509	5.952	0.104	0.631	1.067
4270 (100%)	17147.4	20.46	37	1.931	1.030	1.874	0.004	1.243	0.224	FALSE	FALSE	7.915	0.212	0.511	6.208	0.107	0.643	1.050
4269 (100%)	17140.5	20.26	27	1.931	0.385	1.880	-0.372	1.240	-0.281	FALSE	FALSE	8.249	0.208	0.504	5.744	0.101	0.640	1.030
4281 (90%)	15481.5	19.75	-	-	-	-	-	-	-	TRUE	TRUE	-	-	-	-	-	-	-
4280 (90%)	15471.1	19.51	-	-	-	-	-	-	-	TRUE	TRUE	-	-	-	-	-	-	-
4279 (90%)	15437.3	19.25	-	-	-	-	-	-	-	TRUE	TRUE	-	-	-	-	-	-	-
4282 (90%)	15489	19	17	1.716	1.597	1.660	-0.597	1.199	1.212	FALSE	FALSE	8.051	0.209	0.515	6.556	0.109	0.632	1.135
4284 (90%)	15440.6	18.6	22	1.729	1.872	1.679	0.009	1.197	0.710	FALSE	FALSE	8.642	0.207	0.510	6.369	0.106	0.640	1.100
4277 (90%)	15448.6	18.39	27	1.729	1.401	1.684	-0.062	1.196	0.322	FALSE	FALSE	8.997	0.208	0.502	5.875	0.100	0.637	1.077
4294 (80%)	13737.4	16.1	22	1.541	1.231	1.507	-0.133	1.154	0.597	FALSE	FALSE	10.131	0.216	0.493	5.525	0.094	0.635	1.100
4301 (70%)	12019	16.1	-	-	-	-	-	-	-	TRUE	FALSE	-	-	-	-	-	-	-
4299 (70%)	12026.1	15.6	-	-	-	-	-	-	-	TRUE	TRUE	-	-	-	-	-	-	-
4298 (70%)	12016	15.04	37	1.339	0.636	1.310	-0.933	1.111	1.480	FALSE	FALSE	8.979	0.208	0.460	2.567	0.081	0.539	1.200
4297 (70%)	12019	14.02	22	1.368	0.216	1.345	-0.754	1.113	0.449	FALSE	FALSE	10.758	0.221	0.462	3.345	0.082	0.589	1.110
4296 (70%)	12030	13.44	22	1.385	0.708	1.363	-0.042	1.115	0.131	FALSE	FALSE	11.779	0.235	0.472	4.383	0.085	0.631	1.070
4304 (60%)	10293.3	10.84	32	1.266	0.401	1.253	-0.020	1.083	0.025	FALSE	FALSE	13.385	0.256	0.455	3.600	0.082	0.639	1.025
4309 (50%)	8624.9	9.03	32	1.179	0.331	1.170	-0.026	1.058	0.008	FALSE	FALSE	13.716	0.251	0.449	3.264	0.081	0.632	1.035

Table 19: Model 3 simulation data for NASA Stage 37

Reading	RPM	$\dot{m}$ [kg/s]	Iterations	Π_R	Π_R error [%]	Π_{stage}	Π_{stage} error [%]	T_{stage}	T_{stage} error [%]	Rotor choke	Stator choke	i_R [deg]	Y_R	DF_R	i_S [deg]	Y_S	DF_S	K_A
Design	17188.7	20.188	22	2.071	-1.680	2.030	-0.959	1.264	-0.455	FALSE	FALSE	5.612	0.200	0.520	-0.665	0.090	0.664	0.990
4193 (100%)	17196.8	20.93	22	1.891	5.918	1.755	0.096	1.246	2.641	FALSE	FALSE	4.296	0.236	0.470	-4.722	0.223	0.480	1.040
4192 (100%)	17169.3	20.83	22	1.953	1.882	1.880	0.041	1.255	1.433	FALSE	FALSE	4.442	0.228	0.498	-2.637	0.133	0.581	1.042
4182 (100%)	17254.8	20.74	27	2.049	-0.347	2.006	0.306	1.268	0.549	FALSE	FALSE	4.723	0.216	0.529	-0.302	0.086	0.658	1.035
4188 (100%)	17229.7	20.43	22	2.114	-1.990	2.077	-0.058	1.274	-0.694	FALSE	FALSE	5.244	0.203	0.548	1.231	0.083	0.704	1.020
4187 (100%)	17203.6	19.6	22	2.128	-3.093	2.096	0.125	1.271	-1.967	FALSE	FALSE	6.627	0.204	0.534	0.622	0.082	0.715	0.960
4209 (90%)	15484.7	19.74	-	-	-	-	-	-	-	TRUE	TRUE	-	-	-	-	-	-	-
4208 (90%)	15469.6	19.61	-	-	-	-	-	-	-	TRUE	TRUE	-	-	-	-	-	-	-
4207 (90%)	15468	18.95	27	1.846	-0.402	1.808	-0.611	1.223	0.861	FALSE	FALSE	5.306	0.201	0.557	1.924	0.085	0.694	1.120
4205 (90%)	15481.9	18.01	32	1.878	-0.964	1.847	0.004	1.222	-0.516	FALSE	FALSE	6.888	0.206	0.543	1.328	0.083	0.712	1.033
4204 (90%)	15492.8	17.39	22	1.878	-1.605	1.851	0.206	1.220	-1.308	FALSE	FALSE	7.899	0.218	0.531	0.746	0.082	0.720	0.985
4194 (80%)	13756.7	15.39	17	1.650	-0.179	1.626	0.025	1.174	-0.321	FALSE	FALSE	8.583	0.226	0.533	1.052	0.082	0.720	1.035
4202 (70%)	12046.2	16.25	-	-	-	-	-	-	-	TRUE	TRUE	-	-	-	-	-	-	-
4203 (70%)	12016.4	15.93	-	-	-	-	-	-	-	TRUE	TRUE	-	-	-	-	-	-	-
4201 (70%)	12044.7	15.44	22	1.331	-3.686	1.323	-3.563	1.113	0.619	FALSE	FALSE	5.580	0.200	0.415	-8.209	0.019	0.453	1.150
4198 (70%)	12018.3	14.91	102	1.312	-6.723	1.310	-6.269	1.103	-0.887	FALSE	FALSE	6.469	0.202	0.352	-12.239	0.006	0.384	1.056
4196 (70%)	12036.1	14.19	27	1.441	0.706	1.419	-0.043	1.130	0.684	FALSE	FALSE	7.767	0.212	0.512	-0.611	0.079	0.647	1.120
4195 (70%)	12038.9	13.3	22	1.444	0.151	1.427	-0.033	1.128	-0.056	FALSE	FALSE	9.326	0.235	0.498	-1.230	0.076	0.667	1.035
4215 (60%)	10307	11.05	27	1.301	-0.268	1.294	-0.054	1.092	-0.100	FALSE	FALSE	10.317	0.245	0.475	-2.571	0.044	0.650	1.015
4218 (50%)	8592.5	9.18	22	1.201	-0.089	1.199	0.193	1.064	-0.030	FALSE	FALSE	10.628	0.240	0.471	-2.741	0.014	0.646	1.030

Table 20: Model 3 simulation data for NASA Stage 38

Reading	RPM	$\dot{m}$ [kg/s]	Iterations	Π_R	Π_R error [%]	Π_{stage}	Π_{stage} error [%]	T_{stage}	T_{stage} error [%]	Rotor choke	Stator choke	i_R [deg]	Y_R	DF_R	i_S [deg]	Y_S	DF_S	K_A
Design	17188.7	20.188	57	2.099	-0.269	2.044	-0.301	1.268	-0.052	FALSE	FALSE	5.878	0.194	0.536	0.661	0.082	0.688	1.000
4129 (100%)	17223.9	20.97	487	2.091	16.233	1.804	-0.668	1.282	5.254	FALSE	TRUE	4.557	0.232	0.579	3.415	0.096	0.612	1.106
4128 (100%)	17226.8	20.91	502	2.090	13.192	1.835	0.352	1.279	4.347	FALSE	TRUE	4.669	0.226	0.570	2.803	0.090	0.616	1.089
4123 (100%)	17185.7	20.91	502	2.085	12.232	1.890	0.269	1.280	4.126	FALSE	TRUE	4.613	0.228	0.576	3.188	0.094	0.658	1.101
4121 (100%)	17221.7	20.83	502	2.073	8.438	1.939	-0.240	1.274	2.743	FALSE	TRUE	4.806	0.219	0.554	1.680	0.083	0.655	1.067
4120 (100%)	17227.9	20.67	502	2.054	4.337	1.972	-0.232	1.267	1.174	FALSE	TRUE	5.098	0.208	0.530	0.029	0.084	0.646	1.033
4119 (100%)	17205.9	20.44	217	2.026	1.122	1.935	-2.145	1.258	-0.067	FALSE	FALSE	5.470	0.198	0.505	-1.702	0.110	0.606	1.000
4140 (90%)	15462.1	19.76	-	-	-	-	-	-	-	TRUE	TRUE	-	-	-	-	-	-	-
4139 (90%)	15516.3	19.76	-	-	-	-	-	-	-	TRUE	TRUE	-	-	-	-	-	-	-
4133 (90%)	15447	19.54	-	-	-	-	-	-	-	TRUE	TRUE	-	-	-	-	-	-	-
4132 (90%)	15507.9	19.36	-	-	-	-	-	-	-	TRUE	TRUE	-	-	-	-	-	-	-
4131 (90%)	15478.7	19.02	87	1.859	4.561	1.787	1.481	1.227	2.157	FALSE	FALSE	5.450	0.198	0.572	3.189	0.092	0.707	1.144
4093 (80%)	13735.9	16.76	17	1.613	2.295	1.561	-0.110	1.172	1.615	FALSE	FALSE	6.498	0.196	0.535	0.748	0.082	0.653	1.145
4097 (70%)	12026.2	16.14	-	-	-	-	-	-	-	TRUE	TRUE	-	-	-	-	-	-	-
4098 (70%)	12003.6	15.69	-	-	-	-	-	-	-	TRUE	TRUE	-	-	-	-	-	-	-
4099 (70%)	11999.4	15.27	17	1.424	3.098	1.368	0.058	1.132	2.443	FALSE	TRUE	6.001	0.194	0.543	1.212	0.082	0.631	1.266
4100 (70%)	12002.6	14.92	17	1.373	-1.657	1.359	-1.888	1.117	0.727	FALSE	TRUE	6.621	0.196	0.446	-5.561	0.018	0.518	1.130
4101 (70%)	12005.1	14.5	17	1.434	1.731	1.399	-0.097	1.129	1.336	FALSE	FALSE	7.359	0.200	0.517	-0.254	0.080	0.635	1.159
4095 (70%)	12014.2	13.85	22	1.438	1.244	1.409	-0.096	1.127	0.669	FALSE	FALSE	8.505	0.212	0.503	-0.969	0.076	0.645	1.089
4104 (60%)	10621.2	11.75	27	1.313	0.106	1.308	0.288	1.095	0.221	FALSE	FALSE	9.744	0.226	0.463	-3.410	0.021	0.618	1.035
4102 (50%)	8562.7	9.29	37	1.193	-0.096	1.192	0.236	1.061	0.233	FALSE	FALSE	10.466	0.227	0.454	-3.894	0.009	0.614	1.033

Table 21: Model 4 simulation data for NASA Stage 35

Reading	RPM	$\dot{m}$ [kg/s]	Iterations	Π_R	Π_R error [%]	Π_{stage}	Π_{stage} error [%]	T_{stage}	T_{stage} error [%]	Rotor choke	Stator choke	i_R [deg]	Y_R	DF_R	i_S [deg]	Y_S	DF_S	K_A
Design	17188.7	20.188	32	1.864	-0.043	1.819	-0.046	1.225	0.006	FALSE	FALSE	8.298	0.187	0.456	2.433	0.084	0.564	1.000
4004 (100%)	17220.2	20.95	77	1.840	5.867	1.780	3.871	1.234	2.994	FALSE	FALSE	6.988	0.222	0.485	4.201	0.090	0.577	1.086
3978 (100%)	17119.1	20.82	47	1.847	-1.470	1.788	-2.918	1.233	0.680	FALSE	FALSE	7.087	0.217	0.491	4.696	0.094	0.588	1.086
3977 (100%)	17125.1	20.48	22	1.944	-0.582	1.880	-1.310	1.243	-0.050	FALSE	FALSE	7.705	0.194	0.517	6.907	0.122	0.644	1.060
3974 (100%)	17196.8	20.13	22	1.988	0.130	1.926	0.227	1.247	-0.455	FALSE	FALSE	8.409	0.187	0.519	7.322	0.130	0.667	1.026
3975 (100%)	17224.5	19.54	22	1.988	-1.285	1.939	0.358	1.244	-1.484	FALSE	FALSE	9.431	0.192	0.504	6.478	0.115	0.670	0.979
3976 (100%)	17218.5	18.2	22	1.880	-7.662	1.847	-3.955	1.222	-4.492	FALSE	FALSE	11.534	0.228	0.429	1.478	0.087	0.601	0.879
3979 (90%)	15451.3	19.5	-	-	-	-	-	-	-	TRUE	TRUE	-	-	-	-	-	-	-
3982 (90%)	15477.7	18.97	27	1.683	0.168	1.635	-1.528	1.190	0.646	FALSE	FALSE	7.966	0.189	0.483	4.394	0.091	0.579	1.110
3983 (90%)	15467.9	18.24	27	1.728	-0.067	1.686	-0.731	1.192	-0.298	FALSE	FALSE	9.164	0.189	0.489	5.229	0.097	0.619	1.056
3984 (90%)	15473.4	17.82	37	1.732	-0.940	1.694	-1.021	1.192	-0.872	FALSE	FALSE	9.852	0.195	0.482	4.941	0.095	0.626	1.024
3985 (90%)	15474.3	16.61	17	1.701	-4.502	1.672	-2.709	1.183	-2.844	FALSE	FALSE	11.755	0.228	0.445	2.692	0.084	0.614	0.933
3987 (80%)	13774.4	14.32	17	1.504	-4.248	1.482	-3.437	1.141	-2.281	FALSE	FALSE	12.986	0.252	0.421	1.330	0.083	0.593	0.930
3995 (70%)	12074.9	15.81	-	-	-	-	-	-	-	TRUE	TRUE	-	-	-	-	-	-	-
3994 (70%)	12074.5	15.31	47	1.307	0.518	1.287	-0.298	1.103	1.467	FALSE	FALSE	8.531	0.187	0.408	-1.228	0.047	0.455	1.175
3993 (70%)	12073.2	14.38	27	1.346	0.259	1.323	-0.841	1.107	0.561	FALSE	FALSE	10.160	0.196	0.425	0.691	0.076	0.515	1.105
3990 (70%)	12040.8	13.41	22	1.361	0.333	1.340	-0.384	1.108	0.034	FALSE	FALSE	11.790	0.218	0.429	1.494	0.082	0.561	1.035
3989 (70%)	12022.9	11.79	22	1.372	-0.183	1.357	0.540	1.110	-0.915	FALSE	FALSE	14.559	0.283	0.428	2.268	0.084	0.638	0.914
3997 (60%)	10453.2	10.5	17	1.278	0.249	1.266	0.279	1.085	-0.358	FALSE	FALSE	14.291	0.260	0.446	3.556	0.085	0.651	0.974
4000 (50%)	8582.4	8.99	17	1.181	0.629	1.172	0.327	1.058	0.087	FALSE	FALSE	13.675	0.232	0.455	4.048	0.086	0.639	1.047

Appendix D. Ethics in Research Assessment

Application for Approval of Ethics in Research (EiR) Projects
Faculty of Engineering and the Built Environment, University of Cape Town

ETHICS APPLICATION FORM

Please Note:
Any person planning to undertake research in the Faculty of Engineering and the Built Environment (EBE) at the University of Cape Town is required to complete this form **before** collecting or analysing data. The objective of submitting this application *prior* to embarking on research is to ensure that the highest ethical standards in research, conducted under the auspices of the EBE Faculty, are met. Please ensure that you have read, and understood the **EBE Ethics in Research Handbook** (available from the UCT EBE, Research Ethics website) prior to completing this application form: http://www.ebe.uct.ac.za/ebe/research/ethics1

APPLICANT'S DETAILS		
Name of principal researcher, student or external applicant		Daniel Barlin
Department		Mechanical Engineering
Preferred email address of applicant:		BRLDAN001@myuct.ac.za
If Student	Your Degree: e.g., MSc, PhD, etc.	MSc (Eng) (by dissertation) in Mechanical Engineering
	Credit Value of Research: e.g., 60/120/180/360 etc.	180
	Name of Supervisor (if supervised):	Wim Fuls
If this is a researchcontract, indicate the source of funding/sponsorship		
Project Title		Developing a 1-D method for modelling gas turbines

I hereby undertake to carry out my research in such a way that:

- there is no apparent legal objection to the nature or the method of research; and
- the research will not compromise staff or students or the other responsibilities of the University;
- the stated objective will be achieved, and the findings will have a high degree of validity;
- limitations and alternative interpretations will be considered;
- the findings could be subject to peer review and publicly available; and
- I will comply with the conventions of copyright and avoid any practice that would constitute plagiarism.

APPLICATION BY	Full name	Signature	Date
Principal Researcher/ Student/External applicant	Daniel Barlin		2021/02/05
SUPPORTED BY	Full name	Signature	Date
Supervisor (where applicable)	A/Prof WF Fuls		2021/02/06

APPROVED BY	Full name	Signature	Date
HOD (or delegated nominee) Final authority for all applicants who have answered NO to all questions in Section 1; and for all Undergraduate research (Including Honours).	Prof. Tunde Bello-Ochende		25/03/2021
Chair: Faculty EIR Committee For applicants other than undergraduate students who have answered YES to any of the questions in Section 1.			

Page 1 of 1